Random packing of colloids and granular matter

Universiteit Utrecht

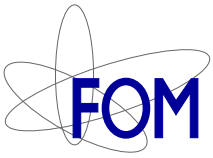

ISBN 0
Subject headings: random packing/hard spheres/spherocylinders/cut spheres/spheroids/granular matter/colloids/computer simulation.

Random packing of colloids and granular matter

Willekeurige stapeling van colloïden en granulaire materie

(met een samenvatting in het Nederlands)

Proefschrift

ter verkrijging van de graad van doctor aan de
Universiteit Utrecht op gezag van de rector magnificus,
prof. dr. J. C. Stoof, ingevolge het besluit van het
college voor promoties in het openbaar te verdedigen
op maandag 18 februari 2008 des ochtends te 10.30 uur

door

Alan Wouterse

geboren op 29 december 1978 te Utrecht

Promotor: Prof. dr. A.P. Philipse

This work is part of the Granular Matter programme of the 'Stichting voor Fundamenteel Onderzoek der Materie (FOM)', financially supported by the 'Nederlandse Organisatie voor Wetenschappelijk Onderzoek (NWO)'.

Contents

1

Introduction

This thesis deals with the random packing of colloids and granular matter. Random packings are disordered collections of particles in contact. The particles can be colloids [1, 2], defined as particles that have a size between 1 nm and 1000 nm in at least one dimension. Colloids can be found in many practical systems, such as the inorganic pigments in paint and ink, the casein micels in milk and the red blood cells in blood. Colloids are small enough to exhibit a noticeable thermal motion, the so-called Brownian motion named after its discoverer, the botanist Robert Brown (1773 - 1858). Though Brownian motion tends to keep the colloids homogeneously distributed, an external force due to gravity or a centrifuge may push the colloids into a dense sediment. If the colloids stay in a disordered configuration (because the colloids are kinetically arrested) the sediment is actually a random packing. Examples are sediments of silica spheres or randomly oriented rods and deposits of colloidal particles obtained via a filtration process [2].

A striking feature of random packings of colloidal spheres or other shapes is their structural similarity to packings of so-called granular matter. This type of matter contains by definition macroscopic particles that are too large to display significant thermal motion. Of the very many examples of granular packings in nature and (food) technology we mention coffee powder, nuts, sand, rice and ball bearings. The similarity just mentioned implies that particle shape rather than size determines the static properties of a random packing. Such properties are the average particle concentration and average contact numbers between particles in a random packing. However, how they follow from a given particle geometry is a difficult, largely unsolved problem.

The aim of this thesis is to further develop our understanding of the random packing problem, i.e. the connection between particle geometry, volume fraction of a packing

and particle contact numbers. To address this problem we employ computer simulations and also make use of caging models for analytical or numerical calculations. The content of the thesis is briefly as follows.

In Chapter 3 we will discuss the specific case of caging spheres with respect to the jamming that occurs in random packings. Next, in Chapter 4 a geometrical cluster ensemble model is proposed that utilizes the concepts of Chapter 3 to calculate global properties using local packing rules. In Chapter 5 the mechanical contraction method is extended to simulate random packings of general convex objects and results for spherocylinders, spheroids and cut spheres are presented. Contact numbers in random rod packings are investigated in Chapter 6, which also comprises a calculation of the caging number for spherocylinders. Finally, in Chapter 7 some preliminary results on simulations of expanding packings are presented and the possible relevance to the movement of certain types of biological cells is discussed. First, however, we review in Chapter 2 a selection of literature on the random packing problem. This chapter places this thesis in its appropriate context and introduces key concepts that are used in later chapters.

2

Random particle packings: A review

2.1. Introduction

The packing of particles is a topic with long standing history: transmitted literature goes back at least to the Ancient Greeks. An interesting early example is the calculation by Archimedes (287 - 211 BC) of the number of sand grains that it would take to fill the universe, given some reasonable estimate of its size [3, 4]. Another early packing study (200 BC) is that by Apollonius of Perga, who thought about an algorithm for the packing of disks that fills space completely [5] the so called "Apollonian Packing". Later in history, Kepler made in 1611 his famous conjecture that the maximum density at which spheres can be packed is a close packed crystal consisting of hexagonal planes where the spheres are placed in the dents of the layer below [6]. The volume fraction of this close packing is $\frac{\pi}{\sqrt{18}} \approx 0.74$. That this volume fraction is indeed the absolute maximum has been proved only recently by Hales, who employed extensive computer calculations to verify Kepler's conjecture [7].

Not only ordered packings are of interest but also random packings are important, as they are abundant in nature and technology [8,9]. Random packings are disordered collections of particles in contact. These random packings can be made from particles with various shapes such as spheres, discs, cubes, plates, rods and ellipsoids. The particle distribution can be monodisperse or polydisperse where in the latter case particles have some distribution in size or shape. Random packings of hard spheres are, for example, used as a model system for the structure of simple liquids [10, 11]. Bernal's sphere packing has been identified as the prototype of the monoatomic glass [12]. The flow of granular matter and storage of grain in silos is an example of an industrial application

of random packings. The properties of concrete are determined by the packing of particles [13,14]. Composite materials and powder technology [8,15–20] use the properties of packings to create a wide range of products with different material properties based on the packing of particles.

One of the first reported quantitative experimental studies on random packing was performed by Smith et al. [21] in 1929, who investigated random packing of lead shot spherical particles in a beaker. Volume fractions were found in the range 0.55 - 0.64. Bernal analyzed steel balls, which were more uniform spheres and reported that 0.64 is the maximum density obtainable for random packings [10]. Various studies yielded consistently a volume fraction of about 0.64 for different systems, which raises the question whether there is a geometrical equation of state for random sphere packings or random packings in general.

The goal of this literature study is to review and summarize various aspects of random packings. Only a selection of articles is discussed because of the overwhelming number of articles available on the subject [8,15–19] the large majority of which, it should be noted, is on sphere packings. See for instance the standard textbook "The packing of particles" by Cumberland and Crawford [20] which already reviews over 300 articles.

This chapter is structured in the following way. In the first section the general parameters that play a role in random packings are introduced. Then in the next section random packings of spheres will be discussed. A comparison is made between experiments, theory and computer simulations. After the discussion of random packing of spherical particles the packing of non-spherical particles is considered. Finally, some conclusions are given on our current understanding of random packing.

2.2. Random packing of particles

Throughout this thesis a random packing of particles is thought of as a disordered collection of particles that are in contact with each other and form a static structure. Fig. 2.1 shows several examples of random packings of particles with sizes ranging from colloids in the sub-micron range to macroscopic particles of several centimeters, which illustrate that the packing of particles considered here is mostly a geometric effect. From Fig. 2.1 relevant parameters are easily identified, namely particle size (polydispersity) and shape, an indication of particle interactions, the number of contacts on a particle (coordination numbers), the number density or volume fraction and the order in the packing. Relations between these parameters can be derived, which is useful for both fundamental insight in random packing and commercial use of random packings. For example fine tuning a random packing in a reactor bed can be useful to modify gas flows inside a packing which can increase reaction yields.

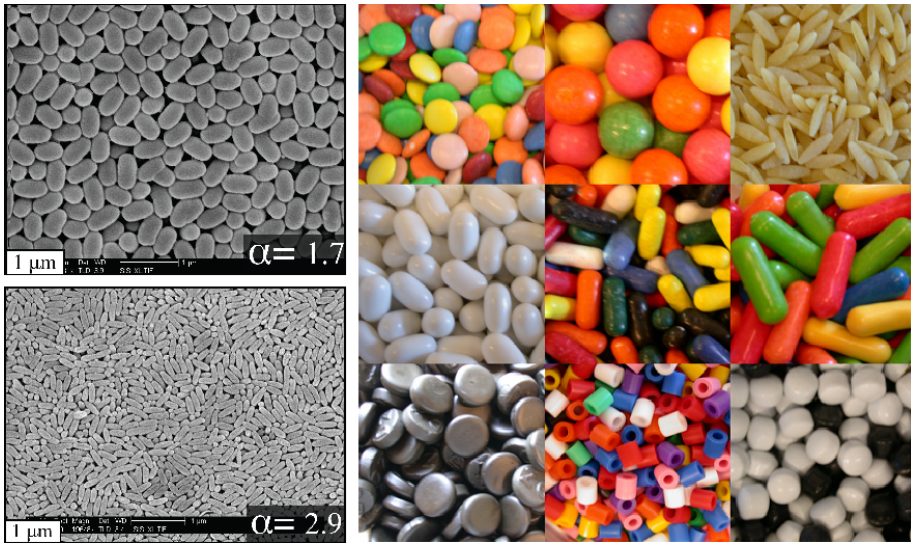

Figure 2.1: (a) Examples of random packing of colloidal ellipsoid-like particles [22] with aspect ratio 1.7 and 2.9 in the sub-micron range. (b) Example of disordered granular material with particles in the size range of centimeters [23]. Note the similarity between the colloidal particles and similar shaped granular material indicating that packing effects are purely of geometric origin.

2.2.1. Particle size and shape

One parameter to characterize the shape of a particle is the sphericity parameter ψ, defined as the ratio of surface area A_s of a sphere having the same volume as the particle to the actual surface area A_p of the particle [24],

$$\psi = \frac{A_s\,(V_s = V_p)}{A_p} \tag{2.1}$$

where V_s and V_p are the volume of the sphere and particle. If the particle is a sphere then $\psi = 1$ by definition. For a spherocylinder

$$\psi = \frac{\left(1 + \frac{3}{2}\alpha\right)^{\frac{2}{3}}}{1 + \alpha} \tag{2.2}$$

where α is the aspect ratio of the spherocylinder. The aspect ratio for rods is defined as

$$\alpha = \frac{L}{D} \tag{2.3}$$

where L is the length and D is the diameter of a spherocylinder. For a spheroid, L would be the length of the long/short axis and D the length of the axis of symmetry.

A hard particle excludes a certain volume in space where other particle centers are not allowed. This excluded volume depends on shape and size of particles. When particles interact the probability of finding a particle center within a certain region of another particle changes depending on the interaction between particles. A definition

of the excluded volume for two spheres that takes the interactions between particles into account is

$$V_{excl} = \int \left(1 - e^{-\frac{\phi(\vec{r})}{k_B T}}\right) d\vec{r} \tag{2.4}$$

where $\phi(\vec{r})$ is the interaction potential between spheres, k_B is Boltzmann's constant and T the absolute temperature. The excluded volume for hard spheres is an instructive example. The hard-sphere potential for a sphere with diameter σ is

$$\begin{aligned} \phi = &\ \infty \quad \text{for } r \leq \sigma \\ = &\ 0 \quad \text{for } r > \sigma \end{aligned} \tag{2.5}$$

Substituting (2.6) in (2.4) gives the excluded volume of a hard sphere

$$V_{excl} = (4/3)\pi\sigma^3 \tag{2.6}$$

As expected this is the volume excluded for the center of a hard sphere by the presence of another hard sphere, which is 8 times the volume of a sphere. If spheres repel each other apart from the hard-core potential, the contribution for $r > \sigma$ to the integral (2.4) becomes unequal to zero and the excluded volume becomes larger than for the hard-core potential. Effectively this means that the probability of finding contacting spheres decreases because of repulsion between two particles. In the case that spheres do not interact, the excluded volume is zero and the spheres are allowed to overlap completely. Another example is the excluded volume for two spherocylinders calculated by Onsager [25],

$$V_{excl} = \frac{\pi}{2} L^2 D + 2\pi L D^2 + \frac{4}{3}\pi D^3 \tag{2.7}$$

In a random packing there are more than two particles interacting with each other and in the next paragraph coordination numbers are discussed, which describe the number of particles surrounding or contacting a central particle.

2.2.2. Coordination numbers: Kissing, parking and caging number

Particles in a packing have contacts and interactions with other particles. The different types of contacts or coordination numbers used in this thesis are described in this section. The ratio between the total number of contacts, N_{con}, in a packing and total number of particles, N, is called the contact number $\langle c \rangle$

$$\langle c \rangle = \frac{N_{con}}{N} = \frac{\langle C \rangle}{2} \tag{2.8}$$

where $\langle C \rangle$ is the average number of contacts per particle. See Fig. 2.2 for an illustration.

The coordination number is the average number of nearest neighbours and the kissing number is the maximum number of particles that can touch the particle in question without creating overlap with other particles. In 1694 David Gregory claimed that a maximum of 13 spheres could fit on another sphere of the same size, whereas Isaac

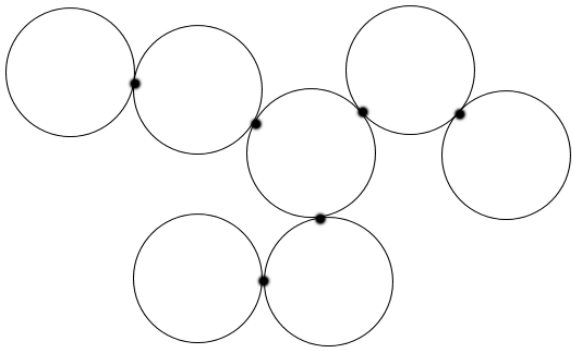

Figure 2.2: Illustration of the contact numbers in (2.8). Here $\langle c \rangle = 6/7$ and $\langle C \rangle = (1+2+3+2+1+2+1)/7 = 12/7$.

Newton stated that this maximum was 12. It took 180 years before Hoppe proved in 1874 that Newton's answer was the right one [26].

The kissing number is obtained by placing particles in an ordered way such that a maximum number of particles is contacting a central particle. Another related number is the parking number. The parking number $\langle z \rangle$ is the average of the maximum number of particles that can be placed *randomly* on a central particle without interpenetration of the surrounding particles with each other (see Fig. 2.3). Mansfield et al. investigated how many spheres can park on a central sphere as a function of sphere ratio [27]. For randomly placed spheres the parking number is

$$\langle z \rangle = K_p \left(\frac{r_1}{r_2} + 1 \right)^2 \tag{2.9}$$

with the constant $K_p = 2.187$. Furthermore, an equation for spheres attaching through diffusion has been found, where the first spheres attach randomly and already attached spheres guide the next spheres. This gives

$$\langle z_{dif} \rangle = K_d \left(\frac{r_1}{r_2} + 1 \right)^2 \tag{2.10}$$

now with the constant $K_d = 2.243$. For equal sized spheres, according to (2.9), the parking number is 8.7. The parking number for other shapes such as spherocylinders or ellipsoids is not well-defined because particles already present, align newly placed particles.

The coordination number of a particle also determines whether or not the particle can translate or rotate. The average *minimum* number of randomly placed particles required to block all movement of a center particle is called the caging number $\langle \gamma_c \rangle$ [28, 29]. By definition this number is less than the parking number, which is the average maximum number of randomly placed particles.

Caging is related to random packing [28] and is a specific case of the more general jamming state [30, 31]. Particles in a random close packing are static. For macroscopic particles like tennis balls in a box it is clear that the tennis balls are static. In a colloidal packing colloids may move because of Brownian motion in the fluid. However, in colloidal random close packings colloids are static on a short timescale just like tennis balls in a box because translations of colloids are blocked by other colloids.

2.2.3. Structure

In the previous section different coordination numbers for particle contacts were presented. However, the number of contacts on a single particle alone is clearly not enough to describe the structure of a packing. To quantify the global density of a packing one usually employs the solid volume fraction ϕ, defined as the total volume of all particles divided by the total volume of the system:

$$\phi = \frac{NV_p}{V} = nV_p \tag{2.11}$$

where N is the number of particles and V_p the volume of a particle. V is the volume of the container and n is the number density. For a distribution of particle sizes a sum is taken over the number of different sizes of the particles

$$\phi = \sum n_i V_i \tag{2.12}$$

An alternative density measure often used in powder technology is the porosity which is defined as $1 - \phi$.

The volume fraction describes the global structure of a packing in terms of volume filled but it does not show how the volume is locally distributed over the available space. To quantify the structure of a set of particles, the probability of finding a particle at a distance r from another particle is calculated. The radial distribution function $g(r)$ is a probability function of finding a particle at a distance r away from another particle normalized by the mean particle density. The $g(r)$ is defined as

$$g(r) = n(r)/(\rho 4\pi r^2 \Delta r) \tag{2.13}$$

Here $n(r)$ is the number of particles in a shell of width Δr at distance r and ρ is the average particle number density. For every particle $g(r)$ can be calculated to obtain an average global $g(r)$, which can be normalized such that it decays to unity for large r.

The vectors connecting a central particle to its neighbours are called bonds and a bond order parameters is introduced to identify the structure of a packing [32]. The order parameter, usually a number between zero and one, is defined in such a way that it is one for the structure of interest and much less than one for other structures. To neighbour bonds polar angles θ,ϕ can be assigned that can be inserted into spherical harmonics. A bond order parameter Q is defined as

$$Q_{lm}(\theta, \phi) = Y_{lm}(\theta, \phi) \tag{2.14}$$

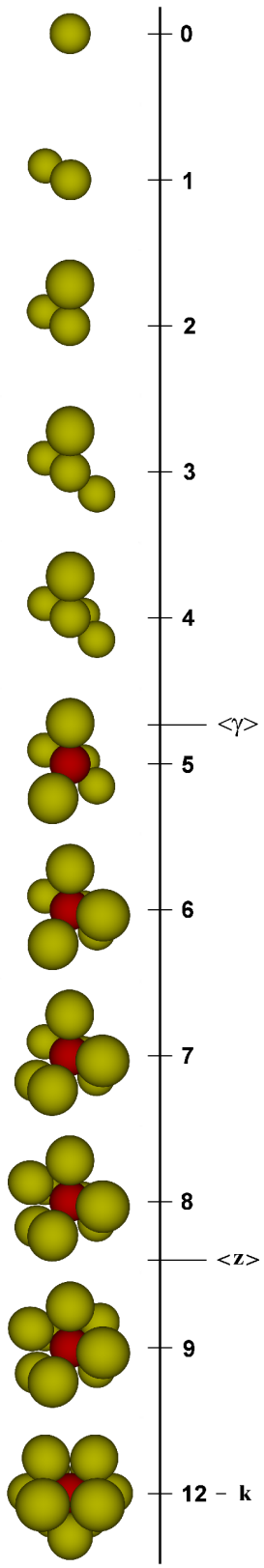

Figure 2.3: From top to bottom, neighbor spheres are added at random contact positions on a test sphere T, under the constraint of non-overlap. The average minimum of such neighbors that immobilise T is the caging number $\langle\gamma\rangle = 4.71$. The average maximum of randomly parked spheres is the parking number $\langle z\rangle = 8.7$. Further increase of the contact number requires reorganisation of contacting spheres, untill the kissing number $k = 12$ is reached.

To obtain a global orientational order parameter all Q's for all bonds in a sample are averaged:

$$\overline{Q}_{lm} = \langle Q_{lm}(\theta, \phi) \rangle \tag{2.15}$$

From the different global order parameters a rotationally invariant order parameter can be constructed as

$$Q_l = \left(\frac{4\pi}{2l+1} \sum_{m=-l}^{l} \left| \overline{Q}_{lm} \right|^2 \right)^{1/2} \tag{2.16}$$

For random packings and crystals Q_6 is often used to determine the order or disorder in a system [32].

2.2.4. Bertrands paradox

In statistics a uniform random distribution generates numbers that occur with equal probability. In this thesis the word 'random' occurs in many places related to particle packings. However, when a contact is created by two particles the non-overlap condition prevents certain contacts from occurring so not all contact positions are equally probable. Despite the non-overlap condition, it is nevertheless custom in the literature to refer to 'random' packings. In this thesis we will follow this custom, keeping in mind that we address actually 'disordered' packings in which local correlations are present. An exception is the random rod packing from Chapter 6, for which correlations vanish in the limit of thin rods.

Another illustrative concept of randomness is given by Bertrands paradox. Consider two circles with radii r_1 and r_2, where circle 1 is inside circle 2 and has half the radius of circle 2. A random chord is drawn that completely intersects circle 2 and the question is what is the probability p_{ic} that the chord intersects also with circle 1. Any chord (provided it does not hit the center) is uniquely determined by the location of its midpoint (Fig. 2.4a). Thus,

$$p_{ic} = \frac{A_{circle1}}{A_{circle2}} = \frac{1}{4} \tag{2.17}$$

From symmetry under rotation, we may assume the chord is vertical (Fig. 2.4b).

$$p_{ic} = \frac{2r_1}{2r_2} = \frac{1}{2} \tag{2.18}$$

Similarly we may assume by symmetry that one end of the chord is at the far left point of circle 2 (Fig. 2.4c). The chord is then defined by the angle θ and hits circle 1 if θ is in the interval $[-\pi/6, \pi/6]$ and

$$p_{ic} = \frac{2\pi/6}{\pi} = \frac{1}{3} \tag{2.19}$$

Thus, three different ways of describing the chord yield three different answers for the probability that a random chord intersects circle 1. Having described various important

parameters for random packings of particles we will now present a summary on the random packing of spheres.

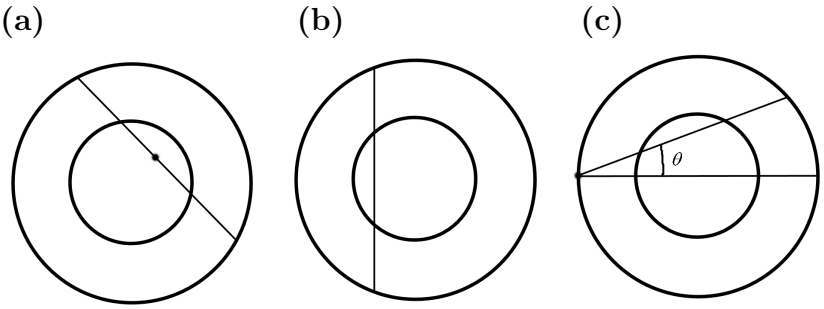

Figure 2.4: Illustration of Bertrands paradox, where the chord is described in three different ways.

2.3. Random packing of spheres

A random packing of spheres has been the archetypical model system for studying random packings of particles, witnessing the amount of literature on the topic [8,15–20]. The preference for spheres clearly is based on the symmetry a sphere possesses. Despite this fact there are still open questions related to packing of spheres and, moreover, it turns out that random thin rod packings [33–35] are more ideal random packings (see also Chapter 6) despite the fact that rods have more degrees of freedom.

This section first discusses experimental data on random sphere packing. Then theory for random packing of spheres is discussed and finally, a brief summary on computer simulations of random sphere packing is given.

2.3.1. Experiments

Experiments performed on macroscopic particle packings show a large similarity with respect to packing properties independently of the material used for the particles, which suggests that there is some well defined geometric mechanism behind random packing. In the next section an overview of various experiments for different types of particles is given.

Macroscopic packings

When spheres are quenched together at a rate faster than the time needed to achieve thermal equilibrium, a random packing is formed that is stable under gravity. Tapping container walls will slightly increase the volume fraction of the random packing. Whatever tapping method is chosen the maximum volume fraction obtained after packing will always be around 0.64 for equal sized spheres. This maximum volume fraction does not depend on the size of spheres but it does depend on the size distribution and deviations from spherical shape. Bernal was one of the first who found that the maximum volume

fraction is around 0.64 and also determined the average number of contacts to be 6.4 for the densest packing [36]. Later Scott and Kilgour repeated the experiments and also found a volume fraction around 0.64 [37,38]. They used small steel balls covered with a thin protective oil coating in a cylinder. The volume fraction depended on the method of shaking, pouring and tapping. Two limits were found, which were called 'random close packing' with $\phi = 0.6366 \pm 0.0005$ and 'random loose packing' with $\phi = 0.60$. Mason [39] calculated the radial distribution function $g(r)$ for Scott's packing using a correction factor to account for incomplete shells near the edge of a packing and found a contact number of about 5. There were nearly 7 neighbours within a distance of 1.02 diameter [39].

In the field of powders and granular matter also a volume fraction of roughly 0.64 was found for spheres [40,41]. Knight et al. [40] reported measurements on the density of a vibrated granular material as a function of time. The material studied consists of monodisperse glass spheres confined to a cylindrical tube. Through vibration of the tube the volume fraction increased from 0.57 to around 0.62. In the follow up experiments performed by Nowak et al. the volume fraction increased to roughly 0.63 with spikes up to 0.64 [41]. Vibration of a tube and thus varying density continuously is equivalent to sampling the possible volume space configurations as defined in the work of Edwards [42] by overcoming geometrical barriers present in the packing.

Using X-ray micro-tomography Seidler et al. determined the real-space structure of a granular bed of relatively monodisperse glass spheres [43]. The spheres were 63 μm $\pm$ 5 μm in size. The volume fraction found was 0.61. The number of contacts was on average 8.3. Aste et al. performed extensive studies on more than 100.000 spheres and found disordered packings with volume fractions from 0.58 to 0.64 [44].

Onoda and Liniger [45] investigated the lowest possible volume fraction for a stable random packing of particles, the random loose packing (RLP). The lowest volume fraction found for a mechanical stable configuration (random loose packing) was $\phi_{rlp} = 0.55$. A mechanical stable configuration means in this case that a packing of spheres is in a static equilibrium under an existing set of externally applied forces in the limit of gravity going to zero.

Colloidal packings

Spherical colloids are widely used as a model system for collections of spheres. For example fluorescent colloids with a radius of 525 nm and a polydispersity of 1.8% were used to determine the real-space structure of a glass. The volume fractions found were between 0.60 and 0.64 [46]. Philipse and Pathmamanoharan [47] studied liquid permeation and sedimentation of dense colloidal hard sphere packings and found randomly dense packed systems of colloidal silica spheres with an average volume fraction of 0.648 $\pm$ 0.032. All these results for macroscopic and colloidal packings clearly illustrate the size-independence of the random packing density.

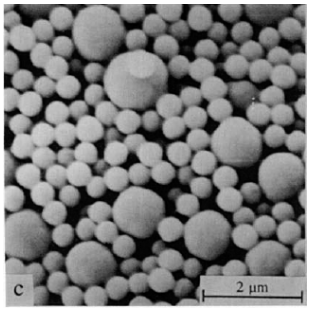

Figure 2.5: SEM picture of a bidisperse mixture of colloidal silica spheres with size ratio 2.6 [50].

2.3.2. Bidisperse and polydisperse systems

Colloidal packings

Bidisperse sphere systems consist of two types of spheres with a different radius and polydisperse systems consist of spheres with a distribution of sphere sizes. Eckert and Bartsch found that polydispersity increases the critical volume fraction ϕ_g for the glass transition [48]. The maximum volume fraction for random close packing ϕ_{rcp} of 0.64 for monodisperse spheres is also increased by polydispersity. The system under study was a binary mixture of polystyrene micronetwork spheres with radii of 150 nm and 185 nm. The polydispersity was about 12%, sufficient to completely suppress crystallization. The increase in volume fraction found can be explained by realizing that smaller spheres can fill gaps created by the bigger spheres.

The effect of particle size distribution on crystallisation and the glass transition of hard sphere colloids has been studied by Henderson et al. [49]. There were two distributions of particle sizes, one was a narrow and roughly symmetrical and the other was a broader distribution and more skewed towards smaller particles. Both systems showed a glass transition at approximately the same ϕ_g of 0.58. Interestingly, it was found that crystallization rates are significantly slower for the polydisperse case than for the monodisperse case.

Thies-Weesie and Philipse [50] studied liquid permeation of bidisperse colloidal hard sphere packings with size ratio 2.6 and measured the volume fraction as a function of volume occupied by the small particles (see Fig. 2.5).

Macroscopic packings

McGeary performed an experimental study on binary, ternary and quaternary packing of steel spheres [51]. For monodisperse spheres a volume fraction of 0.625 was found. For binary sphere packings it was found that a smaller diameter of small spheres yielded a higher volume fraction. For larger big spheres the maximum volume fraction occurs at a lower percentage of big spheres. The percentage remains above 60% for the big spheres (see Fig. 2.6).

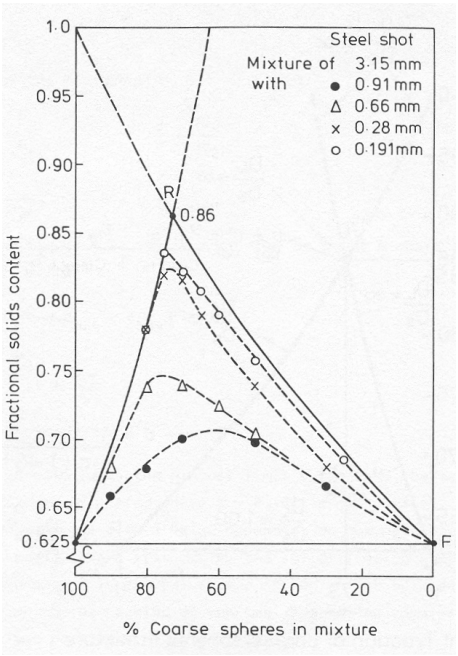

Figure 2.6: Volume fraction of random bidisperse packings as a function of the fraction of large particles [51].

Ternary and quaternary packings show the same behaviour as binary packings. The rate at which the maximum density was reached slows down because the number of particles increases. It can be seen as two types of filters where the third type must go through other particles to fill up the voids. It was found that there should be at least a sevenfold difference in sphere diameter of various components to produce efficient packing. The maximum volume fraction is 0.951 for a quaternary packing of spheres with diameter ratios 1:7:38:316.

2.4. Theory

There are several theories describing properties of random packings. However, most of these theories use approximations or use empirical data as it is very difficult to include all collective effects that play a role in random packing. In the next paragraphs some proposed models for random packing will be discussed. The aim is to illustrate possible approaches, without pretending to be exhaustive.

2.4.1. Predicting random packing properties

Predicting properties of random sphere packing is not easy because of the disorder in positions of spheres and the requirement that particles cannot overlap each other. For random close packings the volume fraction of 0.64 is a reproducible quantity in experiments. This leads to the believe that it can be possible to describe such a random

packing mathematically. Bernal stated in 1937 the importance of statistical geometry for random packings [11].

Finney started describing the geometry of random close packing with the Voronoi polyhedron [52]. A packing of spheres can be described by the coordinates of the sphere centers. The Voronoi polyhedron for one sphere center consists of points that are closer to this center than to other sphere centers. This defines a volume that can be described with a polyhedron. Packing of spheres can now be described in terms of these polyhedra. Distribution of the types of polyhedra were calculated for the Bernal sphere packing.

Gotoh and Finney [53] deduced an overall packing density by relating it to the most probable Voronoi polyhedron. The average contact number was postulated to be six. Finney then postulated that this average polyhedron is a characteristic for the packing, and thus gives the bulk packing density. By changing a parameter in the model the volume fraction can change from 0.6099 to 0.6472 with a mathematical mean of 0.6357.

Bordia developed a way for calculating surface coverage for disks and volume fraction for spheres by looking at two extremes [54]. One packing consists of spheres stacked on top of each other and the other packing is the well-known hexagonal close packing. The value for random dense packing must lie between these two extremes. This value is found by integrating over all possible volume fractions for every packing between these two extremes.

$$\langle\phi\rangle = \int_{\frac{\pi}{3}}^{\frac{\pi}{2}} \phi(\alpha) f(\alpha) d\alpha \tag{2.20}$$

where α is an angle that describes the packing and $f(a)$ is a distribution function that describes the probability for this packing to occur.

$$\int_{\frac{\pi}{3}}^{\frac{\pi}{2}} f(\alpha) d\alpha = 1 \tag{2.21}$$

The surface coverage found was 0.8239 and the volume fraction 0.6369.

Berryman used an approach based on nearest neighbour radius and the radial distribution function for spheres and disks [55]. This radial distribution function is taken from a computer simulation. The surface coverage found for disks was $\phi_{rcp} = 0.82$ and for spheres $\phi_{rcp} = 0.642$.

Liu and Davies derived a relation between the coordination number and the volume fraction of a random packing by starting with a general equation for the particle number distribution function [56]. From this distribution function the number of particles within a radius R were calculated. This was then used to find the coordination number. Two constants are chosen, one in analogy with a free damping vibration equation and the other from experiments of Scott [37]. For $\phi = 0.64$ the coordination number found is 9.11. Liu and Davies [56] claim that the highest random close packing density is 0.687 with a coordination number of 10.26.

Edwards and Mounfield [57] described a configurational statistical mechanical theory for random packing of grains. The crucial point to note is that it is the distribution of grains over the available volume states (subject to external constraints such as stability under gravity and that grains are impenetrable) which gives rise to a volume of configurations. The authors' formal analogy then is to replace energy E by volume V. A granular equivalent of the Hamiltonian H is required namely W, which specifies a volume state of a system in term of constituent grains i.e. $E = W(q)$ and will be referred to as the volume function. The q is taken to mean a particular granular property over which the average of the volume function is performed.

Torquato et al. [58] define a concept called 'jamming' into the field of random packing, which yields a mathematically better defined description of random close packing. An order parameter is introduced and the maximum random jammed state is then the state with maximum volume fraction that minimizes the order parameter. This is similar in spirit to a definition coined by Roux [59, 60] that the upper limit in volume fraction is given by the maximum volume fraction where there are no crystal nuclei. In both cases the volume fraction is well defined. There are a number of jamming types, namely: locally, collectively and strictly jammed configurations [30, 31, 58]. In a locally jammed configuration each particle cannot translate while fixing the positions of the other particles. In a collectively jammed configuration each subset of particles cannot translate due to the presence of the other neighbors and in a strictly jammed configuration all globally non-uniform volume-decreasing deformations of the system boundary are not allowed. Donev et al. used linear programming to calculate jamming and unjamming motions for packings [30].

Jamming is similar to the caging concept that is used to understand properties of glasses, where particles can rattle in a cage. A static concept of caging for 2-d spheres or disks was first introduced by Williams [61] and later further developed by Uhler and Schilling [62]. Bideau et al. showed that for a configuration with no order, the maximum number of neighbour disks needed to cage a disk is 4 [63]. The configuration of disks were treated as an n-sided polygon. The Euler-Poincaré theorem was then used to show that there would be correlations between the angles in the n-sided polygon when the number of disks was larger than 4. The Euler-Poincaré theorem states that in any convex, three dimensional polyhedron

$$V - E + F = 2 \tag{2.22}$$

where V is the number of vertices, E is the number of edges and F is the number of faces. The topological relations used to derive a constraint for the maximum cage size were also used by Bideau et al. [64] to obtain an expression for the surface coverage

$$\phi = \frac{\pi^2}{12}\left[1 + \frac{4 - C}{2}\left(1 - \frac{\pi\sqrt{3}}{6}\right)\right]^{-1} \tag{2.23}$$

where C is the number of contacts per disk. For $C = 4$ this gives $\phi = 0.822$ and for $C = 3$ this gives $\phi = 0.786$.

Peters et al. [28] derive a relation for the caging of d-dimensional spheres by point contacts and present numerical results for the caging of 3-dimensional spheres by equal sized spheres that are not allowed to overlap. In chapter 3 we present our work on the caging number for disks and spheres that are not of equal size. In the next paragraph we review studies on bidisperse packings.

2.4.2. Bidisperse and polydisperse systems

For systems with a distribution in sizes the general idea is that the volume fraction changes because of two opposing effects. Small spheres can fill in voids created by bigger spheres. The other effect is that small spheres push bigger spheres apart. Adding a large sphere to a packing of small spheres will remove voids from where the small spheres were and replaces the voids with solid volume from a big sphere and thereby increasing the volume fraction.

Mounfield and Edwards described polydisperse systems of hard spheres in the same way as for monodisperse spheres but in this case the technique does not work correctly for the dense packed case [42]. The authors were able to show that a packing of polydisperse spheres is more dense than a packing of monodisperse spheres. A packing of near monodisperse spheres obtained by perturbing monodisperse spheres was on average less dense than a packing of monodisperse spheres. On the other hand, when local correlations in the granular configurations were taken into account it was shown that in the case of densely packed spheres this is not necessarily true. The volume fraction depends on the interactions between granules.

Aste studied geometrical and topological rules underlying dispositions and size distribution of non-overlapping, polydisperse circle-packings [65]. The size distribution that densely covers a plane follows a power law. The results for circles were extended to packings of spheres and hyper-spheres of dimension d. From a topological point of view the densest packing of circles is a packing where all spheres are in contact with their neighbours.

Dodds developed a simple statistical geometric method for calculating volume fraction and contact points for multi component random sphere packings [66]. The main assumption is that each sphere touches its neighbours. This is not totally correct since a sphere slightly away is still a neighbour but it is not in contact. Therefore there are no gaps in the packing and the space is divided up into tetrahedral subunits. The model is valid for size ratios from 1 to 6.46.

In a packing with n differently sized spheres the number of different tetrahedral configurations can be calculated. A binary packing consists of five different tetrahedra,

the structure can be described when the relative numbers for these tetrahedral configurations are known. The tetrahedron frequency distribution depends on sphere size distribution and the relative numbers of different sphere sizes making up a packing. Each tetrahedron has a specific volume fraction. The overall volume fraction is then given by sum of volume fractions of the specific tetrahedral weighted by the frequency distribution. The average number of contacts can also be calculated from the frequency distribution of tetrahedra.

Brouwers developed a model for the geometric random packing and void fraction of polydisperse particles and demonstrated that the bimodal packing can be transformed into a continuous particle-size distribution of the power law type. Furthermore, an expression is derived that predicts the packing fraction of the polydisperse power law packing as a function of distribution exponent, size width, mode of packing and particle shape [67].

2.5. Simulations

Deriving analytical results is very difficult for systems containing more than three particles. With the aid of statistical mechanics one can calculate global properties of a system of particles but when systems get more complex it requires many complicated steps to get an exact analytical result. It is often possible to calculate expressions numerically and with the advance in computing power there are more and more possibilities to simulate complex systems.

One can simulate a complex system by creating possible states of the system (Monte Carlo) or by calculating the forces that each particle experiences and then integrating these forces to obtain new particle positions. In this way a single system is simulated (Molecular dynamics) [68–70]. A short description of general techniques in computer simulations will be given and then an overview of techniques specifically for generation of random packings is presented.

2.5.1. Computer Simulations

In a classical Monte Carlo calculation a system of N particles is created. These particles interact through a potential. A sequence of particle configurations is then generated by successive random displacements of particles. A newly generated configuration of particles is either accepted or rejected. The probability of accepting a configuration of particles is done such that accepted particle configurations sample asymptotically configuration space according to an equilibrium probability density to a chosen ensemble. Newly generated states with a lower energy have a higher probability of being accepted according to the Boltzmann distribution.

In the molecular dynamics method one sample of a microcanonical ensemble is followed in time. For a system of N particles the forces and torques that each particle

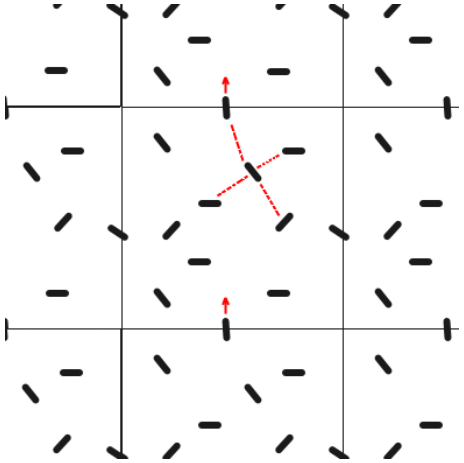

Figure 2.7: Example of a tiled periodic cubic cell. Dotted lines show the neighbours of the central particle. The two arrows show the periodic boundary conditions.

experiences are calculated and then used to solve the Newton-Euler equations of motion. The solutions to the equations of motion are sampling the phase space along a surface of constant energy.

Molecular dynamics (MD) is suitable for the study of time-dependent phenomena. The Monte Carlo method is often used when studying rare events, where it will take to long to follow a system in time with MD until the rare event occurs. The number of particles is a difficulty for both methods. Most experimental systems consist of more than 10^6 particles and the computational time for these systems is too large with computer power that is available at the time of writing but already simulations have been performed on simple systems with these numbers and current developments of computing with a GPU instead of a CPU show promising prospects.

With a small number of particles volume effects can have a significant impact and to reduce these volume effects periodic boundary conditions are used. One example is a periodic cubic cell (see Fig. 2.7). For a single cell the relevant quantities are calculated and the cell is then tiled periodically across space. Calculation of particle interactions in the central cell then takes into account the particles in neighboring tiled cells.

2.5.2. Various algorithms on random packing generation

Most algorithms for constructing random packings fall in one of two categories, namely sequential methods and concurrent methods.

Random sequential addition algorithms

A system has a small seed of fixed particles as a starting configuration. Then in a number of steps particles are added according to a placement rule.

Adding disks randomly to a substrate in such a way that disks are not allowed to overlap results in a surface coverage of 0.5472 [71] and for spheres a volume fraction

of 0.385 [72]. A major disadvantage of this method is that as the number of spheres increases it becomes increasingly hard to add additional spheres. Furthermore the volume fraction is too low for spheres to be jammed.

Bennet developed a mathematically well-defined method for preparing hard-sphere packings on a computer [73]. A suitable seed cluster is generated on which then additional spheres are placed one at a time. The next sphere is placed in hard contact with three spheres below. After placement spheres are static. Volume fractions between 0.60 and 0.63 were found. The average number of contacts was 6.0. The requirement of 3 spheres below the newly placed sphere leads to 3 spheres above this sphere. Adams and Matheson re-invented Bennet's method and found a volume fraction of 0.627 [74].

Hinrichsen et al. used a random sequential addition (RSA) algorithm in combination with a growth method to generate a packing of 2-d disks in a plane [75]. In the next step the plane is divided according to Voronoi-Dirichlet (VD) division of space. Then each disk in its VD polygon is moved to the center of the largest inscribed circle in the VD polygon. The disks are increased until the first two disks are in contact. This proces is repeated until no disks can be increased any more. This iteration process is equaluivalent to an uniform contraction of the surface where the particles have a weak repulsive force in addition to hard-core repulsion. The volume fraction found was 0.772 and the coordination number 3, implying that the obtained volume fraction should be close to the volume fraction of an RLP configuration.

Concurrent methods

With concurrent methods the entire set of particles is present from the start of the simulation. Four categories can be identified: Molecular dynamics, Overlap elimination, Energy minimization and Contact network based, where the naming has been adopted from Donev's thesis "Jammed packings of hard particles" [76].

In molecular dynamics simulations either hard or soft particles are used to produce a packing by either increasing the density or by using dissipative dynamics in a gravitational field. One way to increase the density is by particle growth mechanisms where the size of particles increases until a critical condition is reached. Lubachevsky et al. performed simulations for disks and spheres using a growth mechanism [77]. The basics of the method are the following. N points are placed randomly with uniform distribution in a cell with periodic boundary conditions. These points have a velocity. As time increases these particles grow at a common rate. The diameter of a d-dimensional sphere $a(t)$ increases monotonically and continuously with time. As particles grow the available free space to move becomes less and thus particles will collide more often with each other. When the rate of collisions diverges, the system becomes jammed.

The collision dynamics for expanding particles is non-conservative. The outgoing velocity components along the line of centers receive an extra velocity increase. Therefore

Table 2.1: Surface coverage as a function of growth rate a_0 for disk packings [77].

a_0	10^{-3}	3.2	10^2
ϕ	0.895	0.883	0.852

kinetic energy in the system increases discontinuously at each collision. For disk packings the resulting surface coverage depended on the constant growth rate a_0 (see Table 2.1). The most frequent number of contacts is 6. For 3-d spheres the procedure has been repeated with a diameter growth rate $a_0 = 1.0$, which yielded $\phi = 0.637$ [77]. The main difference between the 2-d and 3-d case is the ordering of spheres. While in the 2-d case most disks have 6 contacts and thus are in a hexagonal lattice, in the 3-d case the spheres are positioned random and the $g(r)$ goes to unity after two diameters. In a hexagonal close packing the number of contacts is 12. This number was not observed in the simulation. The maximum contact number was 10 and $\langle C \rangle = 5.83$.

In 1-d particles pack in a long range order, while in 2-d the packing diversity increases but the packing is still well ordered; in 3-d order has disappeared. Another interesting result of the packings is that there are rattlers present. Rattlers are particles that are not jammed and can move in a cage of surrounding tightly packed particles.

Silbert et al. performed molecular dynamics simulations on model systems of monodisperse spheres under influence of gravity [78]. A system is spatially periodic in the xy plane, with a unit cell of $40r$ x $40r$, and is bounded in the z direction by a rough bed at the bottom and an open top. A starting configuration consisted of randomly positioned non-overlapping spheres, with packing fractions in the range $0.02 < \phi < 0.3$. The system settles under gravity on a rough bed. This method of construction mimics the pouring of granular materials through a sieve to an area far away from sidewalls, without forming a conical heap. The amount of friction particles experienced was varied. For zero friction the average number of contacts per particle was 6.144 and the volume fraction 0.64. For particles with friction the number of contacts and the volume decreased, such packings gave for example, $\langle C \rangle = 4.69$ with $\phi = 0.594$ and $\langle C \rangle = 4.9$ with $\phi = 0.61$. Changing the coefficient of restitution ϵ would not change the static packing. It only affects the relaxation dynamics by increasing the removal rate of kinetic energy. For very large quench rates a system might be expected to stop immediately upon forming the minimum number of contacts necessary to achieve static mechanical equilibrium. Starting with a more dilute state leads to a more compact final state.

Frictionless packings achieve the same structure regardless of construction history and restitution coefficient, frictional packings achieve a multitude of structures that depend on system parameters and construction history [78].

Table 2.2: Volume fraction for randomly close packed spheres as a function of polydispersity [79]

σ	0.00	0.02	0.05	0.075	0.10	0.15	0.20	0.25	0.30	0.35	0.40
ϕ_{rcp}	0.64	0.65	0.66	0.66	0.67	0.68	0.68	0.69	0.71	0.74	0.78

Schaertl and Sillescu created 3-d random packings of spheres with various polydispersity [79]. The starting configuration consisted of 729 particles and periodic boundary conditions. The following steps were taken:

1. Each particle is moved by a distance $(2D_0\tau)^{\frac{1}{2}}$ in one of the randomly chosen directions along each Cartesian axis, where D_0 is the diffusion coefficient of the system without interactions as given by the Stokes-Einstein equation.
2. Any particle overlap detected after the move is corrected by pairwise shifting of the overlapping particles up to their touching distance.
3. The radius of the particle is then increased by a factor of 1.005, which leads to an effective increase of the volume fraction by a factor of 1.015.

This procedure is repeated until the number of touching (and overlapping) particles exceeds 723. The results are given in Table 2.2.

Makse et al. performed simulations on packings of compressible granular materials [80]. Granules interact via normal forces only. Granules slide and rotate freely mimicking rearrangements of grains during shaking in experiments [52, 81]. The found volume fraction of 0.634 is close to ϕ_{rcp}. A discrete element method was used for a system of deformable elastic grains interacting via normal and tangential Hertz-Mindlin forces plus viscous dissipative forces [82, 83]. The following relation was found for the mean coordination number as a function of ϕ

$$\langle C\rangle - C_{min} \propto (\phi - \phi_{critical})^{\theta} \tag{2.24}$$

where C_{min} is the minimum coordination number and $\theta = 0.295$ is a critical exponent. The maximum packing density decreases as surface roughness (friction) of particles increases. For spheres with friction C_{min} approaches 4 (the lowest value found was around 4.5) and without friction goes to 6. No experimental study for RLP has been reported yet to confirm $C_{min} = 4$.

In overlap elimination methods one constructs a dense packing by allowing the particles to overlap during a step but at the end of the step all overlap is eliminated and the simulation is terminated when it is not possible to remove the overlap anymore. He et al. performed a Monte Carlo simulation model for the random packing of unequal spherical particles [84]. A dense packing with overlapping particles is generated. Then overlapping particles are repositioned until a given tolerance and the final packing is achieved. Spheres that have no contacts are moved in contact with their nearest

neighbour. A particle i overlapping with a particle j is repositioned according to,

$$\vec{R}_{ij} = \vec{R}_j + (\vec{R}_i - \vec{R}_j)\frac{r_i + r_j}{|\vec{R}_i - \vec{R}_j)|} \tag{2.25}$$

where r_i is the radius of sphere i and i is re-positioned according to

$$\vec{R}_i = \frac{\sum_{j=1}^{n} \vec{R}_{ij}}{n} \tag{2.26}$$

The resulting $\phi = 0.627$ for equal sized spheres. Furthermore, random sphere packings were created according to a log-normal distribution such that the probability density function of particle radius r is given by

$$f(r) = \frac{1}{\sqrt{2\pi}\sigma r} e^{-(\ln r - \ln \langle r \rangle)^2 / 2\sigma^2} \tag{2.27}$$

where r is the average radius and σ is the polydispersity. The volume fraction depends little on the polydispersity σ for $\sigma < 0.15$. As σ increases the volume fraction increases but the mean coordination number decreases.

2.5.3. Mechanical contraction method for spheres

Williams and Philipse [35] developed a general algorithm for creating random closed packed packings for various particle shapes. Here the specific case of spheres is used to describe the algorithm. In section §2.10.1 and chapter 5 this will be expanded to general convex shapes such as spherocylinders, spheroids and cut spheres. A random packing is formed by quenching the system at a rapid rate in order to force particles in permanent positions before particles get into a thermodynamically more favored phase.

The initial conditions are a cubic cell with periodic boundary conditions in which a dilute equilibrium fluid is created using standard Monte Carlo techniques. Then the following steps are repeated until a termination condition is reached.

1. The volume of the cubic cell is reduced by a small amount ΔV and particle positions are scaled by a factor s. A particle at a corner of the cubic cell will be at the corner of the scaled cubic cell. Thus $sb = b'$, the new volume $V' = V - \Delta V = (sb)^3$ where b is the length of the cubic cell. From this the scaling factor s can be easily calculated.

2. The scaling of particle positions leads to a possibility of particles overlapping. Overlapping particles are then moved outside each other in a number of iterations. The direction to remove overlapping particles can be found by the amount of overlap δ between particles, which is for two spheres $\delta = d - |\vec{k}|$ where $d = r_1 + r_2$ and $\vec{k} = \vec{x}_2 - \vec{x}_1$ where x_i are particle positions and r_i are the radii of respective spheres. The speed at which a particle i changes overlap with a fixed particle j is then given by:

$$\frac{\partial k_j}{\partial t} = k_j^{(1)} a_1 + k_j^{(2)} a_2 + k_j^{(3)} a_3 \tag{2.28}$$

where the a_n's represent the velocity of a particle i. The change in overlap between i and j and thus the change in $\vec{k}$, since d is a constant, is maximum in the direction of $\vec{k}_j$. A particle i is surrounded by C particles, the change in overlap with particle j can then be expressed as the product of the velocity a_n with the direction k_j^n. The sum over all overlapping particles represents a speed s at which the total overlap is changing.

$$s = \sum_{j=1}^{C} \delta_j \frac{\partial k}{\partial t} \tag{2.29}$$

where the factor δ_j is introduced in order to remove particles that overlap the most in an efficient way. The speed s is only determined by overlapping particles. If particle i is moved in the direction where the overlap is reduced the fastest the particle can overlap with other 'new' particles. Therefore a particle is moved half the distance to remove overlap with the first particle. Since the distance to move is already fixed by this criterion the direction to move a particle in a single step needs to be calculated. Therefore a kinetic energy-type constraint is introduced on the velocity of particle i,

$$a_1^2 + a_2^2 + a_3^2 = 1 \tag{2.30}$$

The method of Lagrange multipliers is then used [85] to find the direction of the velocity.

$$a_n = \sum_{j=1}^{C} \delta_j \frac{k_j^n}{k_j} \tag{2.31}$$

Now that direction and distance are known to move a single particle, we can repeat the calculation for all particles and update their positions at the same time. This process is repeated for a large number of steps. If at the end all particles are not overlapping the volume is contracted as in step 1. If there are still particles overlapping the system has reached the most dense state and the volume fraction is determined from the previous non-overlap state. The volume fraction found for a random sphere packing using this method is $\phi = 0.631$ and the number of contacts per particle is about 6. In chapter 5 the mechanical contraction method will be extended to handle general convex shapes.

2.6. Summary and conclusions for sphere packings

From experiments performed on random packings it can be concluded that there is indeed a value that represents a maximum random dense packing volume fraction ϕ_{rcp} and that this value is around 0.64. The average number of contacts a particle experiences in a random dense packing is not known very precisely. Values reported are 5, 6.4 and 8.3. Unfortunately, no contact number is mentioned in the real-space study of a colloidal glass [46]. Introducing polydispersity in the particle sizes increases ϕ_{rcp}.

To predict the value for ϕ_{rcp} several theoretical methods are employed. One method is to look at the most probable Voronoi polyhedron and assume that the number of contacts is 6.0, the ϕ_{rcp} found then is 0.6357. Another method is to average over all

possible packing fractions between two extremes. This method evades the need for a contact number but the method has a varying contact number built in through a variable angle, which yielded $\phi_{rcp} = 0.6369$. Berryman's approach [55] used calculated radial distribution functions that contain errors, therefore it gives only an estimate of ϕ_{rcp}. A method that does take into account the number of contacts through the definition of an average cage predicts roughly the correct value for 2-d disks but finds in 3-d a value close to the random loose packing density $\phi_{rcp} = 0.60$.

An alternative definition of a maximum random jammed state has been proposed to replace the random close packing. This definition leads to a mathematically well-defined state through an order parameter but it is still unclear which order parameter is well suited for random close packing.

Computer simulations confirm found experimental values. For random sequential addition methods the average number of contacts equals 6.0 but the found volume fractions are too low compared with ϕ_{rcp} from experiments. Concurrent methods can give volume fractions that match with experiments but a variety of contact numbers, 4.5, 5.83 and 6.14 is found.

All experimental and theoretical studies so far confirm the existence of a ϕ_{rcp} which lies around 0.64. There seems to be no conclusive evidence for one unique value for ϕ_{rcp}; it rather seems to present a narrow window of volume fractions with some average value depending on the choosen method. The average contact number in a random packing varies for the different methods presented here and this variation is significantly larger than the variation found in ϕ_{rcp}. One possible method to predict a more accurate ϕ_{rcp} is to find a relation between the average number of contacts and volume fraction in a random packing. So far one theoretical relation has been found [29] but this is based on a relation for overlapping spheres where the number of contacts for non-overlapping spheres is used.

Little work has been done on the random loose sphere packing volume fraction ϕ_{rlp}, the value of which is rather uncertain. In the absence of gravity it is 0.55 obtained from the study by Onoda and Liniger [45] and in other experiments that include gravity ϕ_{rlp} is around 0.60. From experiments and simulations it is clear that this value depends on friction between particles: more friction leads to a lower ϕ_{rlp}. This dependence on friction suggests that mechanical stability is an important feature for an experimental random loose packing. It also suggests that ϕ_{rlp} has a much wider range of possible values than ϕ_{rdp}, the latter depending only on sphere shape and not on friction.

2.7. Non-spherical particles

In granular matter and colloidal dispersions most particles are not identical spheres. For example, sandstones are formed from particles with a variety of shapes and sizes. Since sandstones are important reservoirs for oil, water and natural gas, the porosity of

these packings is of great economical importance. It is important for fundamental and economic reasons to describe the structure of non-spherical particle packings.

Packings of non-spherical particles are in several aspects similar to packings of spheres. The particles form random structures where the particles are in contact and show no long-range correlation. As is the case with spheres a random loose packing and a random dense packing can be defined. However, the structure of these packings can vary significantly from the structure of sphere packings. It is also more difficult to describe these packings because the orientation of particles plays an important role. It turns out that the random thin-rod packing is an exception to this.

The structure for the literature overview on non-spherical particle packings is the same as was for the spheres section. First experiments are presented, then theory available on packing of non-spherical particles is outlined and finally, computer simulations on the subject are presented.

2.7.1. Experiments

Much less experiments have been performed on random packing of non-spherical particles than for packings of spheres. For sphere packings only the position of the center and the radius of a sphere is relevant. For non-spherical particles the orientation is also important and the additional length scales require more than one parameter. These extra parameters make the analysis of packings of non-spherical particles more difficult than their spherical counterpart. In the next paragraph an overview of experiments on packing of non-spherical particles is given. Random packings can be formed with macroscopic as well as colloidal non-spherical particles with a variety of materials and shapes.

Macroscopic packings

Villaruel et al. performed compaction experiments on nylon rods of 1.8 mm diameter and 7.0 mm length [86]. The initial volume fraction was 0.49 and after tapping for a short time the volume fraction went up to 0.55. This increase is caused by void relaxation. Particles are oriented dominantly horizontally. The authors compare the reorientation with a nematic glass state as seen in computer simulations. The volume fraction decreased a little and then jumped up to a value between 0.64 and 0.72 depending on tapping intensity.

For different container sizes Zou et al. have shown that porosity increases near the wall for cylindrical containers [87]. Larger containers yield a lower porosity. Higher length to diameter ratios give a higher porosity and as the aspect ratio increases the difference between random loose packed and random close packed becomes smaller. In the experiment wooden rods with aspect ratios from 1 to 64 were used.

Yu and co-workers [88–90] investigated packing of non-spherical particles, including binary, ternary and quaternary mixtures. A mixture of wooden rods with glass spheres

size segregated due to a difference in particle density. No segregation occurred between metal cylinders (disks) mixed with glass spheres though there was also a large difference in particle density. Using a sphericity parameter together with an empirical model developed for spherical particles the porosity of binary mixtures of non-spherical particles can be predicted. This method is also applicable to multi-component systems. A study was performed on how porosity changes as a function of sphericity. The main results are that as sphericity goes to zero porosity approaches one. For random loose packing the initial porosity increased while for random close packing porosity decreases to a minimum and then increases again as sphericity goes to zero. This could be attributed to ordered packing caused by tapping and vibration of a system.

The presented results clearly indicate that there is no one-to-one relationship between porosity and sphericity [91]. Results for packings with a log-normal or a power law size distribution show that packing of cylindrical particles is heavily dependent on this distribution and the dependence cannot be predicted by direct analogy as for packing of spheres. For packings with a wide length distribution the shape effect is dominant over the size effect [92].

Nardin et al. investigated the relation between volume fraction and aspect ratio for random packing of particles with axial symmetry [93] and found that for large aspect ratio the inverse volume fraction varies linearly with aspect ratio. For the other limit, as aspect ratio goes to zero the volume fraction becomes a constant value.

Rahli et al. [94] performed an experimental study in which they made a comparison with the work of Nardin et al. [93] and Milewski [95] and found good agreement between the different experiments. The variation of volume fraction has been investigated as a function of aspect ratio for nylon, bronze and copper rods. Milewski used glass and wood rods and Nardin used steel rods. The same stacking method was performed and the volume fraction depended only on the aspect ratio. An approximate volume fraction from the experimental results [94] was proposed as

$$\phi = \frac{m}{V_{excl}/V_{particle}} \tag{2.32}$$

where m is a quantity that takes into account the number of rods included in the excluded volume V_{excl} and $V_{particle}$ is the volume of a particle. Fitting the experimental data gives a value close to 11 for m.

Blouwolff and Fraden [96] studied random packings of cylinders and found a similar relation as Nardin et al. and Milewski for wooden rods. For high aspect ratios the contact number approached 10. This study confirmed the random contact equation discussed in the next section.

Man et al. [97] investigated random dense packing of ellipsoids with various aspect ratios. Experiments were done with two types of candy. Type 1 was an oblate spheroid with principal axes $2a = 1.34 \pm 0.02$ cm and $2b = 0.693 \pm 0.018$ cm. Type 2 was an

oblate spheroid with principal axes $2a = 0.925 \pm 0.011$ cm and $2b = 0.493 \pm 0.018$ cm. A square box, 8.8 cm x 8.8 cm, was filled to a height of 2.5 cm while shaking and tapping the container. Measurements were performed by adding 9.0 cm to the height and excluding the contribution of the possibly ordered bottom. The volume fractions found were $\phi = 0.665 \pm 0.01$ for type 1 and $\phi = 0.695 \pm 0.01$ for type 2. The experiment was repeated with round flasks of 0.5-, 1- and 5-liters. The volume fractions found were $\phi = 0.685 \pm 0.01$ for both type 1 and 2. The average contact number was 9.82. The absence of order was measured with a two-dimensional nematic order parameter S_2,

$$S_2 = \langle 2\cos^2\theta - 1 \rangle \tag{2.33}$$

where θ is the angle between the axis of symmetry and a director axis. S_2 was around 0.05 which is consistent with absence of orientational order, $S_2 \approx 0$.

Colloidal packings

Philipse et al. [98] studied sediments of colloidal silica rods which form low density isotropic networks. In a study of isotropic-nematic phase separation for colloidal Boehmite rods with an aspect ratio of about 20, the volume fraction found by Buining et al. [99] was 0.25. Zou et al. [88] found for wooden rods with aspect ratio 22.42 a loose packing volume fraction of 0.268. Despite a large size difference, the volume fractions are roughly the same implicating that the geometry of the particles has a large effect on the packing. Sacanna et al. [22] measured the random packing density of colloidal silica ellipsoids with well-defined shape, gradually deviating from the sphere-shape up to prolates with aspect ratios of about five and reported the first experimental observation of a density maximum for a colloidal system at aspect ratio around 1.6.

2.8. Theory

Most of the theoretical work done on non-spherical particle packings is based on monodisperse particles. The introduction of 3 extra variables for the orientation of particles makes the description already difficult enough. Examples of non-spherical particles that can be relatively easily described mathematically are ellipsoids, cylinders and rods also known as capsules. In the first part of this theoretical overview various models for non-spherical particles are presented. In the second part one of the limits of non-spherical particles namely long thin rods are discussed because random packing of long thin rods turn out to be a much simpler system to study then random packing of spheres.

2.8.1. Various models for non-spherical particles

One often used approach in modeling is to start with a simple system and apply a perturbation in order to model the more complicated system. Mounfield and Edwards

used such a perturbative theory to qualitatively describe packing of non-spherical particles and polydisperse spheres [42]. For irregularly shaped particles, a packing with six contacts per particle is mechanically stable for general orientations of particles only if particles have some non-zero coefficient of friction. For frictionless particles the only stable states will be states where the volume as a function of orientation has a local minimum or particles have more than six contacts. Perturbation with an amount x leads to a reduction in volume fraction of an amount x^2 but by taking correlations into account it was shown that this is not necessarly true in the close packed regime.

A relation between aspect ratio and volume fraction for a packing of rods was derived by Parkhouse and Kelly [100]. The main approximation is a 50% probability of being able to fit another rod no further away from the chosen location than about $\frac{1}{4}$ of the length of the rod and within about a quarter of a right angle of the chosen direction. Rods are placed randomly in a square block. A light is shown perpendicular on this box and the rods cast shadows on a square plane. The average area of the shadows is then calculated and normalized by the area of the square. The normalized shadow area depends on the volume fraction. The expected spacing between the unlit patches depends also on the normalized shadow area. Combining these two leads to the following formula for ϕ

$$\phi \approx 2 \ln \alpha / \alpha \tag{2.34}$$

where α is the aspect ratio.

For spheres this equation predicts a volume fraction of zero, it does predict a maximum volume fraction for $\alpha = e$, and for large α it tends to zero. The volume fractions calculated are too high when compared with experiments [33, 96] and the volume fraction maximum occurs at a different aspect ratio compared to simulation [35].

Evans and Gibson worked on random packing of short thick fibres using a theoretical approach from the field of liquid crystals [101]. For rod-like molecules with a fixed aspect ratio there is an isotropic-nematic phase transition at a certain volume fraction. A change from random orientation to an ordered configuration becomes favourable because of packing difficulties in maintaining a random orientation. The maximum volume fraction for random packing was found by treating a rod as a double-cone volume. A rod in contact with another rod sweeps out a doubled-cone volume upon rotating around a contact point. The maximum volume fraction is then estimated from the assumption that the rod cannot rotate and is found to be

$$\phi_{max} = 4 \frac{D}{L} \tag{2.35}$$

This result contains the correct scaling with aspect ratio and predicts volume fractions close to experimental data [33, 96] and simulations [102]. Another theory that predicts

correct volume fraction behaviour for rods with a large aspect ratio is the random contact equation described next.

2.8.2. The random contact equation for thin rods

Rods with a high aspect ratio have a large probability of touching other rods. Long thin rods in a network can not translate because of presence of other long thin rods: the rods are caged. From this fact the random contact equation can be derived, which predicts the experimental volume fraction correctly for long thin rod packings [33, 34].

Consider two rods: a central rod and a neighbour rod separated by a center-to-center vector $\vec{r}$. The central rod forbids a fraction $f_{excl}(\vec{r})$ of the orientations of a neighbour. This excluded fraction is also the probability that a neighbour will contact the central rod. If there is a number density $\rho(\vec{r})$ surrounding the central rod then the average number of contacts per particles $\langle C \rangle$ is given by

$$\langle C \rangle = \int f_{excl}(\vec{r}, \rho)\rho(\vec{r})d\vec{r} \tag{2.36}$$

Using a mean field approximation and assuming that neighbour particles themselves do not interact with each other $\rho(\vec{r})$ is replaced by the average number density ρ and $f_{excl}(\vec{r}, \rho)$ simplifies to $f_{excl}(r)$.

$$\langle C \rangle = \rho \int f_{excl}(r)dr \tag{2.37}$$

The integral in (2.37) is nothing else but the orientationally averaged excluded volume V_{excl}. So the average number density in the packing is equal to:

$$\rho = \frac{\langle C \rangle}{V_{excl}} \tag{2.38}$$

For equal-sized spherocylinders the excluded volume as calculated by Onsager [25] is

$$V_{excl} = \frac{4}{3}\pi D^3 + 2\pi L D^2 + \frac{\pi}{2} D L^2 \tag{2.39}$$

If we define the ratio E as V_{excl}/V_p then for spherocylinders

$$E = \frac{6\alpha^2 + 24\alpha + 16}{2 + 3\alpha} \tag{2.40}$$

Substituting this in (2.38) gives

$$\phi E = \langle C \rangle \tag{2.41}$$

For long thin rods $E = 2\alpha$ so the volume fraction becomes

$$\phi = \frac{\langle C \rangle}{2\alpha} \tag{2.42}$$

This relation does not hold for low aspect ratios because there placement of a second particle is highly influenced by placement of the first particle on a central particle.

A lower boundary for the volume fraction of long thin rods can be estimated by calculating the average number of contacts needed to prevent translation in a direction

perpendicular to the axis of symmetry of a particle [103]. Since in the derivation of (2.41) the interactions between neighbors are ignored, the translational caging of the rod becomes a 2-d problem of the caging of a disk. When viewed along the axis of symmetry, the central rod looks like a disk and since neighbors do not interact the contacts can be considered as uncorrelated point contacts. So the caging number for disks $\langle C\rangle = 5$ is a lower boundary on the contact number. In chapter 6 the caging number for infinite 3-dimensional rods is calculated, where also rotations are blocked.

2.9. Simulations

This paragraph on computer simulations continues the review from §2.5. Many topics treated in §2.5 also apply to computer simulations of non-spherical particles. First various methods for non-spherical particles are discussed and then the mechanical contraction method is extended to handle non-spherical particles.

2.10. Methods for non-spherical particles

A method for generating packings of monodisperse 2-d ellipses was developed by Buchalter and Bradley [104]. First ellipses are placed in a rectangle in a non-overlapping way. The ellipses have a finite set of orientations and are placed on a grid. Then a modified version of a Monte Carlo method is used. A particle is randomly selected, for which a random translation vector and a random angle to rotate the particle is chosen. Translations upwards are forbidden. This particle is moved until it has moved a defined maximum distance or collides with the wall or another ellipse.

The simulation was done for a range of aspect ratios. The volume fraction is 0.75 for $\alpha = 1$, then it increased to 0.8 for $\alpha = 3.5$ and then it decreases with further increasing α. There is always some order in the system because the ellipses attempt to minimize their gravitational energy.

Sherwood developed a RSA method to simulate random packings of spheroidal particles with semi-axes of length (a,b,b) [105]. Spheroids follow the same trend as ellipses in 2-d. For $\alpha = 1$ the volume fraction is a minimum, then as α increases it becomes a maximum for $\alpha = 1.4$ and then the volume fraction decreased again. Due to limited computation time the highest α was 15 with a $\phi = 0.36$.

Donev et al. [106] generalized the method developed by Lubachevsky et al. [77] for spheres as described in section §2.5 to generate random dense packings of ellipsoids. For various aspect ratios the volume fraction and the number of contacts was determined. It was found that spheres have a local minimum for the volume fraction and contact number in the family of ellipsoids. Prolate spheroids have a maximum volume fraction at an aspect ratio of roughly 1.5 and oblate spheroids at about 0.67. The corresponding contact numbers are roughly 9.8 for both. The maximum in volume fraction is

attributed to the expected increase in the number of contacts resulting from additional rotational degrees of freedom for ellipsoids. General ellipsoids show a maximum volume fraction of around 0.735 with a contact number of 11.4.

A method that generates random packings of all kinds of shapes was developed by Nolan and Kavanagh [107]. The main idea behind this method is to approximate non-spherical particles with a collection of spheres. With an infinite distribution of spheres every non-spherical shape can be generated. Fortunately, to generate a random packing only a finite amount of spheres is needed to roughly approximate particle shape. The algorithm for generating a random packing consists of the following steps. The first step is to generate a dense packing with overlapping particles. The second step is to remove overlap through a series of iterations. It is easy to check for overlap because only spheres are checked for overlap. For every sphere overlapping there is a force that is proportional to the distance between spheres that lies along the shortest path between two overlapping spheres. All forces on a single particle from the component spheres of that particle are summed to obtain a net force. This force gives a particle a velocity and it can also produce an angular moment about the centre of mass of the particle.

The particles do not roll in the simulation. Research on close packed structures of spheres has shown that rolling does not affect values of either the mean coordination number or the volume fraction but it is the mechanism that ensures gravitational stability of a packing.

In the simulation from Nolan and Kavanagh unstable particles are moved down a bit in a periodic box until a stable situation is achieved [107]. A stable particle has a contact below the centre of mass of a particle and it experiences positive and negative moments in both the XZ and YZ planes. A packing is stable if 95% of the particles are stable. The packing is considered final when all overlap is removed and the system is stable.

By varying the starting volume fraction a random loose packing or random dense packing can be generated. The found volume fractions were $\phi_{cylinder} = 0.674$, $\phi_{spheroid} = 0.676$ and $\phi_{nail} = 0.519$. These are in agreement with found experimental values of 0.67, 0.67 and 0.52 [107]. Cylindrical particles had a contact number that ranges from 4.4 to 6.5, spheroids have 3.2 to 5.9 and nails have 6.1 to 8.0. Interestingly for a $\phi_{spheroid}$ of around 0.64 the average contact number is about 5.0 and for a $\phi_{spheroid} = 0.55$ it is 4.5. Both numbers are close to the average cage size of 4.79 for spherical particles. For $\phi_{spheroid} = 0.67$ the average coordination number is 6.2.

Another overlap removal scheme was developed by Latham et al. to generate loose random packings of tetrahedra [108]. Pournin et al. developed molecular dynamics codes for simulating packing of spherocylinders that are being vibrated in a tube [109]. Inter particle contacts are modeled with springs and friction can be included in the contact model, which can also easily be extended to general spheropolyhedra.

2.10.1. Mechanical contraction method for rods

The method from Nolan and Kavanagh [107] described in the previous paragraph starts with a high volume fraction of overlapping particles and then iteratively removes the overlap, thereby increasing the volume. In contrast to this, the mechanical contraction method (MCM) starts with a low volume fraction and the volume is contracted [35]. In every iteration the volume is decreased until overlap occurs between the particles as described in §2.5.3.

The MCM for spherocylinders works according to the same principle as for the sphere method, but since rods have an orientation, two extra degrees of freedom are introduced because rotation around the symmetry axis is not taken into account. The k-vector is now the shortest vector connecting the two spherocylinders. If the distance between two spherocylinders is smaller than the sum of both radii then two spherocylinders overlap. The rate at which overlap is removed changes because a rod can also rotate out of its overlapping position. By taking into account this rotation the rate of change in k becomes:

$$\frac{\partial k_j}{\partial t} = k_j^{(1)} a_1 + k_j^{(2)} a_2 + k_j^{(3)} a_3 + l_j k_j^{(4)} a_4 + l_j k_j^{(5)} a_5 \tag{2.43}$$

where l_j is the length from the center of mass of the i-th particle to the contact point with the j-th particle along the axis of particle i.

The kinetic energy type constraint includes a rotational term, where ϵ is related to the moment of inertia for a particle:

$$a_1^2 + a_2^2 + a_3^2 + \epsilon a_4^2 + \epsilon a_5^2 = 1 \tag{2.44}$$

Using the Lagrange multiplier method gives a_4 and a_5. Translational terms stay the same. The rotational terms are:

$$a_n = \frac{1}{\epsilon} \sum_{j=0}^{C} \delta_j l_j \frac{k_j^{(n)}}{k_j},\ n = 4, 5 \tag{2.45}$$

The mechanical contraction method shows similarities with the method developed by Nolan and Kavanagh [107] as described in the previous paragraph. Nolan and Kavanagh's method starts with an unrealistic physical state and uses the k-vector to calculate net-forces on the particles to arrive at a realistic physical state. The MCM starts with a realistic physical state and uses the k-vector to calculate an impulse to remove overlap during compression of the volume.

The MCM is able to generate random rod packings with a large aspect ratio that obey the random contact equation for thin rods and agree with experiments [33, 96]. The MCM also generates a maximum in volume fraction for spherocylinders with a small aspect ratio. The maximum found was 0.695 for aspect ratio $\alpha = 0.4$. The number of contacts as a function of aspect ratio showed the same trends as the curve from the volume fraction as a function of aspect ratio. This similarity strengthens the idea that

the volume fraction can be linked to the number of contacts and the excluded volume. An alternative interpretation (as opposed to the one in section §2.8.2) of the maximum volume fraction is that the amount of contacts needed to cage a particle increases with aspect ratio. For low aspect ratios this effect dominates and the increase in number of contacts increases the volume fraction. As the aspect ratio increases the excluded volume also increases. For larger aspect ratios this effect starts to dominate and leads to a decrease in volume fraction.

2.10.2. Mixtures of particles

Mixtures of colloidal spheres and rods have been found to form a variety of structures. Entropically driven microphase separation can occur to form a layered structure with sheets of spheres followed by columnar rods, a lamellar phase [110].

The combined packing of rods and spheres was investigated by Milewski [95]. Combining two full containers, one with spheres and one with rods, in a new container leaves room left for extra particles to be added due to the increased packing efficiency for certain combinations of aspect ratio and radii. This effect resembles very much the packing of binary sphere mixtures. An accurate model to link the volume fraction to a distribution of pore sizes and the flow of small particles into them has not been found yet.

Abreu et al. [111] studied the influence of particle shape on packing and on segregation of spherocylinders via Monte Carlo simulations. Differences in particle size are the main driving force for segregation. Packings of spherocylinders ranging in aspect ratio from 0 to 3.5 have been investigated. For spheres the found volume fraction was 0.58 indicating that this Monte Carlo method generates a loose random type of packing since the random dense packing value is 0.64. For spherocylinders of aspect ratio 0.5 a maximum was found of 0.65. Lower vibration intensity results in a slightly denser packing. Vibrating bidisperse mixtures of spherocylinders resulted in segregation.

2.11. Summary and conclusions for non-spherical particle packings

When changing the aspect ratio from 0 (a sphere) to infinity (a long thin rod), theory, experiments and simulations show a volume fraction maximum at low aspect ratio upon deviating from spheres. This maximum volume fraction can be explained by the fact that short rods can reorient themselves into pores and thereby creating room for extra rods in the packing. An alternative explanation is that as the aspect ratio increases more contacts need to be placed on a particle thereby increasing the volume fraction. As the aspect ratio increases even more, the excluded volume becomes important and the volume fraction decreases again inversely proportional to the aspect ratio.

The family of ellipsoids show the same effect. Deforming spheres to prolate ellipsoids shows the same qualitative dependence of the volume fraction on aspect ratio as for spherocylinders. This is not surprising since the shape of prolate ellipsoids is very similar to that of spherocylinders. With ellipsoids also aspect ratios lower than one are possible. For spherocylinders this cannot be achieved. Going from spheres to oblate ellipsoids also shows a maximum in volume fraction. Cylinders could be possibly used to show the same cusp as for ellipsoids. However, it is not clear what the effect of the sharp edge of the cylinder will be. Unfortunately there is no data for high aspect ratio ellipsoids yet.

For long thin rods the random contact equation adequately predicts the volume fractions found in experiments [33, 96] and simulations [35]. The work of Parkhouse and Kelly explains the volume fraction maximum for short thick rods but it predicts a different aspect ratio dependence of the packing density then found in simulations [100]. Also it does not give the right scaling for higher aspect ratio rods. The contact numbers found for rods in simulations is lower than theory and experiments predict. There are still many open questions with respect to the random packing of non-spherical particles. Future models for rods and ellipsoids should explain the volume fraction in the whole range of aspect ratios.

3

On the caging number of two- and three-dimensional hard spheres

Abstract

Local structural arrest in random packings of colloidal or granular spheres is quantified by a caging number, defined as the average minimum number of randomly placed spheres on a single sphere that immobilise all its translations. We present an analytic solution for the caging number for two-dimensional hard disks immobilised by neighbour disks which are placed at random positions under the constraint of a non-overlap condition. Immobilization of a disk with radius $r = 1$ by arbritary larger neigbor disks with $r \geq 1$ is solved analytically, whereas for contacting neighbors with radius $0 < r < 1$, the caging number can be evaluated accurately with an approximate excluded volume model that also applies to spheres in higher Euclidian dimension. Comparison of our exact two-dimensional caging number with studies on random disk packing indicates that it relates to the average co-ordination number of random loose packing, whereas the parking number is more indicative for coordination in random dense packing of disks.

3.1. Introduction

Contact numbers in sphere packings have in several cases a special physical significance. The *kissing* number represents the maximum number of spheres that can be placed simultaneously on the d - 1 dimensional surface of a d-dimensional sphere S. For disks in a plane (d=2) the kissing number is six and for three-dimensional spheres the number is 12 [26]. These maximum contact numbers occur in regular close-packed sphere solids as encountered, for example, in colloidal crystals [112]. The kissing number is a single-valued quantity, in contrast to the distributed contact numbers found by placing spheres on randomly chosen, fixed positions on the surface of S until the probability for finding sufficient parking space vanishes. This distributive contact number, the *parking* number, equals 8.7 for three-dimensional spheres [27]. It is the average outcome of a random parking process with the constraint that spheres are forbidden to overlap. This parking process models irreversible adsorption and has been generalized [27] to the attachment of spheres with arbitrary size on the surface of S. Thus, the kissing number is the absolute maximum contact number achieved for regular close-packed spheres while the parking number is a lower constrained maximum that is more relevant for less dense "amorphous" sphere stackings. To increase the co-ordination of S above the parking value the disordered neighbours must be rearranged into a more ordered configuration.

One might identify the parking number as the typical number of spheres required to immobilize a sphere in a random packing. However, the parking process is merely a maximization under the constraint of random positioning and non-overlap which pays no heed to the issue whether or not sphere S is able to translate. Of course, the parked neighbours do restrict the mobility of S and, in fact, when the number of contacting neighbours equals the parking number, S will be unable to translate. An important point is that to achieve this arrest, on average much less spheres are required than the parking number. Thus, to describe local arrest of a single sphere, a *caging* number has been introduced [28,29,103] defined as the average *minimum* number of randomly placed spheres that blocks all translational degrees of freedom of sphere S. The construction of such geometric cages has been discussed in detail elsewhere (see for example the simulations of sphere caging in arbitrary Euclidean dimension in Ref. [28]). In essence, a cage is constructed via the parking process referred to above, with the additional rule that the process is terminated when S is caged. Consequently, the resulting caging contact numbers fall significantly below parking and kissing numbers in any Euclidean dimension [29].

To avoid confusion we note here that caging effects in transport phenomena are time dependent, in contrast to our static definition of caging. In dense colloidal fluids, for example, local structural arrest is described in terms of slowly fluctuating neighbour

cages that trap spheres, on approach of a glass transition, over increasing time intervals. In our present analysis a cage is purely geometric, as in a static snapshot of thermal colloids or a packing of macroscopic 'granular' spheres. This is not to say that the caging number is irrelevant for thermal spheres, because the progressive arrest of spheres near a glass transition is ultimately caused by purely geometrical restrictions [79]. So calculation of caging numbers is useful to better understand or perhaps even quantify co-ordination numbers in random sphere packings or colloidal sphere glasses, a point to which we return in the discussion in Sec. 3.6.

The main challenge in a geometrical caging problem is to account for excluded volume effects, which cause positions of contacts on a sphere to be strongly correlated. For randomly parked, overlapping neighbour spheres, i.e. for a distribution of completely uncorrelated contact points on the surface of sphere S, caging numbers have been calculated analytically for spheres of arbitrary dimension [28]. For non-overlapping hard spheres, caging numbers have only been determined by computer simulation [28]. We report in Sec. 3.3 an analytical solution for the caging number of a two-dimensional hard sphere with radius $r = 1$ for neighbouring spheres with radius $r \geq 1$, which is validated by numerical calculations. In Sec. 3.4, we also investigate the caging number for contacting neighbour spheres with radius $0 < r < 1$. We compare caging numbers with parking numbers, which exhibit an interesting difference depending on sphere size ratio. In Sec. 3.5, we discuss the caging number for three-dimensional hard spheres. In Sec. 3.2, we first briefly re-examine the caging number for uncorrelated contacts for comparison with the results for correlated contacts in later sections and to provide a more concise derivation than given previously [28].

3.2. Caging by uncorrelated contacts

Let p_n be the probability that n arbitrarily placed contacts cage sphere S. The probability that n contacts do not cage S equals

$$1 - p_n = P(\gamma > n) = \sum_{k=n+1}^{\infty} P(\gamma = k) \tag{3.1}$$

where $P(k)$ is the conditional probability that k contacts cage S, given that $k-1$ contacts still allow sphere S to translate. The caging number is defined as the expectation value,

$$\langle \gamma \rangle = \sum_{k=0}^{\infty} kP(\gamma = k) = \sum_{n=0}^{\infty} \sum_{k=n+1}^{\infty} P(\gamma = k) = \sum_{n=0}^{\infty} 1 - p_n \tag{3.2}$$

The contacts on the surface of S may stem from touching spheres or any other neighbour shapes such as cylinders or thin rods [113]. If the neighbours are particles that cannot interpenetrate each other, the contacts are correlated. When the neighbours are allowed to overlap without any restriction, the contacts on S are uncorrelated (the neighbours

are randomly inserted) and the contact distribution is equivalent to a set of blocking points placed at random, fixed positions on the surface of S.

The probability that n contacts do not cage a d-dimensional sphere equals the probability that one equator on S can be found such that all n contacts share the same hemisphere of S. For example, a one-dimensional sphere can only translate along a straight line, so there are only two 'hemispheres'. The probability that all uncorrelated contacts are on one hemisphere is therefore

$$1 - p_n = \left(\tfrac{1}{2}\right)^{n-1} \quad \text{for } n > 0 \text{ and } p_0 = 0 \tag{3.3}$$

which on substitution in (3.2) yields for the caging number for uncorrelated contacts on a one-dimensional sphere,

$$\langle\gamma\rangle = 1 + \sum_{n=1}^{n=\infty} \left(\frac{1}{2}\right)^{n-1} = 3 \quad \text{for } d = 1 \tag{3.4}$$

For two-dimensional spheres the caging problem for uncorrelated contacts is more complicated because from an infinite set of possible hemispheres one has to determine whether or not at least one member is common to all n contacts. The general problem for a d-dimensional sphere has been solved by Peters et al [28]. Here we present an alternative treatment for $d = 2$ employing a formula derived by Wendel [114] for the probability of finding n randomly placed points on the same hemisphere of a d-dimensional sphere (see Appendix A):

$$p_{d,n} = \begin{cases} \left(\tfrac{1}{2}\right)^{n-1} \displaystyle\sum_{k=0}^{d-1} \binom{n-1}{k} & \text{for } n > d \\ 1 & \text{for } 0 \le n \le d \end{cases} \tag{3.5}$$

Thus for two-dimensional spheres,

$$p_{2,n} = \begin{cases} 1 - p_n = n\left(\tfrac{1}{2}\right)^{n-1} & \text{for } n \ge 2 \\ 1 & \text{for } n = 0, 1 \end{cases} \tag{3.6}$$

which according to (3.2) yields for the caging number for uncorrelated contacts in two dimensions,

$$\langle\gamma\rangle = 1 + \sum_{n=1}^{n=\infty} n\left(\frac{1}{2}\right)^{n-1} = 5 \quad \text{for } d = 2 \tag{3.7}$$

Equations (3.4) and (3.7) are instances of the general result $\langle\gamma\rangle = 2d+1$ for uncorrelated contacts, rederived in Appendix B using the Wendel formula (3.5). The caging number $\langle\gamma\rangle = 2d + 1$ for d-dimensional spheres is clearly an upper bound because the non-overlap condition for hard spheres increases the average distance between contacts and, hence, will decrease the number of contacts needed for caging, as demonstrated in the next section for two-dimensional spheres.

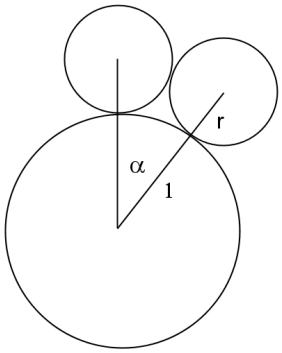

Figure 3.1: Hard disks are not allowed to overlap. This leads to an excluded arc on the circumference of the center disk.

3.3. Caging by three hard disks

The caging of sphere S by non-overlapping hard spheres of any size has the trivial solution $\gamma = 2$ in one dimension. In two dimensions, the caging probability for three disks can be exactly calculated taking into account the non-overlap condition. For finite-size caging disks, there is a minimum angle given by a triangle of three contacting spheres that is equal to

$$\alpha = 2\arcsin[r/(r+1)] \tag{3.8}$$

where r is the size ratio of the radii of the caging disks with respect to S (see Figs. 3.1 and 3.2). Hence, each contact on the circumference of S excludes an arc with angle α on each side of it for any other contact. S is caged when the largest arc between any two adjacent contacts is smaller than π. The caging number as a function of r must satisfy two limiting cases. When r tends to zero, the caging number $\langle\gamma\rangle = 5$ for uncorrelated particles should be recovered. On the other hand, for sufficiently large r, a two-dimensional disk S can only accommodate a maximum of three contacting neighbors and since two disks cannot cage S, it follows that the caging number should monotonically decrease from five to three for increasing r. A numerical solution (Fig. 3.3) indeed confirms this behavior. The caging number diminishes rapidly when the point contacts at $r = 0$ start to inflate and saturates already for $r > 1$.

For equal-sized disks, $\alpha = \pi/3$, Bideau et al. [63] showed that for a configuration with maximum disorder four disks are an upper limit for the contact number. Four disks do *not* cage S when they touch each other forming a connected row of four as in a hexagonal unit with two disks missing. In this case the largest arc corresponds exactly to π. Since the probability for this configuration to occur is zero for randomly placed disks, $p_{2,4} = 1$. Therefore, for $\alpha > \pi/3$ or equivalently $(r > 1)$, the calculation of $p_{2,3}$ is sufficient to obtain the caging number. For the sake of generality, $p_{2,3}$ will be given for arbitrary values of α.

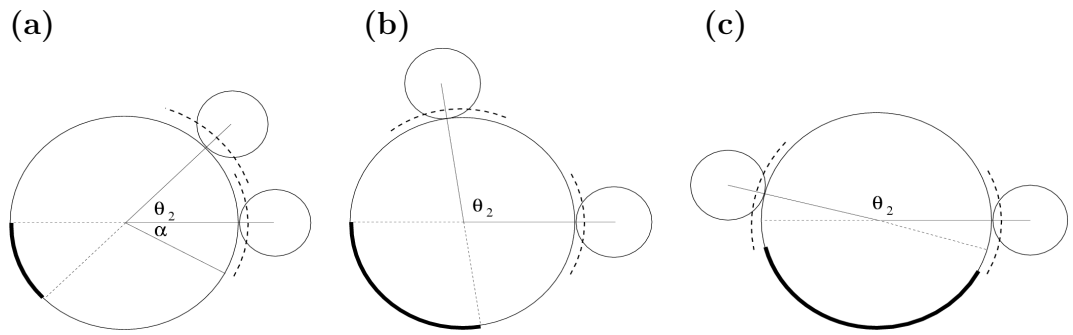

Figure 3.2: Illustration of excluded arcs (thick dashed lines), free segment, and caging segment (thick line). The thin dashed lines indicate the "image" points of the contacts with respect to the sphere center. (a) Overlapping excluded arcs; (b) disjoined excluded arcs; (c) image points in excluded volumes.

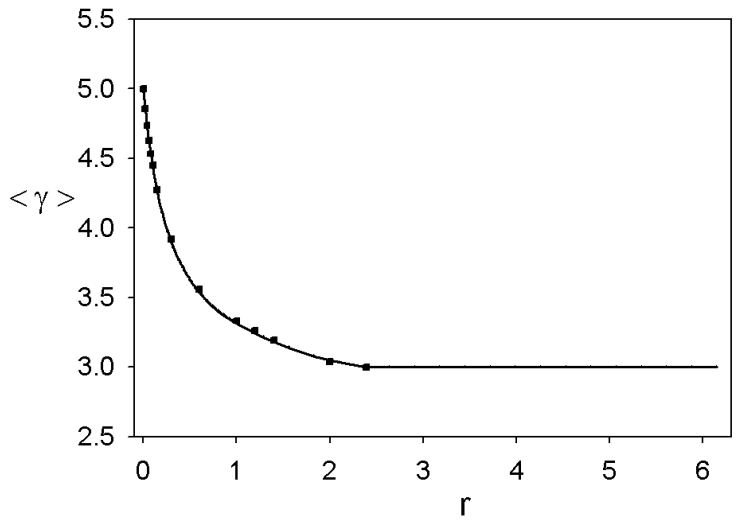

Figure 3.3: Plot of two-dimensional caging number $\langle\gamma\rangle$ as a function of the radius of the contacting disks. Squares represent the approximation with excluded length given by (3.8) and the computer simulation is shown as a straight line.

Let us denote the angular coordinates of the three contact points by θ_1, θ_2, and θ_3, where the index indicates the ordering of the successive additions. Since the position of the first contact is arbitrary, we can choose $\theta_1 = 0$. Since the "upper" and "lower" half circle are as of yet equivalent, we can restrict θ_2 to values $0 < \theta_2 \leq \pi$. Furthermore, because of the excluded volume, θ_2 must satisfy $\theta_2 \geq \alpha$. To obtain $p_{2,3}$, we need to calculate for each possible choice of θ_2 the probability that the third contact cages the sphere, and average this probability over all possible values for θ_2. For a given θ_2, this probability is equal to the lengths of the segments of the circle in which the third

contact point cages the sphere, divided by the length of the total available space for the third contact.

For $\alpha < \pi/3$ or equivalently ($r < 1$), three different situations have to be considered as θ_2 increases, see Fig. 3.2. For $\alpha < \theta_2 < 2\alpha$, the excluded volumes of the two disks overlap (no third disk can be placed in between), and the total available length for placing the third contact is $2\pi - \theta_2 - 2\alpha$. In order to cage the sphere, the third contact must be placed such that there is no free arc of length π or more. It can be easily seen from Fig. 3.2a that this happens only in the segment located in between the two "image" points of the two first contacts with respect to the sphere center. Therefore, the length of this segment is just θ_2. For $2\alpha < \theta_2 < \pi - \alpha$ (Fig. 3.2b), the excluded volumes are disjoint (now, the third disk can also be placed between the first two), and the total available segment length for the third contact is always equal to $2\pi - 4\alpha$, whereas the length of the caging segment is still equal to θ_2. Finally, for $\pi - \alpha < \theta_2 < \pi$ (Fig. 3.2c), the "image" points of the first two contacts fall into the excluded volume. The total available length is still $2\pi - 4\alpha$, but the length of the caging segment is reduced to $2\pi - 2\alpha - \theta_2$. The expression for $p_{2,3}$ that results from putting the three pieces together is

$$p_{2,3} = \frac{1}{\pi - \alpha}\left(\int_{\alpha}^{2\alpha} \frac{\theta_2}{2\pi - 2\alpha - \theta_2} d\theta_2 + \int_{2\alpha}^{\pi-\alpha} \frac{\theta_2}{2\pi - 4\alpha} d\theta_2 + \int_{\pi-\alpha}^{\pi} \frac{2\pi - 2\alpha - \theta_2}{2\pi - 4\alpha} d\theta_2\right) \tag{3.9}$$

Similar considerations apply in the case $\alpha > \pi/3$. Only, since now $2\alpha > \pi - \alpha$, the "image" points enter the excluded volumes before the latter get disjoint. Therefore, the bounds of the individual integrals have to be changed, and the total and caging segment lengths re-evaluated for the second integral, which gives

$$p_{2,3} = \frac{1}{\pi - \alpha}\left(\int_{\alpha}^{\pi-\alpha} \frac{\theta_2}{2\pi - 2\alpha - \theta_2} d\theta_2 + \int_{\pi-\alpha}^{2\alpha} \frac{2\pi - 2\alpha - \theta_2}{2\pi - 2\alpha - \theta_2} d\theta_2 + \int_{2\alpha}^{\pi} \frac{2\pi - 2\alpha - \theta_2}{2\pi - 4\alpha} d\theta_2\right) \tag{3.10}$$

The evaluation of these integrals yields, for $\alpha > \pi/3$,

$$p_{2,3} = \frac{1}{\pi - \alpha}\left(\frac{7}{2}\alpha - \frac{5}{4}\pi + (2\pi - 2\alpha)\ln\frac{2\pi - 3\alpha}{\pi - \alpha}\right) \tag{3.11}$$

Note that this expression is valid only for $\alpha \leq \pi/2$; for $\alpha = \pi/2$, $p_{2,3} = 1$, which corresponds to the fact that three disks with $\alpha > \pi/2$ cannot be placed on the same hemi circle, and thus S is always caged.

In particular, for equal-sized disks with $\alpha = \pi/3$, $p_{2,3} = \ln(9/4) - 1/8$, which upon substitution in (3.2) yields the two-dimensional caging number $\langle\gamma\rangle = 1 + 1 + 1 + 9/8 - \ln(9/4) \approx 3.31407$. This result equals the value found from simulations in Ref. [28] and is confirmed by simulations described in the next section. The result for correlated

contacts is, as expected, below the caging number for uncorrelated contacts because of excluded volume effects. The caging number is also lower than the parking number for two-dimensional disks, since one can always park four equal-sized disks at random on a central disk. We determined the parking number for two-dimensional disks numerically to be 4.484.

3.4. Caging and parking numbers for hard disks of different size

No analytical solution is yet available for the caging number for $r < 1$ ($\alpha < \pi/3$), since there are non-caging configurations with four and more contact points. Therefore, an evaluation of the caging number would require the calculation of $p_{2,n}$ for $n > 3$ while taking into account the sequential addition of disks, which is very cumbersome. Fortunately, as a good approximation an exact calculation can be performed for a slightly modified problem. The condition of sequentially adding disks is replaced by positioning n disks simultaneously. The new problem is defined as follows.

Let a central disk of unit radius be surrounded by n disks of radius r. Count all possible configurations for the n surrounding disks and determine the fraction that has all n disks in a hemisphere of the central disk. This can be done in the following way: the space of configurations is defined by the positions of the small disks. All configurations where all n disks are separated from each other by the same angles are equivalent because one can always transform one configuration into the other by rotating the reference axes. Therefore, only the angle differences between disks are useful variables in two dimensions. Let θ_i again be the angle of the ith contact with respect to an arbitrary reference axis; this time, since all contacts are present from the start, the index can count the contacts counter clockwise. We define the angle differences as: $\varphi_i = \theta_{i+1} - \theta_i$ for $i = 1$ to $n-1$ and $\varphi_n = \theta_1 + 2\pi - \theta_n$ in order to make all $\varphi_i > 0$. For n contacts there are n differences. However, they are not all independent since

$$\sum_{i=1}^{n} \varphi_i = 2\pi \tag{3.12}$$

The total number of configurations is the number of possible ways to choose sets of φ_i satisfying (3.12). For continuous variables this becomes the volume of phase space spanned by the φ_i. This can be written as, preserving the symmetry between all variables,

$$V = \int d\varphi_1 \int d\varphi_2 \cdots \int d\varphi_n \delta\left(\sum_{i=1}^{n} \varphi_i - 2\pi\right) \tag{3.13}$$

where δ is the Dirac delta function. The integration bounds are determined as follows: For point contacts, there is no other restriction than $0 \leq \varphi_i \leq 2\pi$. For finite-sized disks,

φ_i has to be larger than the angle α. There is also a maximum angle: n disks touching each other occupy $(n-1)\alpha$, so the maximum "gap" is $2\pi-(n-1)\alpha$. Including theta functions conveniently incorporates these restrictions on the phase space volume,

$$V=\int d\varphi_1\int d\varphi_2\cdots\int d\varphi_n\delta\left(\sum_{i=1}^{n}\varphi_i-2\pi\right)\theta(\varphi_1-\alpha)\theta(\varphi_2-\alpha)\cdots\theta(\varphi_n-\alpha) \tag{3.14}$$

This way the integration bounds can stay open ($-\infty$ to $+\infty$) and adding the theta function is equal to starting at angle α. This is also a convenient way to take into account the upper boundary without breaking the symmetry between the variables. One can see that the value of the entire integral is independent of the ordering of the integration variables.

The fraction of non-caging configurations is given by the configurations where at least one $\varphi_i>\pi$. There can be only one such φ_i because of the constraint (3.12). The volume of phase space filled by such configurations can therefore be calculated as

$$V=\sum_{l}\int d\varphi_1\int d\varphi_2\cdots\int d\varphi_n\delta\left(\sum_{i=1}^{n}\varphi_i-2\pi\right)\theta(\varphi_1-\alpha)\cdots\theta(\varphi_n-\alpha)\theta(\varphi_l-\pi) \tag{3.15}$$

where the new element is the last theta function which counts only the configurations with $\theta_l>\pi$. The outer sum is necessary because any of the φ_i can become greater than π. Since all variables are symmetric, this can immediately be simplified, giving for the total probability of finding all disks on the same hemisphere,

$$p_{2,n}=\frac{n\int d\varphi_1\int d\varphi_2\cdots\int d\varphi_n\delta\left(\sum_{i=1}^{n}\varphi_i-2\pi\right)\theta(\varphi_1-\alpha)\cdots\theta(\varphi_{n-1}-\alpha)\theta(\varphi_n-\pi)}{\int d\varphi_1\int d\varphi_2\cdots\int d\varphi_n\delta\left(\sum_{i=1}^{n}\varphi_i-2\pi\right)\theta(\varphi_1-\alpha)\cdots\theta(\varphi_n-\alpha)} \tag{3.16}$$

Note that this is an exact formula valid for any α (and thus r) and n. Rather than evaluating the integrals explicitly, we will use a graphical illustration which immediately gives the result for the $p_{2,n}$.

First the probability for three disks will be discussed and then it will be extended to n disks. The total phase space is spanned by $(\varphi_1,\varphi_2,\varphi_3)$. The Dirac δ function restricts the phase space to a plane that can be defined by the points (2π,0,0), (0,2π,0) and (0,0,2π). For point contacts the theta functions exclude all $\varphi_i<0$ and $\varphi_i>2\pi$. The resulting domain of phase space is an equilateral triangle. This is known (up to a rescaling) as the Gibbs simplex, used abundantly in ternary alloy phase diagrams. The non-caging part of the phase space is given by the volume where one $\varphi_i>\pi$. This gives three equilateral triangles with side π (Fig. 3.4). Stripes are cut off from the phase space triangle to take into account the excluded volume thetas, i.e. the non-overlap condition for hard disks. The stripes are cut from the outer rim of the triangle. The remaining inner triangle is the total volume of phase space. Since all subvolumes are equilateral triangles, the ratios of their surfaces are the ratios of the side lengths squared. The side

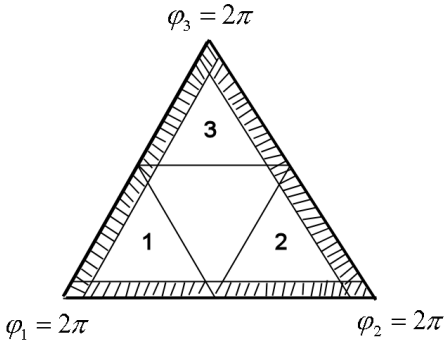

Figure 3.4: The phase space spanned by $\{\varphi_1, \varphi_2, \varphi_3\}$ is an equilateral triangle with length 2π. The non-overlap condition for disks is taken into account by requiring that the minimum of each φ_i is α. Therefore the outer rims of the triangle are stripped off. A disk is non-caged if any of the φ_i is larger than π. This is the case for the labled three small equilateral triangles.

length of the total volume is $2\pi - 3\alpha$ and the side length of one of the three non-caging volumes is $\pi - 2\alpha$. From this the non-caging probability follows:

$$p_{2,3} = \begin{cases} 3(\pi - 2\alpha)^2/(2\pi - 3\alpha)^2 & \text{for } \alpha < \pi/2 \\ 0 & \text{for } \alpha > \pi/2. \end{cases} \tag{3.17}$$

The argument with the Gibbs simplex is general and can be applied to any n. For example, for $n = 4$, the Gibbs simplex is a tetrahedron, and the non-caging volumes are four small tetrahedra located in the corners of the large one. Therefore the immediate generalization,

$$p_{2,n} = \begin{cases} n\left(\frac{\pi-(n-1)\alpha}{2\pi-n\alpha}\right)^{n-1} & \text{for } \alpha < \pi/(n-1) \\ 0 & \text{for } \alpha > \pi/(n-1) \end{cases} \tag{3.18}$$

Note that in the limit $\alpha \to 0$ the probability for point contacts is obtained. Substitution of (3.18) in (3.2) gives the approximated caging number as a function of contacting disk radius as plotted in Fig. 3.3. The upper boundary of the summation in (3.2) was adjusted to π/α because only a finite number of disks can be placed on the same hemicircle.

The accuracy of (3.18) was verified with a computer simulation of the sequential addition of disks using a method similar to [28] for equal-sized spheres. The difference between simultaneously positioning n disks and the numerical solution of sequentially adding disks is surprisingly small over the whole range as shown in Fig. 3.3. In the numerical simulation, the probability for a given configuration depends on the order in which the disks were placed and is thus non-uniform, whereas for adding n disks simultaneously on the central disk the probability for a given configuration is uniform.

To compare the caging number with the parking number a computer simulation was performed to determine the parking number as a function of contacting disk radius (see

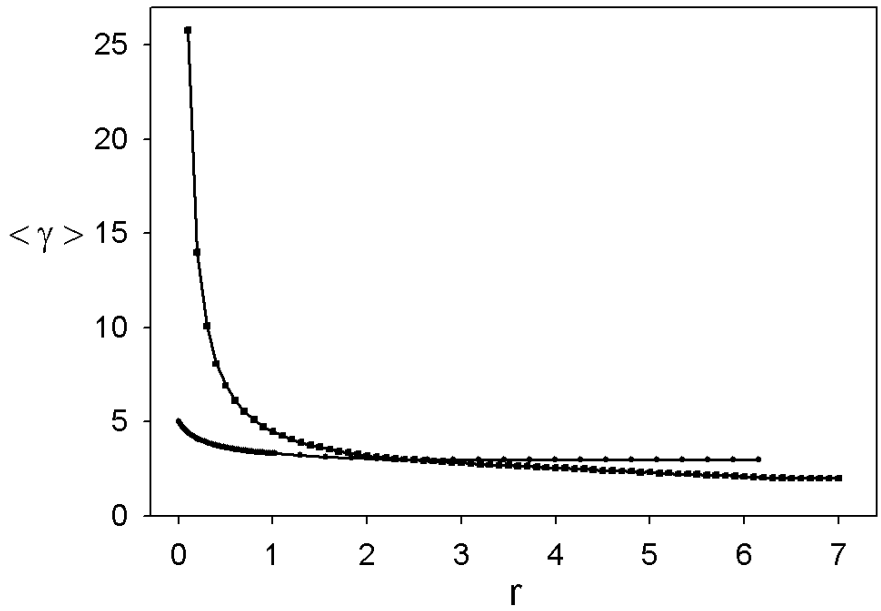

Figure 3.5: Caging (circles) and parking (squares) numbers plotted as functions of contacting disk radius. Two radii can be identified, r_{min} and r_{max}. r_{min} is the intersection point of the caging and parking numbers. r_{max} is the maximum radius for which a unit sphere can have three contacts. Note the difference in parking and caging number for $r \to 0$ and $r \to r_{max}$.

Fig. 3.5). For uncorrelated point contacts the parking number goes to infinity, while for large radii the parking number reaches its minimum value of two.

3.5. Caging numbers for three-dimensional spheres

The approach previously discussed can be extended to three-dimensional spheres caged by hard spheres of arbitrary size. A hard sphere contact excludes an area (a spherical cap) on a unit sphere surface where no other spheres can be placed,

$$A_{excl} = 2\pi(1 - \cos[2\arcsin(r/(r+1))]) \tag{3.19}$$

The n contacts divide the surface of the three-dimensional sphere into $(\frac{1}{2}n^2 - \frac{1}{2}n + 1)$ sectors. Calculation of the total phase space involves double integrals over the area sectors on the sphere, taking into account the non-overlap condition, which is very hard to do. Instead, we approximate the fraction of non-caging configurations in the same way as for the two-dimensional case. Rewriting the probability for finding n points on a three-dimensional hemisphere yields

$$p_{3,n} = \left(\frac{1}{2}n^2 - \frac{1}{2}n + 1\right)\left(\frac{2\pi - (n-1)A_{excl}}{4\pi - nA_{excl}}\right)^{n-1} \tag{3.20}$$

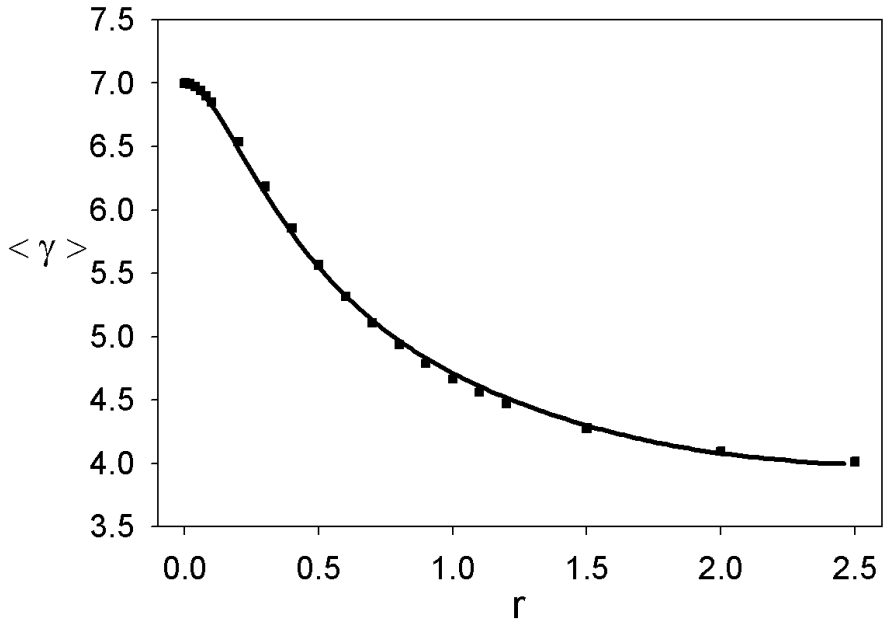

Figure 3.6: Plot of three-dimensional caging number $\langle\gamma\rangle$ as a function of the radius of the contacting spheres. The approximation method is extended to three dimensions (squares). Determination with computer simulation (line). The flattening of the caging number as $r \to 0$ is caused by the cosine term in the excluded area in (3.19).

where now areas are used instead of angles with respect to (3.18). However, $A_{excl} = \pi$ for $r = 1$. This means that according to (3.20) the probability of finding three spheres on a hemi-sphere is zero. This is clearly invalid. The area in (3.19) is the area excluded for other sphere centers. These other sphere centers exclude the area themselves and thus part of the excluded area is shared and double-counted in (3.20). To get a more meaningful result, the excluded area in (3.20) is taken to be the area that belongs exclusively to a single sphere contact, namely,

$$A_{excl} = 2\pi(1 - \cos[\arcsin(r/(r+1))]) \tag{3.21}$$

Using (3.20) and (3.21) to calculate (3.2) with upper boundary $2\pi/A_{excl}$ gives the caging number as a function of contacting sphere radius as shown in Fig. 3.6. Again the approximation agrees well with the simulation over the whole range. The caging number found numerically is 4.71 for equal-sized spheres, in agreement with the numerical value 4.79 ± 0.02 found in Ref. [28].

3.6. Discussion

We have rederived the general caging number in d dimensions using the Wendel formula (3.5). The minimum number of uncorrelated contacts necessary to cage a

sphere is $d + 1$, but on average an additional number of d spheres is needed in view of the caging number $\langle\gamma\rangle = 2d + 1$. This result for uncorrelated contacts is clearly an upper limit for the caging number for correlated sphere contacts. Our analytical result for equal-sized disks $\langle\gamma\rangle = 3.314$, which agrees precisely with simulation results, illustrates that excluded volume effects indeed reduce the caging number substantially. The physical significance of this two-dimensional caging number becomes clear when compared with other studies on hard disks.

Williams [61] attempted, using a local arrest criterion, to calculate the average contact number that stabilizes a two-dimensional random packing and found an average contact number of 3.2. Uhler and Schilling [62] showed that the contact number found by Williams is not correct because not all configurations had been taken into account. They estimated the coordination number for a loose-packed configuration by calculating the probability of a disk having n neighbours in a stable configuration. The central disk is stable if it cannot move without moving any of its neighbours. The value obtained for the average n is in the range of 3.33 - 3.42. We present here an analytical solution for the problem posed by Williams and extended the problem to disks with size ratio larger than one. Furthermore, we extended the approach from Uhler and Schilling to disks and spheres of arbitrary size. Computer simulation of disk packings were performed by Hinrichsen et al. [75] who found a coordination number around three and implied that the generated disk packing was very close to a RLP configuration. The interesting finding is that at least for two-dimensional spheres the caging number seems to be related to random loose packing. This raises the question whether it is possible to identify a contact number relevant for random *close* packing.

Uhler and Schilling attempted a local description for random dense packing but could not find a satisfying analytical description. Experiments performed by Quickenden and Tan on random dense disk packings [115] yielded a coordination number of four. The parking number for equal sized disks is 4.484, which is indeed closer to the experimental value of [115] than the caging number. A random close packing is a *maximum* in volume fraction, while the parking number is the average *maximum* number of disks that can be parked randomly on a central disk. The difference between the parking number and the coordination number in a packing is probably due to global correlations between disks, so the parking number is merely an indication for the average coordination number in a random dense packing.

It can hardly be a coincidence that the caging number is close to contact numbers found in random loose packings. In random loose packing there is no long-range ordering and the packing should be static. From the static condition it follows that the net sum of forces on a particle is zero. The "loose" in random loose packing signifies the lowest reachable volume fraction that satisfies the two mentioned conditions. The caging of spheres described in this work yields a local description of random configurations of

spheres. Each of these configurations satisfies the condition that a combination of forces can be chosen which make the net sum of forces on the central sphere zero. The generation of a single configuration is stopped as soon as the central sphere is caged. Thus a minimum number of spheres is added and thus the local volume fraction is also a minimum or at least close to it. A random loose packing could therefore be modelled as a distribution of these cages since each cage satisfies the requirements for random loose packing. The distribution of cages needs to be such that no long-range order is introduced.

It should be noted that the parking and caging numbers constitute a local description of coordination numbers in random packings. Global correlations in a packing due to collective effects of particles are not taken into account. For random loose packing the collective effects, as mentioned earlier, seem to be small enough to allow a purely local description via the caging number. However, for random close packing more global correlations, as manifested, for example, by the full pair distribution function, cannot be ignored. In the field of dynamical arrest lattice models have been developed to incorporate collectivity [116, 117]. It is interesting to see in future work, whether the concepts of these lattice models can be used to incorporate global effects in our continuum model.

In lack of an analytical solution for caging by disks with a size ratio $r < 1$ we have used an approximation to account for excluded volume effects that reproduces the numerical results quite well. The difference in value between the approximation and computer simulation of the caging number are due to rewriting the problem from sequentially placing n disks to stating that there are already n disks present, which modifies the probability distribution.

From Fig. 3.3 two radii can be identified in the curve for the caging number. The minimum radius at which the caging number is always three and the maximum radius where the central disk just fits in the pore created by three large spheres. These radii are given by

$$r_{min} = \frac{1}{\sqrt{2}-1} \approx 2.41 \quad \text{and} \quad r_{max} = \frac{1}{(2/\sqrt{3})-1} \approx 6.46 \tag{3.22}$$

Comparing the caging number and the parking number we see that for $r \leq r_{min}$, the parking number is larger than the caging number as expected. However, for $r > r_{min}$ the parking number is below the caging number, because in the calculation of the caging number, non-caging configurations are not taken into account. These non-caging configurations are counted in the calculation of the parking number because it is possible to generate configurations with only two disks. For large r the parking number is thus between two and three. This excluded volume effect also occurs in random bidisperse packings where a small disk can get stuck between two large disks while not being caged. For small r the parking number is much larger than the caging number. In bidisperse

packings, where the number of small particles is much larger than the number of large particles, the number of contacts on large particles clearly exceeds the coordination number in a packing of equal-sized disks. This could be seen as a parking process of small disks on a large disk. It is interesting to study this effect in bidisperse packings in more detail [118]. Sitharam and Shimizu [119] found a coordination number around 3.3 for loose packings and a coordination number around 4.1 for dense packings of a log-normal distribution of disk sizes. Sinelnikov et al. [120] found a contact number for a bidisperse disk system on a plane that did not exceed three for a 'loose' packing from the standpoint of mechanical stability. After compression to the center the average contact number was 4. From the caging numbers in Sec. 3.4 for disk contacts of arbitrary size, it is clear that the number of contacts should indeed be in the range from 3.0 to around 4.0 (see Fig. 3.3).

The approximation in three dimensions shows the same trend as the two-dimensional case. The minimum radius at which the sphere is always caged with four contacts appears to be 2.41, which is the same as in two dimensions. Three disks with this radius always cage a central disk. Now extend the disks to three-dimensional spheres. The central sphere is caged in the plane. Adding a fourth sphere blocks one translation perpendicular to the plane and leaves one free. The probability to have three spheres in one plane that contains the central sphere is infinitesimally small and thus the four spheres will always cage the central sphere. The maximum radius in which the central sphere can fit in the pores of the four larger spheres is given by

$$r_{max} = \left(\frac{1}{2}\sqrt{6} - 1\right)^{-1} \approx 4.45 \tag{3.23}$$

For equal sized three-dimensional spheres the caging number $\langle\gamma\rangle = 4.71$ is again much smaller than the parking number $\langle z\rangle = 8.7$ and smaller than the caging number for point contacts $\langle\gamma\rangle = 7$. An analytical expression for the caging of spheres in three dimensions as was found for the two-dimensional case is a very difficult task because not only p_3 has to be calculated but also p_4 till p_8. To find these probabilities one needs to integrate over the surface of a sphere, which is much more complex than the line integrals needed for two-dimensional disks.

3.7. Conclusions

We report an analytical solution for the caging of a two-dimensional sphere by sequentially placed, contacting neighbour disks with a size ratio equal to or greater than unity. The analytical caging number, which fully incorporates excluded volume effects, agrees well with a numerical simulation of the two-dimensional caging problem.

The caging problem for contacting disks smaller than the central disk can be slightly modified to the calculation of the caging probability for n disks placed simultaneously on the central disk. This modified problem can be solved exactly and the outcome

approximates the numerical result for caging by sequential addition of neighbour disks quite well. In a similar approximate manner we calculate fairly accurate caging numbers for three-dimensional spheres. Extension to d dimensions is possible provided the $(d-1)$-dimensional excluded volume is known.

Our results for non-overlapping hard spheres show that excluded volume effects substantially reduce the caging number in comparison with caging by uncorrelated contacts. The latter forms an upper bound for the caging number which we rederive using Wendel's formula for the probability for n randomly placed points to share one hemisphere on a d-dimensional sphere.

We have also numerically evaluated the parking number for non-equal sized disks. A comparison with caging numbers shows that the latter are indicative for the average contact number in random loose packings of monodisperse spheres, whereas parking numbers seem to approach the average coordination number in random close packing. The physical significance of caging and parking numbers is also apparent in random bidisperse packings where, in addition to caging effects for equal-sized particles, one observes the parking number for many small disks simultaneously contacting a large one.

Our calculations relate to a *local* description of coordination in granular matter or colloidal sphere packings. A next step is to model more global correlations, for example by including additional shells of neighbours in the caging or parking model for random sphere packing to include collective effects.

APPENDIX A: The Wendel formula

Wendel's formula (3.5) appears to be unknown in the context of sphere arrest. For later reference we briefly rederive it. A contact x_i on a d-dimensional sphere is a d-dimensional vector. A vector y is perpendicular to none of the x_i and (y, x_i) represents a dot product. Then the sequence $s_y = \{\text{sign}(y, x_i)\}$ is a random point in the set $S = \{s\}$ of all ordered N-tuples consisting of plus and minus signs. A specified s is said to occur if there is a y such that $s_y = s$.

A d-dimensional sphere is a non-caged sphere if all n points lie on one single hemisphere. If all n points are on the same hemisphere then there exists a vector y for which the sequence $s_+ = \{+, +, \cdots, +\}$ exists. By definition the probability that a d-dimensional sphere is not caged, $p_{d,n}$, is the probability that s_+ occurs. Since any s can be changed into any other by reflecting appropriate x_i through the origin it follows that all s are equally likely to happen. Hence

$$2^n p_{d,n} = Q_{d,n} \tag{3.24}$$

where n is the number of contacts, and $Q_{d,n}$ is the number of different s that occur. To calculate $p_{d,n}$ it suffices to know $Q_{d,n}$. A contact point x_i is the normal for a hyperplane

X_i that cuts a d-dimensional sphere in two. Then Q is the number of sectors formed by hyperplanes X_i because each sector consists of all vectors y for which s_y has a fixed value.

Adding a hyperplane X_n cuts a number of sectors Q^1 in two and leaves a number Q^2 intact. Thus $Q_{d,n-1} = Q^1 + Q^2$ and $Q_{d,N} = 2Q^1 + Q^2$. It follows that

$$Q_{d,n} = Q_{d,n-1} + Q^1 \tag{3.25}$$

The intersection of the hyperplane X_n and the d-dimensional sphere is a $(d-1)$-dimensional sphere. The sets of intersections $X_i \cap X_n$ are hyperplanes in $(d-1)$-dimensional space. The union of intersections $\cup_{i=1}^{n-1} X_i \cap X_n$ cut the $(d-1)$-dimensional sphere in $Q_{d-1,n-1}$ sectors. Thus there are $Q_{d-1,n-1}$ intersections upon adding X_n. So

$$Q_{d,n} = Q_{d,n-1} + Q_{d-1,n-1} \tag{3.26}$$

This recurrence relation (3.26) was also derived by Peters et al. [28] and then used to calculate the caging number directly. Here the probability of finding n points on the same hemisphere will be calculated from the same recurrence relation. From (3.24) and (3.26) it follows

$$p_{d,n} = \frac{1}{2}(p_{d,n-1} + p_{d-1,n-1}) \tag{3.27}$$

solving this recurrence relation together with the boundary conditions [121]

$$p_{1,n} = \left(\tfrac{1}{2}\right)^{n-1} \quad \text{and} \quad p_{d,n} = 1 \quad \text{if} \quad 0 \le n \le d \tag{3.28}$$

gives

$$p_{d,n} = \left(\frac{1}{2}\right)^{n-1} \sum_{k=0}^{d-1} \binom{n-1}{k} \tag{3.29}$$

For example, in two dimensions ($d = 2$) each contact creates two new sectors. Therefore the number of sectors for the nth contact is $2n$. Substitution in (3.24) yields then $p_{2,n} = n(1/2)^{n-1}$ as is also found by directly substituting $d = 2$ in (3.29).

APPENDIX B: Derivation of the caging number in d dimensions

Here we derive the caging number for uncorrelated contacts in d dimensions, making use of Wendel's result for the probability of finding n contacts on a d-dimensional sphere. Substitution of (3.5) in (3.2) produces

$$\begin{aligned}\langle\gamma\rangle_d &= 1 + d + \sum_{n=d+1}^{\infty} \left(\frac{1}{2}\right)^{n-1} \sum_{k=0}^{d-1} \binom{n-1}{k} \\ &= 1 + d + \sum_{n=d}^{\infty} \sum_{k=0}^{d-1} \left(\frac{1}{2}\right)^{n} \binom{n}{k}\end{aligned} \tag{3.30}$$

The first term in the summation of (3.30) is the power series

$$\sum_{n=d+1}^{\infty} x^{n-1} = -\frac{x^d}{x-1} \tag{3.31}$$

The other terms in (3.30) can be calculated using (3.31)

$$\sum_{n=d+1}^{\infty} x^{n-1} \binom{n-1}{k} = \frac{x^k}{k!}\frac{\partial^k}{\partial x^k} \sum_{n=d+1}^{\infty} x^{n-1} = \frac{x^k}{k!}\frac{\partial^k}{\partial x^k}\left(\frac{-x^d}{x-1}\right) \tag{3.32}$$

The kth derivative of (3.31) is

$$\frac{\partial^k}{\partial x^k}\left(\frac{-x^d}{x-1}\right) = \sum_{i=0}^{k} \frac{(-1)^{k+1-i}\binom{d}{i} k! x^{d-i}}{(x-1)^{k+1-i}} \tag{3.33}$$

Combining pairs of two terms of the summation in (3.30) such as $k = 0$ and $k = d-1$, $k = 1$ and $k = d-2$, gives for the kth pair,

$$\begin{aligned}
&\sum_{n=d+1}^{\infty} x^{n-1}\left[\binom{n-1}{k} + \binom{n-1}{d-1-k}\right] \\
&\qquad = x^k \sum_{i=0}^{k} \frac{(-1)^{k+1-i}\binom{d}{i} x^{d-i}}{(x-1)^{k+1-i}} \\
&\qquad + x^{d-1-k} \sum_{i=0}^{d-1-k} \frac{(-1)^{d-k-i}\binom{d}{i} x^{d-i}}{(x-1)^{d-k-i}}
\end{aligned} \tag{3.34}$$

By setting x to $\frac{1}{2}$ one obtaines

$$\begin{aligned}
&\left(\frac{1}{2}\right)^{d-1}\left[\sum_{i=0}^{k}\binom{d}{i} + \sum_{i=0}^{d-1-k}\binom{d}{i}\right] \\
&= \left(\frac{1}{2}\right)^{d-1}\left[\sum_{i=0}^{d}\binom{d}{i} - \sum_{i=d-k}^{d}\binom{d}{i} + \sum_{i=0}^{k}\binom{d}{i}\right]
\end{aligned} \tag{3.35}$$

Using

$$\sum_{i=0}^{d}\binom{d}{i} = 2^d \tag{3.36}$$

and realizing that the last two terms in (3.35) cancel yields

$$\left(\frac{1}{2}\right)^{d-1}\sum_{i=0}^{d}\binom{d}{i} = 2 \tag{3.37}$$

In the summation in (3.30) there are $\frac{1}{2}d$ pairs that all contribute two to the summation, if d is even, and $(d-1)/2$ pairs if d is odd. Inserting (3.37) in the summation in (3.30)

leads to

$$\sum_{n=d}^{\infty}\sum_{k=0}^{d-1}\left(\frac{1}{2}\right)^{n}\binom{n}{k}=\frac{d}{2}*2=d \tag{3.38}$$

For odd d, the single term for $k=(d-1)/2$ needs to be evaluated, this term contributes one, so the sum in (3.30) is also equal to d for uneven d. Substitution of (3.38) in (3.30) yields finally

$$\langle\gamma\rangle_d = 2d+1 \tag{3.39}$$

4

Geometrical cluster ensemble analysis of random sphere packings

Abstract

We introduce a geometric analysis of random sphere packings based on ensemble averaging of hard-sphere clusters generated via local rules including a non-overlap constraint for hard spheres. Our cluster ensemble analysis matches well with computer simulations and experimental data on random hard-sphere packing with respect to volume fractions and radial distribution functions. To model loose as well as dense sphere packings various ensemble averages are investigated, obtained by varying the generation rules for clusters. Essential findings are a lower bound on volume fraction for random loose packing that is surprisingly close to the freezing volume fraction for hard spheres and, for random close packing, the observation of an unexpected split peak in the distribution of volume fractions for the local configurations. Our ensemble analysis highlights the importance of collective and global effects in random sphere packings by comparing clusters generated via local rules to random sphere packings and clusters that include collective effects.

4.1. Introduction

Random particle packings [9] are ubiquitous in nature and technology and can be found in divergent topics such as granular media (sand, powders), stacks of catalyst carriers and random fibers in biological cells [122]. Despite the fact that packed particles very often have a non-spherical shape [33, 35, 98], studies of random packings have focused mostly on spheres [36, 37, 44, 45, 123]. Such studies have revealed two distinct limits of random packing, namely random close packing (RCP) and random loose packing (RLP).

Random close packing is associated with a maximum density for a collection of randomly positioned spheres. In the extensive experiments recently performed by Aste et al. [44,123], as well as in recent computer simulations [78,106] a value of around 0.64 is found as an upper limit for the RCP sphere volume fraction, in line with earlier literature [36,37,44,45,123] on random sphere packings. A debated issue is whether a unique well-defined RCP density exists for this maximum random state. Torquato et al. [58] argue that random close packing is actually ill-defined and introduce the alternative concept of a maximally random jammed state. This state refers to the largest density for which an order parameter is minimized, a criterion also used by Stachurski to define an ideal amorphous solid [124]. Another definition for RCP introduced by Roux [59] states that ideal random close packings of hard spheres are equilibrium states devoid of crystal nuclei that remain stable without friction. Compaction procedures are regarded as recipes to minimize the effects of friction. The definitions of both Torquato [58] and Roux [59] imply the existence of a well-defined maximum density: either an order parameter has to be minimized or the constraint of no crystal nuclei has to be enforced to find the maximum RCP density.

While RCP refers to the density maximization of a disordered sphere packing, RLP is associated with minimizing the packing density to the lowest value for which a collection of randomly positioned spheres is mechanically stable in the limit of zero gravity [45]. Mechanically stable means here that the packing is in static equilibrium under a set of externally applied forces.

Solving any of the global packing problems mentioned above is quite a challenge. In this paper our primary aim is to investigate an alternative to such global extremum problems, starting from the perspective of random sphere packings composed of sphere *clusters* rather than single spheres. As typical cluster radius we choose the distance over which the pair distribution decays such that the main peaks of a distribution function from an experimental sphere packing are captured, i.e. where the distribution function starts to oscillate around one. This approach reminds of De Gennes's model for structural glasses where clusters of atoms or particles rather than single entities are the building blocks of a structural glass [125].

In more detail our approach is as follows. We calculate the packing density from the frequency distribution of Voronoi volumes similar to the approach of Finney [44,52,123] who gave an estimate for the RCP volume fraction calculated from a Voronoi analysis of experimental determined sphere configurations. Shahinpoor [126] used Voronoi volumes to construct a statistical mechanical analysis of stable random packings of granular materials where ensemble averages are obtained from a probability distribution as a function of void ratio. In this paper we combine the concept of clusters as building blocks with the statistical mechanics description from Shahinpoor to calculate ensemble averages of properties of random packing such as the probability distribution of Voronoi volumes. To obtain this distribution in our analysis a random sphere packing is considered as an ensemble of clusters of identical hard spheres, which models the constraints of non-overlap and random positioning. These clusters are generated according to well-defined local rules. Properties such as volume fraction, contact numbers and radial distribution function are calculated as a "geometric" ensemble average over these clusters, which can be seen as the geometric equivalent of an ensemble average over phase space in the statistical mechanics of thermal systems. Generation rules for constructing sphere clusters are varied to model properties of random loose as well as close packing. First we review in Sec. 4.2 some important concepts in random packing, followed by a description of generation methods for cluster ensembles in Sec. 4.3. In Sec. 4.4 we discuss results from the cluster ensemble analysis, and make a comparison to experimental sphere packings, in particular the experimental data of Aste et al. [44,123] who to the best of our knowledge has analyzed the largest number of spheres so far.

4.2. Preliminary

The essential approximation underlying our cluster ensemble analysis is that any sphere and its neighboring spheres in a random packing form a local configuration that is statistically independent from the other sphere configurations. This approximation enables us to use a mathematically well-defined criterion for generating geometric local cluster configurations with corresponding ensemble averages of, for example, the packing fraction. The ensemble averages are compared to values obtained from experimental and simulated random packings. Using local rules only allows to assess any influence of global and collective effects on the properties of a random packing.

The rules for generating a cluster should produce sphere configurations that mimic the local structure in a random packing. In a stable random packing the majority of spheres are arrested at their positions whereas a minority of about $1-3\%$ of spheres can rattle [118] when the whole packing is shaken. The generated clusters must also have most spheres arrested. Donev et al. [30, 31] distinguish for packed spheres three types of jamming, namely spheres that are locally jammed, collectively jammed or strictly jammed. A sphere is locally jammed if it cannot translate when the positions of all other

spheres in the packing are fixed. Collectively jammed and strictly jammed are more stringent conditions [30] where a collection of spheres or all spheres cannot translate or rotate. Peters et al. [28] analyze a specific case of local jamming, namely the caging of a sphere with the corresponding caging number defined as the average *minimum* number of spheres that need to be placed at random on the surface of sphere S to block all translational degrees of freedom of S with the condition of non-overlap for spheres [28, 127]. In a disorded sphere packing it is expected that as a first approximation the contacts on each sphere are distributed randomly over the sphere surface, constrained by the non-overlap condition. Thus in our approach, for spheres in a random packing to be locally jammed, the average number of contacts at least equals the caging number if contacts are distributed randomly on the surfaces of spheres.

The mathematical criterion for a sphere S to be non-caged, namely that a hemi-sphere on S can be chosen such that all contacts are part of that hemi-sphere [28, 127], can be cast into a problem of contact normal forces to give a more physical picture. For a non-caged sphere S all vector sums of non-zero normal forces applied at the contact points are non-zero [113]. The contact forces can only push spheres. This definition of non-caging plus the requirement that contact forces are always directed to the center sphere yields the following equation:

$$f_1\mathbf{n}_1 + f_2\mathbf{n}_2 + \cdots + f_n\mathbf{n}_n = \mathbf{0} \quad \text{with} \quad f_i \geq 0 \tag{4.1}$$

which can be written as the system of linear equations

$$\begin{aligned} f_1\mathbf{n}_1 \cdot \mathbf{n}_1 + f_2\mathbf{n}_2 \cdot \mathbf{n}_1 + \cdots + f_n\mathbf{n}_n \cdot \mathbf{n}_1 &= \mathbf{0} \\ f_1\mathbf{n}_1 \cdot \mathbf{n}_2 + f_2\mathbf{n}_2 \cdot \mathbf{n}_2 + \cdots + f_n\mathbf{n}_n \cdot \mathbf{n}_2 &= \mathbf{0} \\ &\cdots \\ f_1\mathbf{n}_1 \cdot \mathbf{n}_n + f_2\mathbf{n}_2 \cdot \mathbf{n}_n + \cdots + f_n\mathbf{n}_n \cdot \mathbf{n}_n &= \mathbf{0} \end{aligned} \tag{4.2}$$

or

$$A\mathbf{f} = \mathbf{0} \quad \text{with} \quad \mathbf{f} \geq 0 \tag{4.3}$$

Here A is a $n \times n$ matrix whose elements are the dot products of the normal vectors n_i and f is a vector which contains the force magnitude of the ith contact with normal n_i. The trivial solution to this system of equations is $\mathbf{f} = \mathbf{0}$. If a non-trivial solution exists then a sphere is caged and the relative acceleration of two spheres at each contact point can be made zero under the application of a set of non-zero contact forces. In a static packing each local configuration has to satisfy (4.1) with exception of rattlers.

In addition to contact forces from other spheres, particles in an experimental random packing may also be affected by the container wall. Spheres in a box might crystallize since the face centered cubic (FCC) or hexagonal close packed (HCP) lattice minimizes gravitational potential energy. However, when spheres in a box are quenched fast

enough a stable disordered state is formed. There are several examples of sphere packings being tapped and shaken yet they stay disordered and do not settle into an FCC or HCP lattice [40, 41]. In the present work sphere cluster ensembles are generated in unbounded space, which is convenient because it allows to study random packing without influence of a wall, in the bulk of a random packing. Having described the criteria a cluster has to satisfy, we will now outline the various methods for generating clusters with specific packing properties.

4.3. Methods

We have investigated three types of algorithms to generate configurations based on a local rule to which we refer to, respectively, as the caging method, the parking method and the drop and roll method. For comparison, an additional algorithm was developed for taking collective effects into account, namely a small modification of the mechanical contraction method [35,118]. The cluster ensemble analysis for the different algorithms is compared to computer simulations of random packing in a box with periodic boundary conditions and to experimental disordered sphere packing.

4.3.1. Caging method

The caging method starts with placing a central sphere S at the origin. Neighboring spheres are subsequently added to S at random fixed positions until S is caged according to the definition in Sec. 4.2. The added neighbor spheres in the first coordination shell are in turn caged by adding more spheres at random that yield the second shell. After the second shell, a third shell is created in the same manner. Fig. 4.1a illustrates the model in two dimensions and Fig. 4.2a shows a three-dimensional example.

4.3.2. Parking method

The parking method is very similar to the caging method except that it is based on the parking number [27], defined as the average maximum number of spheres that can be placed at random on a single sphere including a non-overlap condition. Now a first shell of neighboring spheres is formed by adding spheres at random fixed positions on a central sphere until it is no longer possible to park more spheres. The added neighbor spheres form again the first shell. Note that owing to the definition of the parking number the central sphere is always caged. The spheres from the first shell then form the basis for the second shell. A second shell is formed by randomly parking the maximum number of fixed spheres on the first shell, a procedure which can be repeated for additional shells (Figs. 4.1b and 4.2b).

4.3.3. Drop and roll method

Our third method is a "drop and roll" model inspired by Ref. [128]. The first coordination shell is created just as in the parking model, but the next shells are formed

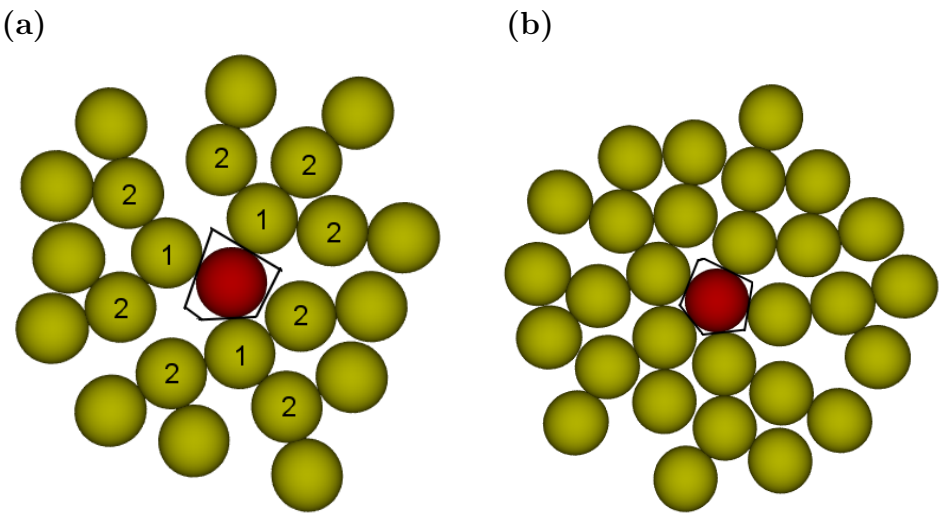

Figure 4.1: Examples of two-dimensional clusters generated. The volume fraction follows from the area of the center disk divided by the area of its Voronoi cell. Shells 1 and 2 are denoted with their respective numbers. Both clusters show a string-like structure. (a) Typical cluster generated with caging method. (b) A cluster generated with the parking method has a higher volume fraction than a caging cluster.

by a drop and roll mechanism, i.e. a sphere is dropped on the cluster from a random direction and then rolled over the cluster surface until it contacts at least three other spheres. This is repeated for a fixed number of spheres (Fig. 4.2c).

4.3.4. Mechanical contraction method for clusters

The fourth procedure is a modified version of the mechanical contraction method for spheres [35, 118]. For a convenient comparison with the previous three local methods a central sphere S is held fixed at the origin around which a gas of spheres is generated. The largest distance from a sphere center to the origin defines the radius of a bounding sphere that comprises all sphere centers. The volume of the bounding sphere is reduced and the spheres are moved towards S by scaling their position. Overlap between the spheres is removed as described elsewhere for the mechanical contraction method (MCM) [35].

When the volume of the bounding sphere is minimized, the enclosed spheres start to crystallize to fit inside the bounding sphere since the most efficient packing to fill space is the FCC or HCP packing [7]. To prevent global crystallization in the container any overlap between a sphere and the bounding sphere is not removed. Local crystallinity is monitored by local bond order parameters and contact numbers. As the bounding sphere shrinks, the volume fraction will at some point exceed 0.64 and a new bounding sphere is calculated. The above steps are repeated until a termination condition is

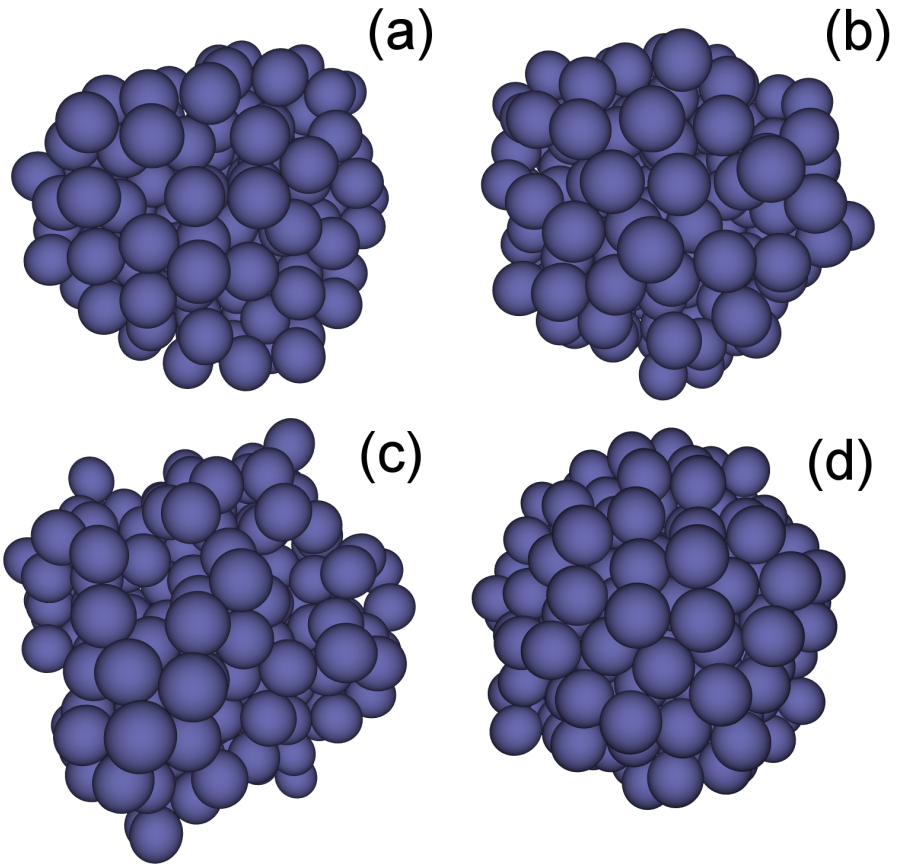

Figure 4.2: Graphical representations of the generated clusters. The volume fraction increases in each picture. (a) Example of a cluster from the caging method. (b) The parking method. (c) Drop and roll method. (d) Mechanical contraction method.

met, namely when the newly calculated bounding sphere is larger then the previously calculated bounding sphere. At the termination point the cluster will dilate because spheres have to move outwards to remove overlap caused by scaling their position and then the bounding radius increases. This algorithm models collective effects from the presence of other spheres, in contrast to the previous three local models involving only positioning of a single sphere per step. A typical example of a cluster is shown in Fig. 4.2d.

4.3.5. Computing average properties of a cluster ensemble

For comparison to the volume fractions of a random sphere packing we calculate the ensemble average of the local cluster volume fraction. The latter is calculated employing a Voronoi cell, i. e. the region of space closer to a specific point than other points in the same point set. The volume of the Voronoi cell is the volume closest to the center of a sphere and the local volume fraction is obtained by dividing the volume of a sphere by its Voronoi volume [52, 123, 129] (see Fig. 4.1). Contact numbers and the radial

distribution function for the central sphere are also calculated by averaging over the ensemble of clusters. The calculated ensemble averages have an uncertainty because a sphere packing consists of clusters that are merged together and it is not clear how exactly the merging of clusters will influence the calculated averages.

Furthermore, the Q_4 and Q_6 orientational bond order parameters [32] were calculated to compare the orientational order with experimental data from [123]. Q_4 and Q_6 are calculated by considering the local bonds connecting a sphere to its neighbors from the Voronoi diagram in stead of the neighbors within a fixed distance [123]. Q_l is defined as:

$$Q_l = \left(\frac{4\pi}{2l+1} \sum_{m=-l}^{l} |\langle Y_{l,m}(\theta(\mathbf{r}_i), \phi(\mathbf{r}_i))\rangle|^2 \right)^{1/2} \tag{4.4}$$

where the angular brackets $\langle ... \rangle$ denotes the average over the local bonds i consisting of the vectors connecting a sphere with its neighbors.

4.3.6. Modified mechanical contraction method

Properties of the clusters are also compared to random sphere packings generated by the mechanical contraction method (MCM). Here a slightly different method is used: instead of contracting a system of spheres, the radii of the spheres are increased which has the same effect. In the original MCM sphere positions are scaled by a factor depending on the volume of the simulation box. This volume dependence is removed by keeping the simulation box fixed and instead to increase the radius of the spheres similar to the extended Lubachevsky-Stillinger algorithm by Kansal et al. [130]. Overlapping spheres are separated employing the same overlap removal scheme as in MCM. As the spheres grow in size it becomes impossible at a certain point to remove the overlap. Then the volume of the simulation box is increased and the mentioned steps are repeated a fixed number of times. In the next section the results for the various algorithms are evaluated.

4.4. Results and Discussion

The geometric ensemble averages over 1000 clusters for the four algorithms from Sec. 4.3 are listed in Table 4.1. It should be noted that the averages over the total cluster must be treated with care since it is not known how to combine the clusters into a packing. Part of the outer shells can be shared which modifies the global average. A visualization of a typical cluster generated by each algorithm is shown in Fig. 4.2. The distribution in contact numbers for the center sphere and the first shell is plotted in Figs. 4.3 and 4.4. The distribution of local volume fractions for the center sphere and first shell are given in Figs. 4.5 and 4.6. The normalized radial distribution function (rdf) for the central sphere was calculated and averaged over all generated clusters in

Table 4.1: Ensemble averages for the four cluster algorithms.

	N^a	N_c	N_1	N_2	ϕ	ϕ_c	ϕ_1	ϕ_2
Cage method	3.54	4.711	4.593	3.3105	0.495	0.497	0.502	0.494
Park method	3.59	8.392	4.42	3.186	0.528	0.625	0.551	0.519
Drop and roll	7.442	8.38	6.618	7.623	0.603	0.650	0.616	0.599
MCM cluster	6.341	6.274	6.333	6.344	0.645	0.633	0.641	0.646
MCM packing	5.8				0.62			

a) N is the average contact number of the first two shells. N_c, N_1 and N_2 is the average contact number, respectively, for the center sphere, the first shell and the second shell. ϕ is the average volume fraction of the first two shells. ϕ_c, ϕ_1 and ϕ_2 are the average of the local volume fraction for respectively, the center sphere, the first and second shell.

the ensemble (see Fig. 4.7). For all methods the rdf has a first peak at one diameter, corresponding to spheres in contact with the central sphere. For the caging method the rdf shows almost no structure after the first two peaks and the second peak is not split into two, in contrast to the other methods that yield a split second peak and a broad peak for r less than three sphere diameters. The first peak of the split peak is due to tetrahedral arrangement of the spheres, which is absent in the caging method. Alignment of three spheres in a row produces the second peak. In Fig. 4.8, the Q_4 and Q_6 for a cluster ensemble are plotted as pairs and compared with the Q's calculated for a perfect crystal structure, namely the FCC, body centered cubic (BCC), HCP and icosahedral arrangement. The four cluster algorithms show a distribution of Q_4-Q_6 pairs, where the majority of pairs is different from the Q_4-Q_6 pairs for the crystal structures which shows that the generated clusters are indeed random structures. Similar to what is reported by Aste [123] there is no icosahedral ordering present in the clusters or in the sphere packings (Figs. 4.8e,f).

4.4.1. Caging results

For the caging method we find the same caging number of 4.71 as reported earlier [127] as contact number for the center sphere. In the next two shells the contact number is lower than the caging number. The volume fractions found with the caging method are surprisingly close to the freezing volume fraction 0.495 of hard spheres and are roughly constant through all shells. The similarity between the freezing volume fraction and caging volume fraction can be tentatively explained as follows. Spheres in a fluid are

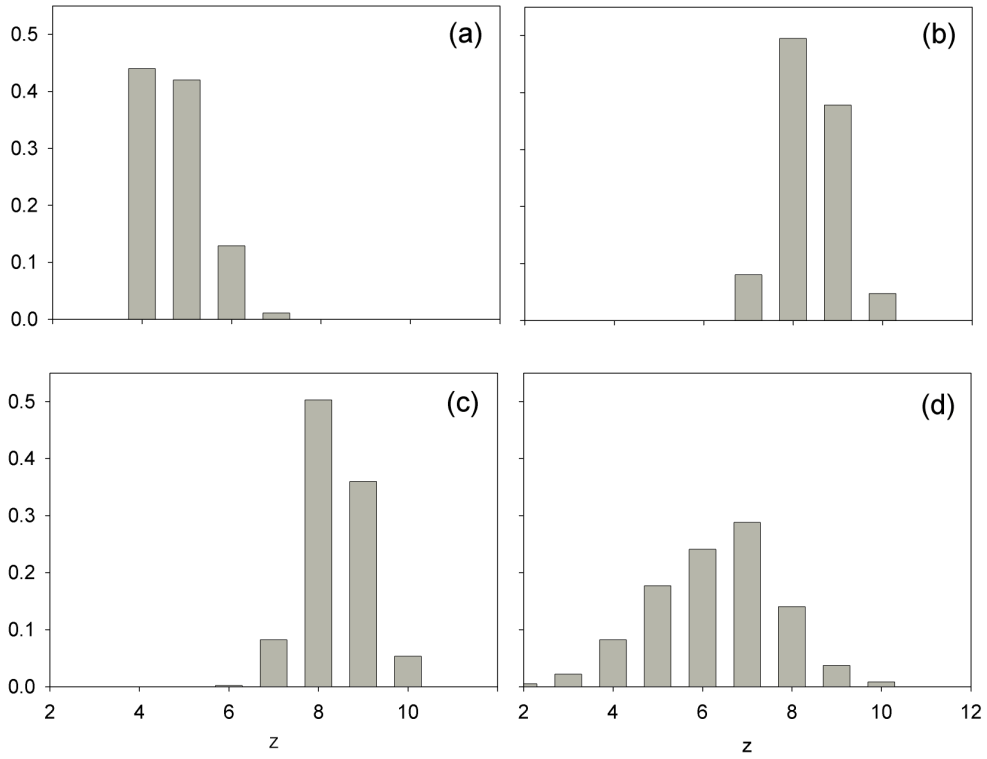

Figure 4.3: Distribution of contact numbers for central sphere. (a) Caging method. (b) Parking method. (c) Drop and roll method. (d) Cluster MCM method.

immobilized due to geometric restrictions when a system of hard spheres starts to freeze upon increasing the density. Spheres in the caging cluster ensemble represent a static snapshot of such a disordered immobilized state. Freezing of hard spheres, of course, is a thermal process so when the motion of spheres is blocked, either the internal energy of the spheres needs to increase or the structure of the system needs to change. Since freezing occurs at constant temperature this means that the structure must change. The caging cluster method generates disordered structures in which spheres cannot translate and thus indeed might represent a density at which freezing occurs. This explanation, it should be noted, is clearly tentative since freezing is a dynamic process whereas caging in our definition is a pure geometrical concept. The volume fraction of a caging cluster ensemble is compared with experimental data on random sphere packings by extrapolating a plot (see Fig. 4.9) of volume fraction versus contact number from Aste [123]. A best linear fit of the data was made without imposing the constraint that the fit has to intersect $z = 4$ at volume fraction 0.55. For the local caging number 4.71 a volume fraction of 0.54 is found. With the constraint the fit gives a volume fraction 0.57. The caging volume fraction 0.495 is lower than the random loose packing volume fraction of 0.55 found by Onoda and Liniger [45]. It makes sense that for a global configuration of spheres a higher volume fraction is necessary to achieve a stable

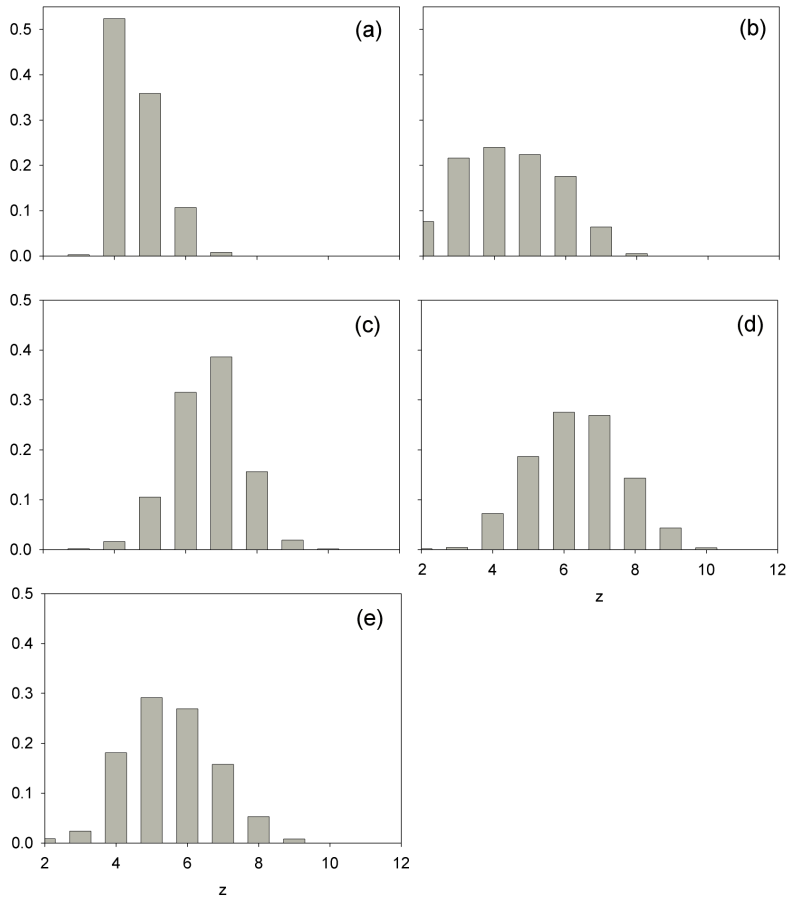

Figure 4.4: Distribution of contact numbers for spheres in the first shell. (a) Caging method. (b) Parking method. (c) Drop and roll method. (d) Cluster MCM method. (e) Distribution of contact numbers for spheres in a MCM packing.

packing and this is also illustrated by the two-dimensional example (Fig. 4.1a). It is clear from the figure that a slight stress may further compact the two-dimensional cluster to make it more stable.

Silbert et al. [78] performed molecular dynamics simulations on frictionless and frictional sphere packings, and found that the contact number of the packings depends on the friction coefficient and the coefficient of restitution of the spheres. In the limit of infinite friction the contact number asymptotes to the minimum value of four. The contact numbers for packings with a reasonably small friction coefficient are around the caging number [78]. The low friction coefficient allows the spheres to slip and for the spheres to be jammed the force in the normal direction is more important. To balance normal forces with randomly positioned contacts a contact number close to the caging number is needed. For a contact number 4.69 that is very close to the caging number, the volume fraction in packings generated by Silbert et al. [78] is 0.59, which in turn

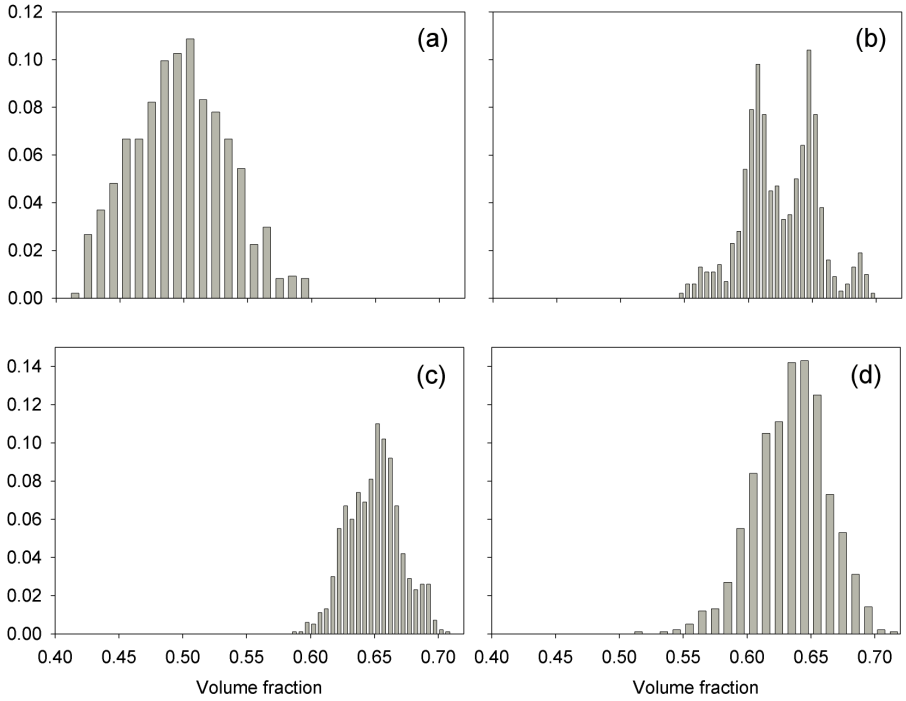

Figure 4.5: Distribution of local volume fraction for center sphere. (a) Caging method. (b) Parking method. (c) Drop and roll method. (d) Cluster MCM method.

is close to the volume fraction 0.601 in Ref. [123] where a sphere cannot move without displacing its first neighbors.

4.4.2. Parking results

For the parking method we find a reproducible, average contact number of 8.39, which is lower than the parking number 8.7 reported in [27]. For the next shell a value of 4.42 is found. Interestingly, it is not possible to achieve a value close to the parking number for the neighboring spheres. Thus by maximizing the contact number for sphere S_1, the contact number for a touching sphere S_2 is lowered because the already parked spheres on S_1 exclude volume for new spheres to be parked on S_2. In the second shell the contact number decreases further. For the parking method the volume fraction of 0.625 for the central sphere is close to the RCP density commonly found in experimental packings of 0.62 - 0.64 but for shells surrounding the central sphere this is no longer the case due to the mentioned excluded volume effects. The cluster dilutes as it grows via parking more spheres. The already parked spheres influence the placement of new spheres and this promotes growth of a string-like structure, as shown in Fig. 4.1b for two dimensions. The parking model describes the structure of a random packing reasonably well as can be seen from the radial distribution functions in Fig. 4.7 but the overall density of 0.53 is still roughly 20% below the RCP density of 0.64. Another interesting feature

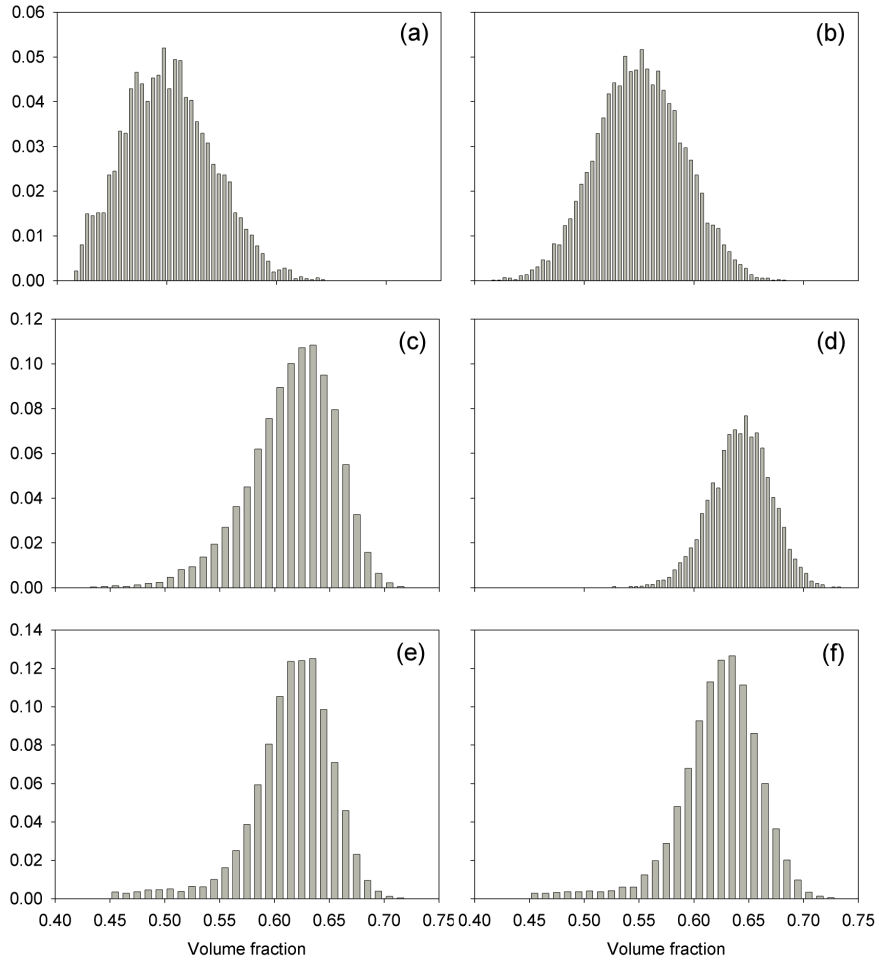

Figure 4.6: Distribution of local volume fraction for center sphere and for spheres in the first shell. (a) Caging method. (b) Parking method. (c) Drop and roll method. (d) Cluster MCM method. (e) Distribution of local volume fraction for spheres in a MCM packing. (f) Distribution of local volume fraction in an experimental random packing of hard spheres.

is present in the distribution of volume fractions for the central particle where a split peak can be seen (Fig. 4.5b) with one peak at 0.60 and one at 0.64. The origin of the split peak in the distribution is not precisely clear, but apparently there is a preference for some particular configurations due to the excluded volume effects from the non-overlap condition. Fig. 4.3b suggests a relation between the contact number and the peaks in the volume fraction distribution where the two main peaks could correspond to spheres with contact number 8 and 9. Analysis of the contact number for spheres with volume fraction in the first peak ranging from 0.595 - 0.625 and the second peak 0.625 - 0.665 confirms that 98% of spheres in the first peak have contact number 8 and 86% of spheres have contact number 9 in the second one. The distribution for the central

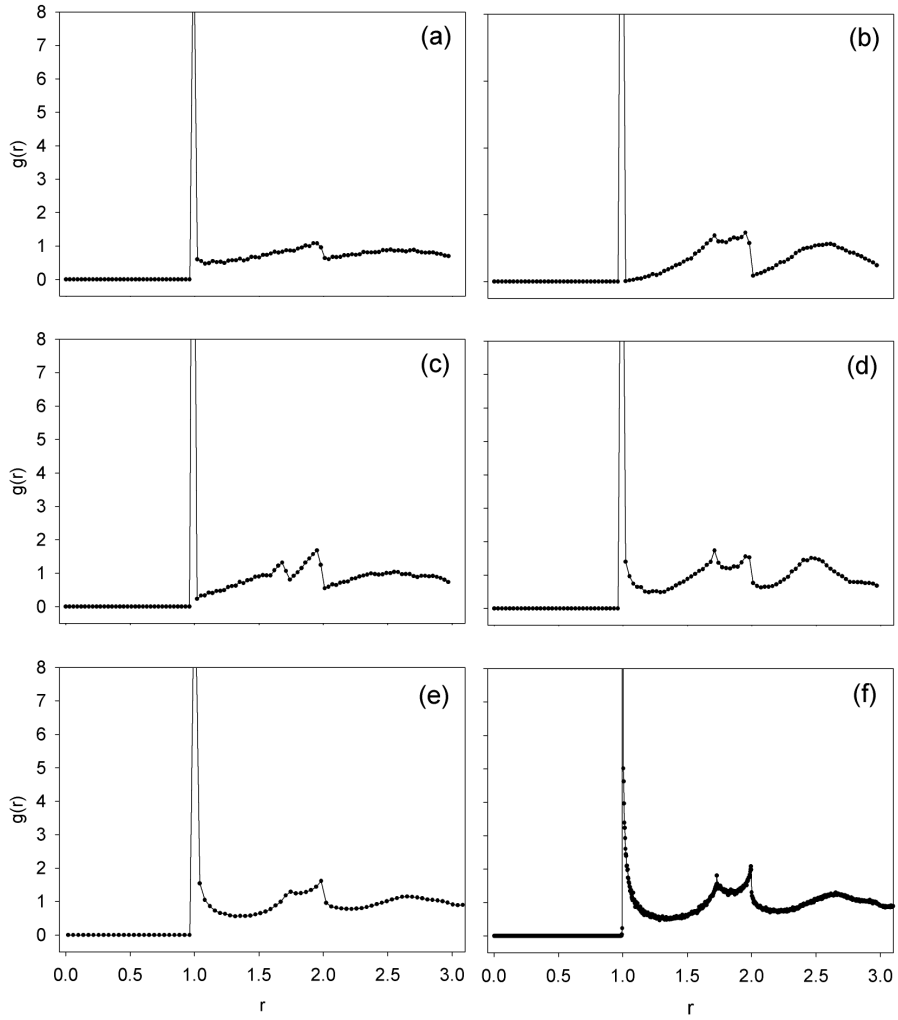

Figure 4.7: Radial distribution functions for the center sphere. (a) Caging method. (b) Parking method. (c) Drop and roll method. (d) Cluster MCM method. (e) MCM random packing. (f) Experimental random packing of hard spheres [123].

sphere supports the experimental observation that shaking and tapping a container of a random packing of spheres densifies the packing [40, 41]. Tapping apparently changes the ratio of 0.60 and 0.64 structures in a disordered sphere packing by increasing the average contact number.

4.4.3. Drop and roll method

For the drop and roll method the average number of neighbor spheres on the center sphere is the parking number as expected. For the next shell the number of contacts per sphere decreases to 6.62 and for the second shell the contact number is 7.62. The contact numbers are higher than for the parking method because the drop and roll method prevents the string-like structure as in the cluster method since the spheres are rolled

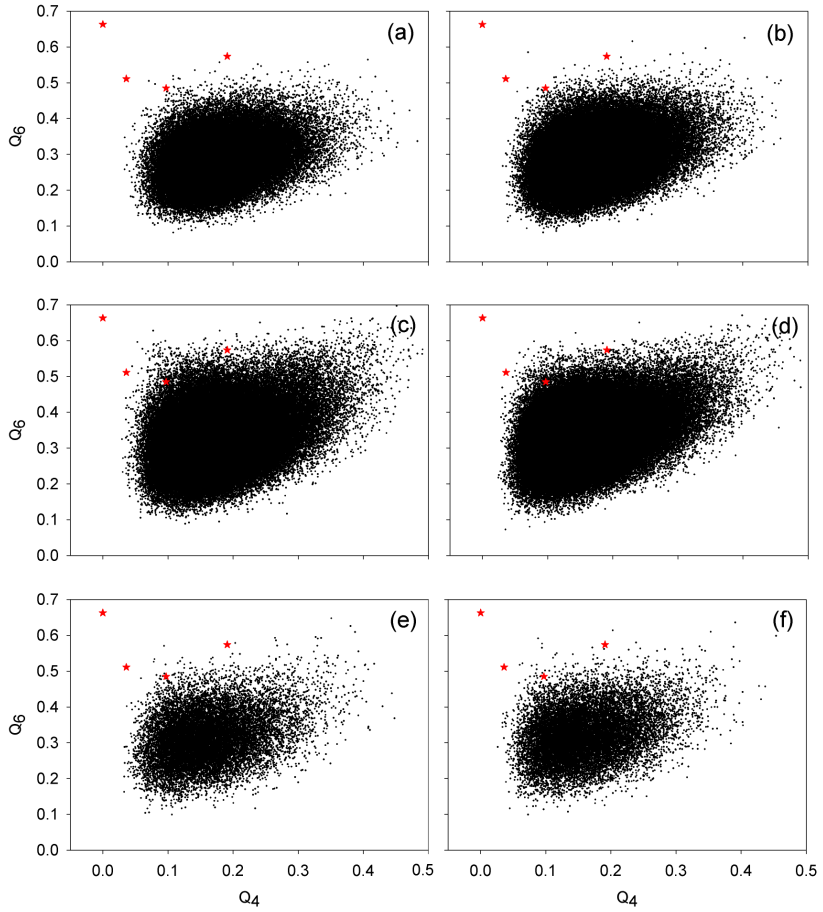

Figure 4.8: Q_4 and Q_6 orientational bond order parameters. The stars represent Q_4 and Q_6 in fcc, hcp, bcc and icosahedral ordering. (a) Caging method. (b) Parking method. (c) Drop and roll method. (d) Cluster MCM method. (e) MCM random packing. (f) Experimental random packing of hard spheres.

until they touch at least three other spheres. The result is a higher volume fraction for the central sphere and for the surrounding shells than with the parking method. The volume fraction decreases with shell number because as spheres are dropped from a random direction, the probability of hitting a sphere from a certain direction becomes non-uniform, which results in an anisotropic structure (Fig. 4.2c). However, the contact numbers for these clusters are higher than the numbers found in random packing. Furthermore, some spheres have 12 neighbors, though there are only a small percentage as can be seen from the Q_4-Q_6 graph (Fig. 4.8c). The rdf shows a clear split peak which is the result of rolling spheres until there are three contacts. This promotes the formation of tetrahedral arrangements.

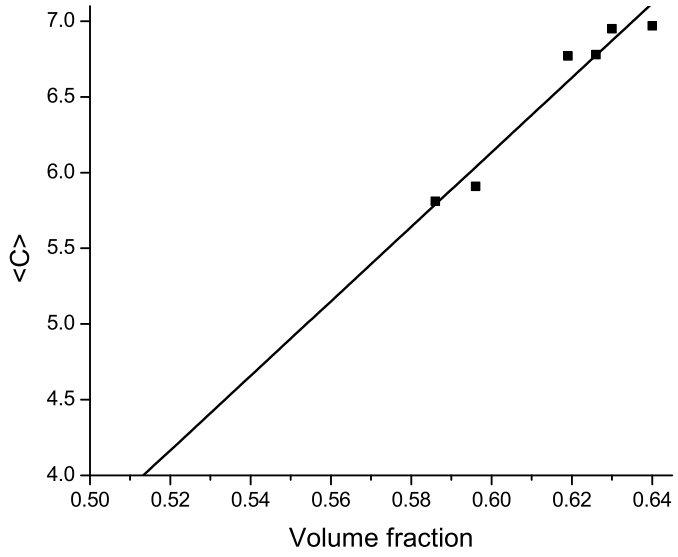

Figure 4.9: Linear fit through the experimental data from [123]. Extrapolating the data yields for the caging number 4.71 a volume fraction of 0.54.

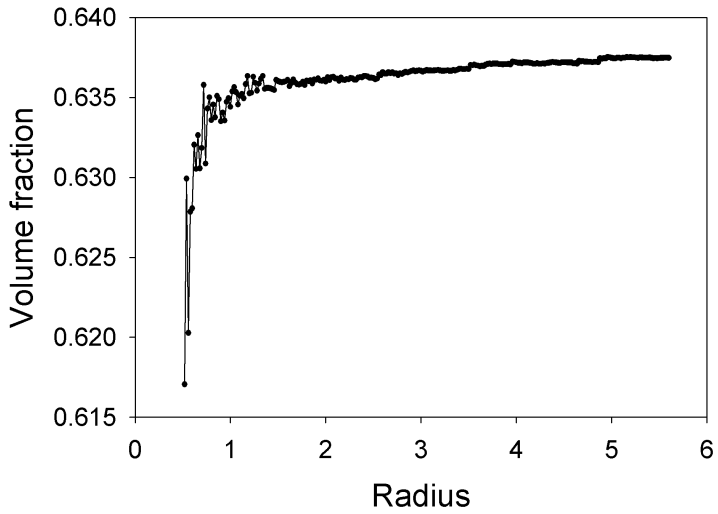

Figure 4.10: Volume fraction as a function of particle radius for the modified mechanical contraction method.

4.4.4. MCM cluster method

For the MCM cluster method the contact number is roughly constant for each sphere shell with a value of 6.3. The MCM cluster method models the features of a random close packing better than the two other methods. The rdf matches reasonably with the rdf for the MCM and experimental packing. The peaks in the rdf occur at roughly the same position but the shape of the peaks differs. The contact number for the central

sphere is larger in the parking method than for the MCM clusters. However, the volume fraction of the center sphere is higher in the MCM model and also denser in the next shells than in the case of the parking method. The average volume fraction 0.645 is close to the random close packing volume fraction usually cited to be around 0.64. Maximizing the coordination number locally as is done in the parking method does not maximize the overall volume fraction of the cluster. The MCM cluster method clearly shows the importance of collective effects occurring due to the geometric constraints on the spheres. By lowering the contact number for the central sphere, the first and second shell can pack more densely compared to the parking method. The collective movement of the spheres creates a more isotropic structure than for the drop and roll method. The local models only mimic the behavior of a random packing reasonably well for the central sphere and its first shell. The second shell is not representative since collective effects become more important. There are no sphere configurations formed with contact number 12 as can be seen from Figs. 4.3d and 4.4d. From the bond order parameters (Fig. 4.8d) it can be seen that the majority of local configurations of the MCM are different than for a fcc or hcp crystal.

4.4.5. Modified MCM for random sphere packing

The modified MCM method is an iterative volume fraction maximization procedure. The volume of the simulation box is increased at each step and spheres can reorganize themselves more efficiently. The volume fraction increases as the spheres grow in size. After a fixed number of steps the volume fraction reaches a plateau at 0.637 (see Fig. 4.10). The plateau of 0.637 indicates that the packing is trapped in a local volume minimum.

4.5. Conclusions

The cluster ensemble analysis turns out to be a versatile method to investigate properties of random sphere packings. The ensemble averages yield a lower bound for the random loose packing (RLP) volume fraction and show quantitative agreement for random close packed (RCP) volume fraction, contact numbers and radial distribution functions. Furthermore, the ensemble analysis is useful to at least qualitatively understand the origin of RLP and RCP from a simple local geometric analysis based on the physics of the packing formation.

The caging cluster method yields a volume fraction of 0.495, remarkably close to the hard sphere freezing volume fraction, providing a lower bound on volume fraction for random loose packing. An unexpected split peak is found in the distribution in volume fractions for the parking method, related to the contact number of the center sphere. We show that local models provide insight into the properties of random packing of equal sized spheres. Calculated radial distribution functions for the clusters show

the same peaks as experimental data and computer simulations. A local orientational bond order analysis confirms that the generated clusters are indeed disordered. The radial distribution function for the parking cluster resembles the radial distribution of a random packing better than the drop and roll model where the two peaks in the rdf are clearly split. The radial distribution function of the MCM cluster method agrees with the rdf for a MCM packing and experimental sphere packings in features but the height and width slightly differ.

The parking cluster method and the drop and roll method both generate configurations with properties similar to random close packing. These methods show that by increasing the contact number the local volume fraction increases. However, there are still some differences in properties with respect to experimental packings due to collective and global effects. The MCM cluster method remedies these effects and models a random close packing more closely since it accounts for collective effects. The MCM cluster is denser than the clusters from the local methods and a maximization of the volume fraction is realized. For a more detailed description of random packing more complicated models are needed, which model collective effects in the generation of clusters or packings.

5

Effect of particle shape on the density and microstructure of random packings

Abstract

We study the random packing of non-spherical particles by computer simulation to investigate the effect of particle shape and aspect ratio on packing density and microstructure. Packings of cut spheres (a spherical segment which is symmetric about the sphere's centre) are simulated to assess the influence of a planar face on packing properties. It turns out that cut spheres, in common with spherocylinders and spheroids, pack more efficiently as the particle's aspect ratio is perturbed slightly from unity (the aspect ratio of a sphere) to reach a maximum density at an aspect ratio of approximately 1.25. Upon increasing the aspect ratio further the cut spheres pack less efficiently, until approximately an aspect ratio of two, where the particles are found to form a columnar phase. The amount of ordering is sensitive to simulation parameters and for very thin disks the formation of long columns becomes frustrated resulting in a nematic phase, in marked contrast to the behavior of long thin rods, which always randomly pack into entangled isotropic networks. With respect to coordination numbers it appears that cut spheres always pack with significantly less contacts than required for isostatic packing.

5.1. Introduction

Random particle packings [9] have been widely investigated and form important materials such as granular media (sand, powders), randomly oriented clay particles [131] and fibers in biological cells [122]. Packed particles very often have a non-spherical shape [33,35,98], which for example is important for shape-induced frustration of hexagonal order in polyhedral colloids [132], random packings of ellipsoids [97,105] and liquid crystals [133]. Random packings of spheres and spherocylinders further demonstrate the effect of shape on packing properties. Previously we found using the mechanical contraction method [35] that spherocylinders reach a packing volume fraction maximum upon slightly deviating from spherical shape. Later Donev et al. showed, using event driven molecular dynamics, that spheroids display a similar behaviour [106]. To compare these two simulation methods [35, 106] we apply in the present study the mechanical contraction method to spheroids. Both spherocylinders and spheroids are smooth convex objects, which raises the question as to what role this property plays in determining the density as well as the microstructure of a random packing. Therefore we have investigated the random packing of non-smooth particles with planar faces, namely cut spheres (Fig. 5.1c).

The latter have the advantage that one can gradually transform a sphere-like shape to a disk-like shape with truly planar faces in a controlled way [134], which allows us to study the influence of a flat surface on the packing geometry. The aspect ratio of a cut sphere is defined as D/L, where D is the sphere diameter and L is the thickness. Furthermore, in the limit of large aspect ratio thin cut spheres become identical to short cylinders (disks).

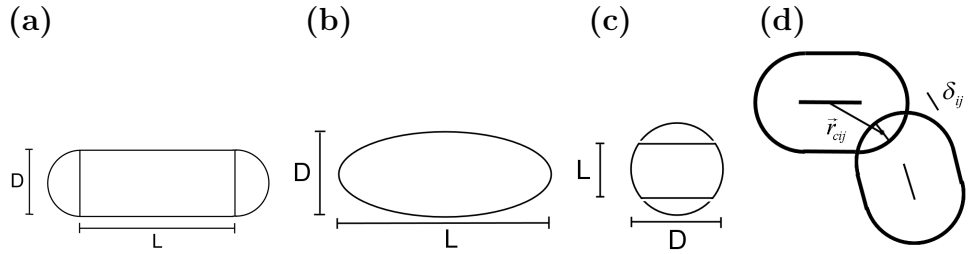

Figure 5.1: Sketch of a spherocylinder (a), spheroid (b) and cut sphere (c) with aspect ratios of (L+D)/D, L/D and D/L. (d) Graphical illustration of variables that are calculated within the mechanical contraction method: $\vec{r}_{cij}$ connects the contact point to the center of particle i and the distance δ_{ij} quantifies the amount of overlap.

The primary aim of this work is to assess whether characteristic features for spheroids and spherocylinders, which are similar in shape, such as the near-sphere density maximum are particular to these smooth convex bodies or whether this maximum also occurs

for particles with planar faces. In addition to the effect of shape on packing density we also investigate the packing microstructure, in particular with respect to the influence of planar faces on orientational correlations.

5.2. Method

The mechanical contraction method [35] is an attempt to inhibit any overlap between the system's particles, by minimally disturbing their positions, as the system is compressed. A dilute random configuration of non-overlapping particles is prepared in a cubic box with periodic boundary conditions. In each step of the simulation the volume of the periodic box is reduced by a small amount ΔV and all particle positions are uniformly dilated while their orientations do not change. At a certain number of steps particles start overlapping and this overlap is then removed. The simulation is stopped when it is no longer possible to remove the overlap between particles with a reasonable amount of computational effort. The final configuration is the one from the previous simulation step where none of the particles were overlapping.

To remove overlap between cut spheres or spheroids the overlap removal scheme as described for the mechanical contraction method for spherocylinders [35] has to be adapted. When two particles i and j overlap, the amount of overlap δ_{ij}, a contact normal n_{ij} and a contact point at the center of overlap are calculated (Fig. 5.1d). If particle i is translated and rotated, the rate with which the overlap changes with particle j can be quantified to first order as

$$\frac{\partial \delta_{ij}}{\partial t} = (\vec{v}_i + \vec{\omega}_i \times \vec{r}_{cij}) \cdot \hat{n}_{ij} \tag{5.1}$$

where v_i and ω_i are the respective translational and angular velocity and r_{cij} is the vector connecting the contact point with the center of mass of particle i. In order to remove overlap efficiently in the case of C contacts an overlap removal speed s is introduced as

$$s_i = \sum_{j=1}^{C} \delta_{ij} \frac{\partial \delta_{ij}}{\partial t} \tag{5.2}$$

where the factor δ_{ij} is included in order to bias the rate at which the particles break contact in favor of those which are overlapping the most. To fix the ratio between translational and rotational velocity a kinetic energy-type constraint is introduced for particle i,

$$\vec{v}_i \cdot \vec{v}_i + \vec{\omega}_i I \vec{\omega}_i = 1 \tag{5.3}$$

where I is a diagonal matrix that relates to the particle's moment of inertia. The direction which maximizes the rate of overlap removal is sought by the use of Lagrange

multipliers with (5.2) and constraint (5.3) to obtain v_i and ω_i,

$$\vec{v}_i = \sum_{j=1}^{C} \delta_{ij} \hat{n}_{ij} \tag{5.4}$$

and

$$\begin{aligned}
\omega_i^{(x)} &= \frac{1}{I_{xx}} \sum_{j=1}^{C} \delta_{ij} (n_{ij}^{(z)} r_{cij}^{(y)} - n_{ij}^{(y)} r_{cij}^{(z)}) \\
\omega_i^{(y)} &= \frac{1}{I_{yy}} \sum_{j=1}^{C} \delta_{ij} (n_{ij}^{(x)} r_{cij}^{(z)} - n_{ij}^{(z)} r_{cij}^{(x)}) \\
\omega_i^{(z)} &= \frac{1}{I_{zz}} \sum_{j=1}^{C} \delta_{ij} (n_{ij}^{(y)} r_{cij}^{(x)} - n_{ij}^{(x)} r_{cij}^{(y)})
\end{aligned} \tag{5.5}$$

Once $\vec{v}_i$ and $\vec{\omega}_i$ are calculated, particle i is moved such that it moves half the distance of the smallest δ_{ij}. Particle i is actually displaced slightly further in the simulation to alleviate problems with numerical inaccuracy for small overlaps. The parameter δ_{ov} is an additional displacement that creates a small constant separation between particles. Packings of $N = 4000$ were typically generated with 10^4 attempts to remove overlap between particles and a minimum of $\Delta V = 0.01$. The parameter δ_{ov} was chosen in the range 10^{-2} to 10^{-4}. Varying the moment of inertia I_{xx} often lead to slightly denser packings.

5.2.1. Measures

The following measures were used to describe the structure of the generated packings. Contact numbers were determined by scaling up the cut spheres by a factor s, while keeping the aspect ratio constant, and the resulting overlapping particles were counted as contacts. The number of contacts was then plotted as a function of the threshold, s. A linear extrapolation was employed to obtain the number of contacts when the threshold s is set to zero (Fig. 5.2).

Positional order was measured with the normalized radial pair distribution function (calculated in the same way that is done for spheres), defined as

$$g(r) = n(r)/(\rho 4\pi r^2 \Delta r) \tag{5.6}$$

where n is the mean number of cut spheres in a spherical shell Δr at distance r and ρ is the mean number density.

In thermal systems cut spheres can form nematic and columnar phases [134], where in the nematic phase the particles have no positional order but orientational order in one direction; for the columnar phase there is positional as well as orientational order. To quantify the amount of order in generated packings an orientational alignment matrix

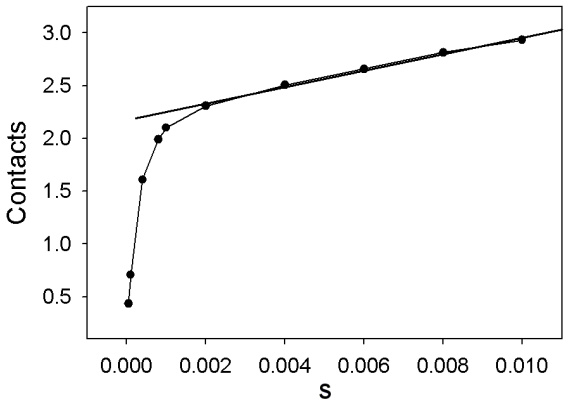

Figure 5.2: Typical example of the determination of the contact number through a linear extrapolation to zero of the threshold s for cut spheres with aspect ratio 20.

Q is used [134], defined as

$$\langle Q \rangle = \frac{1}{N} \sum_{i=1}^{N} \frac{3}{2} \hat{u}_i \hat{u}_i^T - \frac{1}{2} I \tag{5.7}$$

where $\hat{u}_i$ is a unit column vector normal to the planar part of a cut sphere, I is the identity matrix and the nematic order parameter is given as,

$$S = -2\lambda_0 \tag{5.8}$$

where λ_0 is the middle eigenvalue of the matrix $\langle Q \rangle$ given by (5.7). When all vectors $\hat{u}_i$ point in the same direction then $S = 1$, whereas an isotropic distribution is quantified by $S = 0$.

From the graphical renderings (Fig. 5.6) of the packings it was indeed found that the cut spheres tend to align in columns. Whether or not a particle belongs to a column was determined via two threshold values, namely, δ_{pc} to decide whether or not the particle's face is nearly parallel with that of its neighbour and δ_{nc} to assess whether or not the particle's centre is close enough to its neighbours in the direction given by the neighbours axis of symetry. The criterion for a particle in a column can then be stated as $|\hat{u}_i \cdot \hat{u}_j| > 1 - \delta_{pc}$ and $|\vec{r}_{ij} \cdot \hat{u}_j| < L + \delta_{nc}$ together with $|\vec{r}_{ij}| < D$, where $\vec{r}_{ij}$ is a vector connecting the two centers of a pair of cut spheres. The average column length L_{col} is given by $L_{col} = N_{col} L$, where L is the thickness of the cut sphere and N_{col} is the average number of particles per column. We note that these criteria are not sensitive to columns, which have been deformed by having particles slid perpendicular to their axis of symmetry and that this sensitivity becomes more acute as the disks become thinner. While we will not pursue this here we could test for this effect by introducing a third parameter δ_{sc} with the condition, $\frac{1}{2}|\vec{r}_{ij} - \vec{r}_{ij} \cdot \hat{u}_i \hat{u}_i| + \frac{1}{2}|\vec{r}_{ij} - \vec{r}_{ij} \cdot \hat{u}_j \hat{u}_j| < \delta_{sc}$.

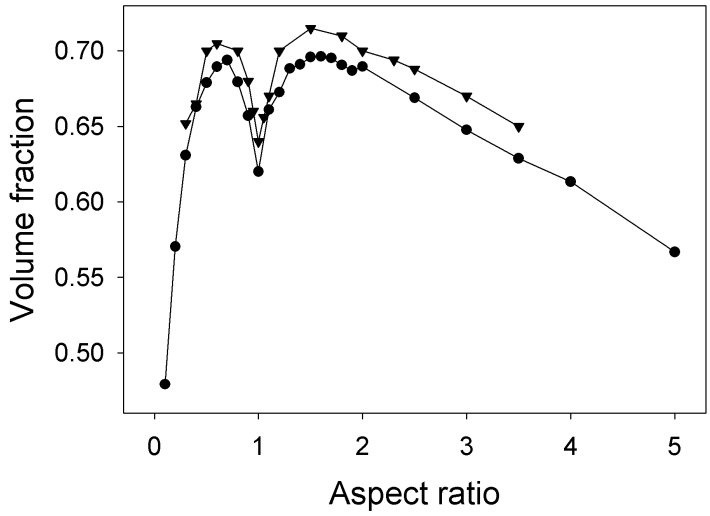

Figure 5.3: Volume fraction as a function of aspect ratio for spheroid packings. Spheres at aspect ratio one form a singular point. (triangles) Event driven simulation from Donev et al. [106], (circles) MCM for spheroids.

5.3. Results and Discussions

5.3.1. Comparison of spherocylinders and spheroids

The volume fractions obtained for oblate and prolate spheroids using the mechanical contraction method (MCM) are plotted in Fig. 5.3 and compared to event-driven molecular dynamics simulations of spheroids [106].

As can be seen from Fig. 5.3, though event driven simulation produces slightly higher volume fractions, the volume fraction dependence on aspect ratio is qualitatively the same for both methods. Using the MCM method a comparison between spherocylinders and spheroids can now be made (Fig. 5.4). To compare spherocylinders with spheroids, we do not use L/D (as previously [35]) for the aspect ratio for spherocylinders but $(L + D)/D$ instead and L/D for spheroids.

Fig. 5.4 shows that spheroids and spherocylinders exhibit a very similar volume fraction dependence on aspect ratio. It would be interesting to see whether an event-driven molecular dynamics simulation of spherocylinders shows the same behaviour but with a slightly higher volume fraction as was the case for spheroids. Both spheroids and spherocylinders show a maximum in volume fraction at roughly aspect ratio 1.5, which is close to spheres that in Fig. 5.4 have an aspect ratio of one. Spherocylinders, at least in our simulations, pack slightly less efficient than spheroids. It is known [33, 35] that for sufficiently high aspect ratios the volume fraction scales inversely proportional to the excluded volume and if we assume that the average number of contacts to constrain a long spheroid or spherocylinder do not differ much, we can attempt to relate the trend

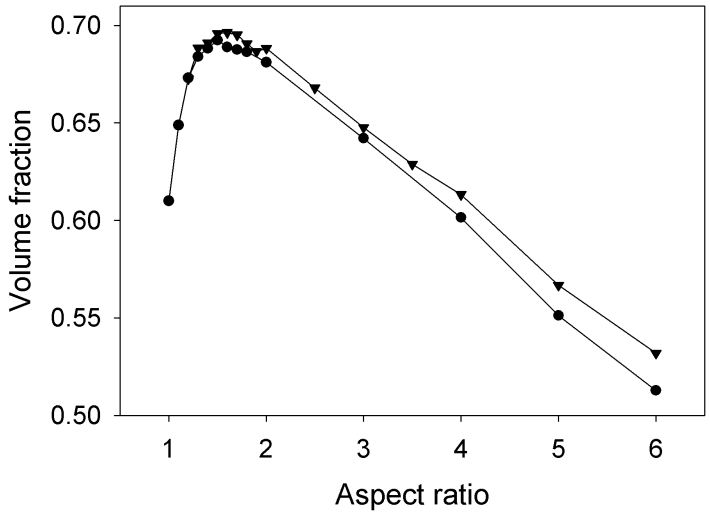

Figure 5.4: Volume fraction dependence as a function of aspect ratio for spherocylinders (circles) and spheroids (triangles) simulated with the mechanical contraction method.

in Fig. 5.4 to a difference in excluded volume. The orientationally averaged excluded volume for equal spheroids [135] with volume $V_{spheroid}$ is

$$\frac{V_{excl}}{8V_{spheroid}} = \frac{1}{4} + \frac{3}{16}z\left[1 + \frac{(1-\epsilon^2)}{2\epsilon}\ln\left(\frac{1+\epsilon}{1-\epsilon}\right)\right]\left[\sqrt{1-\epsilon^2} + \frac{\arcsin(\epsilon)}{\epsilon}\right] \tag{5.9}$$

where $z = L/D$ for prolate spheroids and D/L for oblate spheroids and $\epsilon^2 = 1 - \frac{1}{z^2}$, whereas the orientationally averaged excluded volume for spherocylinders [25] is

$$V_{excl} = \frac{4}{3}\pi D^3 + 2\pi L D^3 + \frac{\pi}{2}DL^2 \tag{5.10}$$

In the high aspect ratio limit we expect the scaling [33]:

$$\phi \propto \langle c\rangle \frac{V_p}{V_{excl}}; \quad \frac{L}{D} >> 1 \tag{5.11}$$

which for long thin spherocylinders becomes:

$$\phi \propto \frac{\langle c\rangle}{2}\frac{D}{L}; \quad \frac{L}{D} >> 1 \tag{5.12}$$

whereas for spheroids substitution of (5.9) in (5.11) yields the asymptote:

$$\phi \propto \frac{4\langle c\rangle}{3\pi}\frac{D}{L}; \quad \frac{L}{D} >> 1 \tag{5.13}$$

This suggests that in the thin-rod limit spherocylinders actually pack slightly denser than spheroids. Possibly the small difference between spherocylinders and spheroids (which is reproducible) in Fig. 5.4 is therefore related to details of the contraction method. Next the effect of a planar face on packing properties is investigated upon cutting equal slices from a sphere.

5.3.2. Effect of a planar face on packing properties

Cut spheres with a low aspect ratio, i.e. a particle with a small planar face relative to the total surface, show similar packing properties as for the smooth curved particles discussed previously. A slight deviation from spherical shape leads to an increase in volume fraction (Fig. 5.5b). However, upon increasing the contribution of the planar face, we find significant different packing effects in comparison to smooth convex particles. For large aspect ratios the volume fraction clearly differs from the results for curved particles. The planar face induces considerable alignment and ordering of particles that reduces the excluded volume and, consequently, allows for a denser packing. Such an ordered packing cannot be considered random anymore. At small aspect ratios random packings of cut spheres are insensitive to simulation parameters and we expect that different techniques, such as molecular dynamics and experiments, should be able to reproduce these results. At high aspect ratios the degree of ordering depend sensitively on the simulation parameters. Such alignment, of course, would also increase the packing density for high-aspect ratio (sphero-)cylinders. However, in the latter case the long thin rods form entangled structures that prohibit local alignment, which appears to be an essential difference between packings of high aspect ratio rods and high aspect ratio discs.

When the parameters in the simulation are varied in order to maximize the density, the cut spheres of larger aspect ratio start to crystallize in a columnar phase. This can be seen in Fig. 5.5a, where large fluctuations in the volume fractions obtained from individual simulations are indicative of packings that are sensitive to crystallization. Increasing the aforementioned simulation parameter δ_{ov} results in more order in the packing and shows the sensitive dependence of the packing volume fraction on simulation parameters at aspect ratios where crystalline ordering occurs. Graphical images of various packings, most showing significant crystalline order, can be seen in Fig. 5.6. The strong ordering seen here is due to the large value of the parameter $\delta_{ov} = 0.01$ that has been used. However, the ordering only occurs for particles of larger aspect ratio than 2 as can be seen in Fig. 5.5b. The contraction method yields reproducible packings, which are not sensitive to arbitrary simulation parameters below an aspect ratio of 2 where the disordered structures appear stable under compression. We argue that this sensitivity of crystallization on arbitrary simulation parameters is not merely an artifact of our simulation method but relevant to experimental systems as well. For example friction between particles, the employed packing procedures and other experimental details could all be sensitively important to the propensity of the packing to crystallize. An example of this is the finding of sediments of colloidal platelets [131] that pack less dense than is expected for a columnar phase but agrees well with Fig. 5.5c.

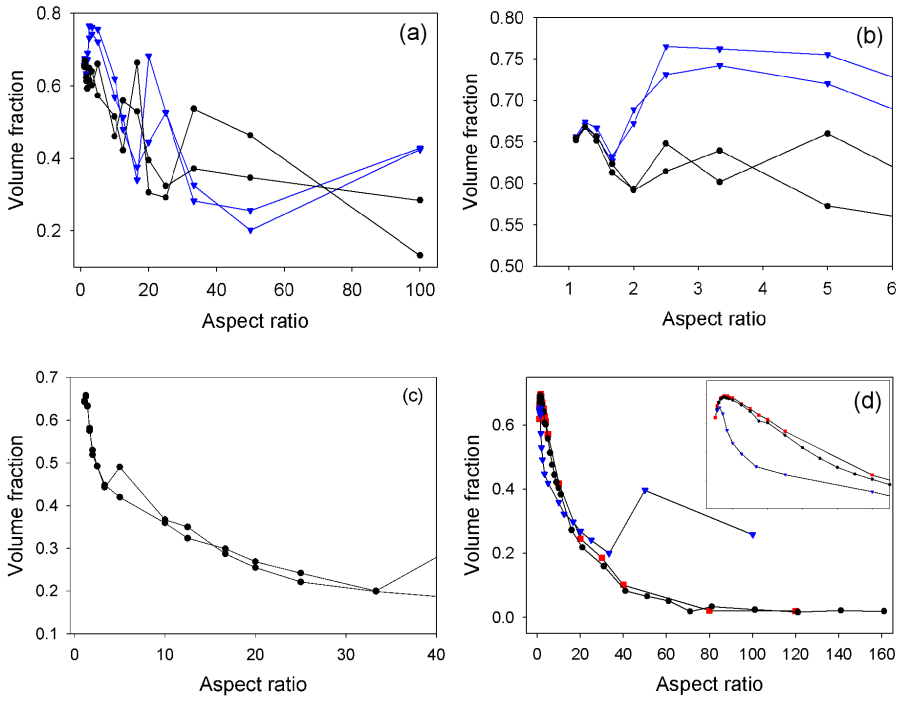

Figure 5.5: (a) Volume fraction dependence for the packing of cut spheres as a function of aspect ratio. The spikes are caused by a columnar phase of the crystallized packing. Two simulations that only differ in starting configuration are shown for two cases with varying δ_{ov}. (triangles) $\delta_{ov} = 10^{-2}$ and (circles) $\delta_{ov} = 10^{-3}$ (b) A close-up of (a). A slight deviation from aspect ratio 1 (sphere) leads to an increase in volume fraction. (c) Two simulations for cut spheres with $\delta_{ov} = 10^{-4}$. (d) Comparison of spheroids (squares), spherocylinders (circles) and cut spheres (triangles).

For cut spheres, starting from spherical shape, the volume fraction initially increases with aspect ratio. However, for larger aspect ratios the volume fraction does not decrease as rapidly as it does for spherocylinders and spheroids due to ordering of the cut spheres (Fig. 5.5d). This can also be seen from the images of cut sphere packings (see Fig. 5.6). For spherocylinders and spheroids the excluded volume effects start to dominate for larger aspect ratios where it is not possible to align themselves due to entanglement and jamming, whereas in a cut-sphere packing, the cut spheres can reduce their excluded volume by alignment. The effect of this alignment is that the cut sphere packings mimic a polydisperse packing of cylinders that are formed from columns of connected cut spheres. The volume fraction for polydisperse particle packings is often higher than for monodisperse ones [118,130]. For larger aspect ratios the cylinders that are formed display significant ordering resulting in more efficient packing.

The statistics of the columns seen in Fig. 5.6 were studied by computing the average number of cut spheres in a column N_{col} and the average length of a column L_{col} as

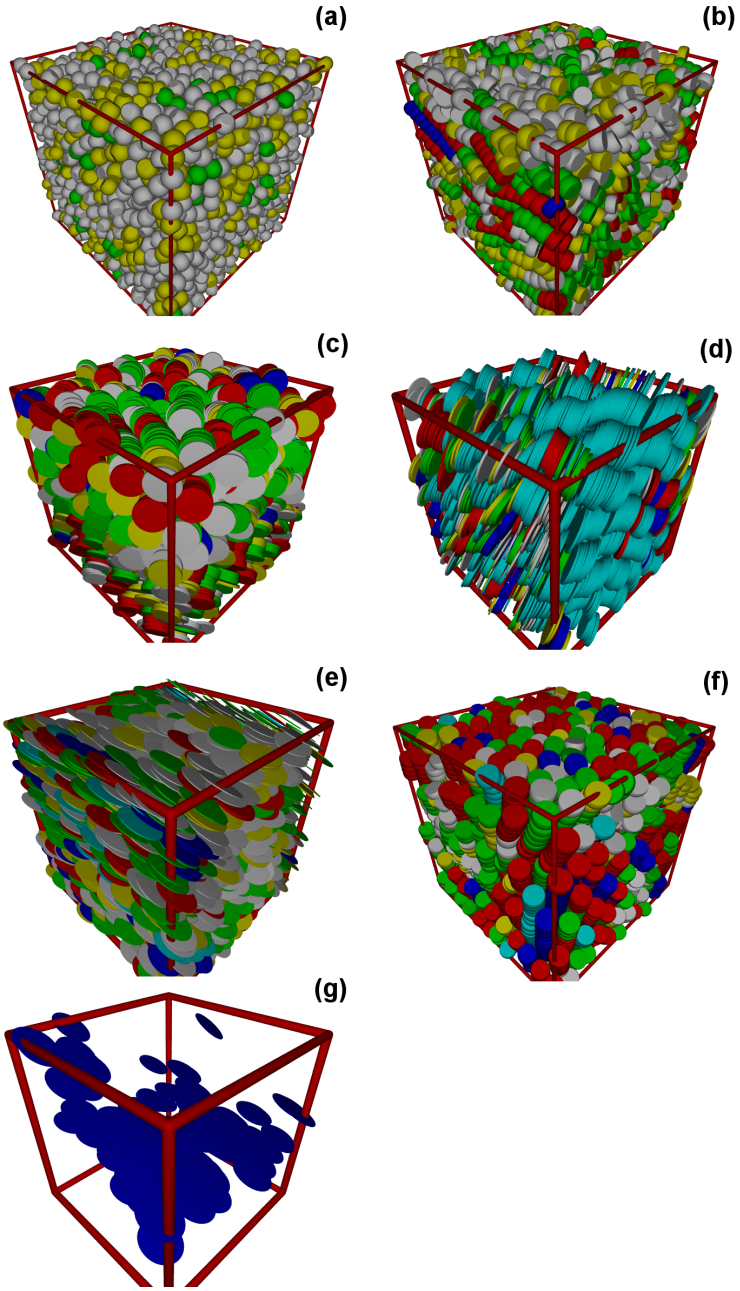

Figure 5.6: Graphical examples of cut spheres ($N = 4000$) with $\delta_{ov} = 0.01$. (a) aspect ratio 1.25 (b) aspect ratio 2 (c) aspect ratio 10 (d) aspect ratio 20 (e) nematic phase of aspect ratio 50 (f) columnar phase of aspect ratio 2.5, $\phi = 0.765$. The cut spheres are colour coded according to the length of the columns. (g) Illustration of the nematic effect.

detailed in the methods section, with results shown in Fig. 5.7. For large aspect ratios a nematic phase is observed. In this case particles in a stairway-like alignment are being counted as belonging to a single column. An example of this stairway alignment is given in Fig. 5.6g, which is a rendering of only the dark gray particles of Fig. 5.6e that shows

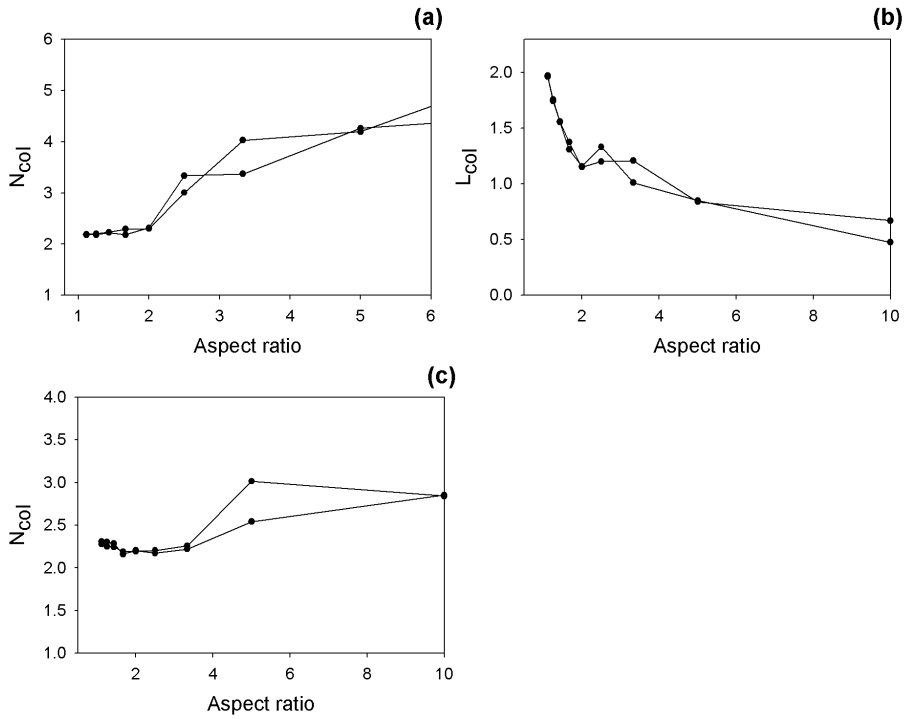

Figure 5.7: Statistics of columns in cut sphere packings of the two runs, with $\delta_{ov} = 10^{-3}$, that did not exhibit a strong tendency to crystallize. (a) Average number of particles per column $\langle N_{col} \rangle$. (b) Average length of a column $\langle L_{col} \rangle$. (c) same as (a) but with $\delta_{ov} = 10^{-4}$ which resulted in still less tendency to crystallize.

strong orientational but poor positional order, i.e. a nematic phase. Given that the nematic phase can be clearly seen in Fig. 5.6 we decided to allow the identification of these stairway like columns rather than use the additional criteria with the parameter δ_{sc} to remove them as discussed in the methods.

The number of particles per column N_{col} increases with aspect ratio (Fig. 5.7a) but slower than the inverse aspect ratio D/L, with the net result that the average column length $\langle L_{col} \rangle$ decreases (Fig. 5.7b).

5.3.3. Contact numbers

In a system of particles, ignoring finite size effects, there are Nd degrees of freedom where N is the number of particles and d is the number of degrees of freedom per particle. For a sphere, which has orientational symmetry, we need only consider the translational degrees of freedom and thus $d = 3$. For a cut sphere there is only one, of a possible 3, orientational axes of symmetry and thus $d = 5$. The isostatic conjecture [136] states that the number of constraint equations is at least equal to the number of degrees of freedom Nd and that disordered packings have the minimal number of contacts necessary for mechanical stability. Each contact is shared by two particles and thus, by

this conjecture, the average number of contacts per particle $\langle C \rangle$ is given by $\langle C \rangle = 2d$. Chaikin et al. provide a convincing argument why the isostatic conjecture may fail for non-spherical particles [137]. In particular when the flat faces of a pair of cut spheres are in contact a translational degree of freedom is constrained as well as two orientational degrees of freedom. A pair of cut spheres can constrain three degrees of freedom with a single contact and thus, in this case, one would expect the isostatic conjecture to fail.

The contact number as a function of aspect ratio is shown in Fig. 5.8 for the cases $\delta_{ov} = 10^{-2}$ and 10^{-4}. The spikes in the graph for $\delta_{ov} = 10^{-2}$ are indicative of the sensitivity to crystallization. For aspect ratios close to unity the contact number is close to $\langle C \rangle = 6$, which is consistent with the isostatic conjecture for spheres as is well known from previous studies [136, 137]. Consistent with previous work on spherocylinders [35] and spheroids [106] we do not find any evidence for the average contact number rising discontinuously to $\langle C \rangle = 10$ upon departing from spherical symmetry. In Ref. [138] it was found that randomly parking the maximum number of spheres does not produce optimal packings and that denser packings are formed by having a contact number lower than the parking number of 8.4. Slightly deforming spheres does not change the volume and surface area dramatically and therefore it is expected that $\langle C \rangle$ will not rise discontinuously to 10 to produce optimal packings for near-spheres. However, in experimental spherocylinder packings the contact number clearly does approach $\langle C \rangle = 10$ at large aspect ratios [96], while for spheroids experimental data at high aspect ratios have yet to be reported. In view of the argument of Chaikin et al. [137] it is not surprising that we see no evidence of $\langle C \rangle = 10$ for cut spheres, violating the isostatic conjecture due to a single contact being able to constrain more than one degree of freedom.

For high aspect ratios the contact number approaches the limit of approximately two for both the disordered and ordered packings, which implies an aligned cut sphere above and below each particle on average. This suggests that almost all the particles in these configurations are still able to move in the direction of the planar face of the cut sphere (i.e. essentially all the particles are rattlers) and the system is not jammed. In the case of the disordered packings we expect structural integrity to be lacking. While it may be able to support a compressive load under some conditions, it will be very unstable to further ordering.

Again we note the considerable order that the system requires to become tightly packed at large aspect ratios and the apparent frustration in the ordering process. This suggests the columns may be jammed while the particles forming them are able to slide or rattle in a direction perpendicular to the column. For the crystalline phases, be they columnar or nematic, we argue that structural integrity may be present. The number of contacts, two, is consistent with constraining the particles in a column with the degrees of freedom perpendicular to the column still being free. In the limit of long

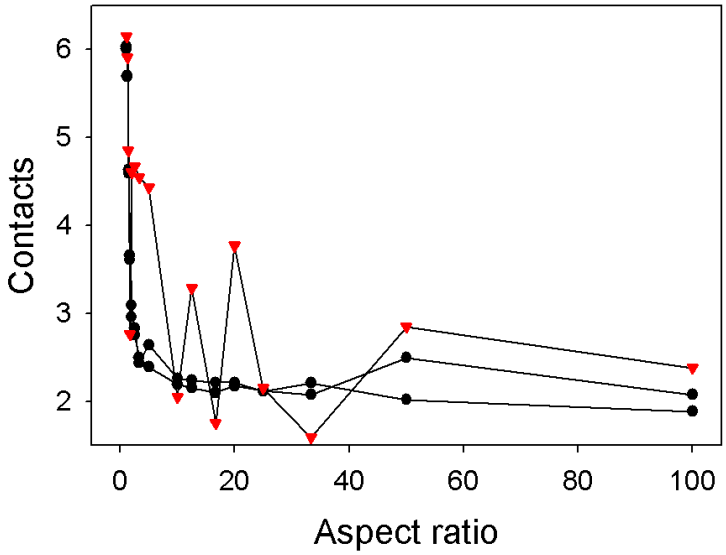

Figure 5.8: Contact number as a function of aspect ratio for cut sphere packings generated with $\delta_{ov} = 10^{-4}$ (circles) and $\delta_{ov} = 10^{-2}$ (triangles).

columns, formed from many cut spheres, and treating each column to be effectively a single particle we obtain a stable structure. The same can be said for a nematic phase consisting of planes made from very thin cut spheres in the limit of large surface area. In either case the contacts necessary to constrain the columns or plains become insignificant in the limit. Thus we obtain a structure consisting of jammed columns or planes, which are formed from thin disks that are able to slide or rattle in a direction perpendicular to the column or in the plane respectively.

Two contacts per particle is also consistent with the nematic phase as seen in Fig. 5.6e. There are large fluctuations in the number of contacts when $\delta_{ov} = 10^{-2}$ due to the frustrated ordering process.

5.3.4. Radial distribution functions

The normalized radial distribution function (rdf) of a random packing of cut spheres with aspect ratio 1.11 is similar to the rdf of a random sphere packing (Fig. 5.9b) of both computer simulation [138] and experiments [44, 123]. In Fig. 5.9b there is a small peak at $r = 0.9$ which corresponds to two touching parallel cut spheres (since the thickness of the cut sphere is 0.9) and a peak at $r = 0.95$, due to the contact between a spherical face of one particle with the cut face of another. The columnar crystal phase in Fig. 5.9c shows considerable structure in the radial distribution function due to the high degree of order present.

The nematic order parameter S as a function of aspect ratio (Fig. 5.10) shows interesting behavior. For aspect ratios less than 2.0 the packings are disordered. When

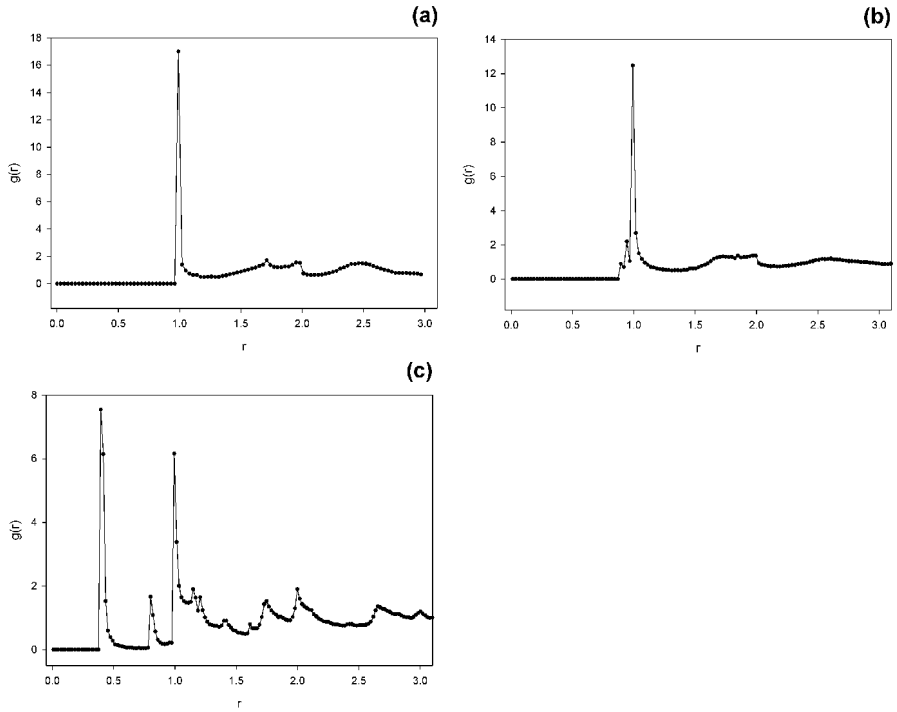

Figure 5.9: Normalized radial distribution functions (a) Disordered sphere packing. $\delta_{ov} = 10^{-6}$ (b) Cut spheres with aspect ratio 1.11 and $\delta_{ov} = 10^{-4}$ (c) Columnar crystal of cut spheres with aspect ratio 2.5 and $\delta_{ov} = 10^{-2}$.

the overlap parameter is large, $\delta_{ov} = 0.01$, the influence of the planar face shows up as an increased amount of order with increasing aspect ratio. When the overlap parameter is small, $\delta_{ov} = 10^{-4}$, the systems ability to form an ordered structure is highly frustrated. At aspect ratio 10 the order is lower than expected for an ordered system (Fig. 5.10b). In these cases the MCM is no longer able to successfully rearrange the system to make it crystallize. Whether or not a system is able to form an ordered structure in an experiment, and if it does at what aspect ratio, depends very likely also on factors such as friction between the particles and the method used to prepare the packing. Nevertheless thin colloidal Gibbsite platelets with an aspect ratio of about 13 were found to pack into a sediment with a volume fraction of around 0.4 [131], which actually agrees quite well with our simulation results in Fig. 5.5c.

5.4. Conclusions

For the case of spheroids our mechanical contraction method (MCM) produces random packings with a marginally lower volume fraction than existing data generated with event-driven molecular dynamics methods [106]. We have shown in addition that spherocylinders and spheroids exhibit very similar packing behavior, consistent with

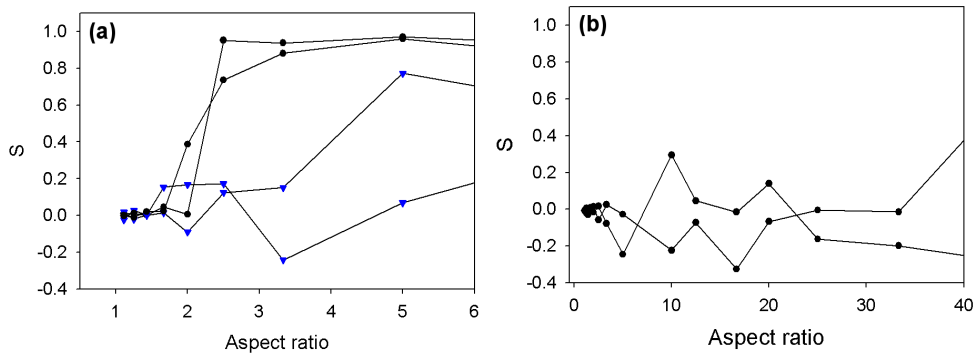

Figure 5.10: Nematic order parameter S as a function of aspect ratio of cut spheres for simulation runs with (a) $\delta_{ov} = 10^{-2}$ (circles) and 10^{-3} (triangles) and (b) $\delta_{ov} = 10^{-4}$. Simulations were repeated twice in each instance to check reproducibility.

their similarity in shape, with respect to the density maximum for near-spheres and the density decrease at higher aspect ratios.

A slight deviation from spheres by use of cut spheres yields random packings with a higher volume fraction similar to elongating spheres as with spherocylinders or deforming spheres as is the case with spheroids. The low aspect ratio (near spherical) cut spheres form disordered packings with a structure similar to disordered sphere packings as shown by the normalized radial distribution functions. The results for low aspect ratio cut spheres are insensitive to simulation parameters and should be reproducible with different simulation techniques. For higher aspect ratios the packing behavior of cut spheres is very different from spheroids and spherocylinders. Under favourable simulation parameters the planar part of the cut sphere promotes order in the packing by particle alignment, which reduces the excluded volume and allows for denser packings than for random packings of high aspect ratio spherocylinders and spheroids that form highly entangled structures. Thus, the jamming of thin cut spheres is qualitatively different from jammed packings of spherocylinders and spheroids. Columns of particles are formed with different orientations and the packing can no longer be considered random or disordered. The nematic order parameter increases with aspect ratio, which is indicative of this alignment effect. While at small aspect ratios the obtained disordered packings are not sensitive to simulation parameters, the same cannot be said for the large aspect ratios. Here the tendency to form an ordered structure is sensitive to the chosen simulation parameters and we argue that this is due to the lack of a stable amorphous structure for thin disks under a compressive load. At these aspect ratios the system is very susceptible to ordering in a manner that depends on the details much more sensitively than in the case of sphere like particles. We conclude that packings of thin disks are far more sensitive to crystalisation than is the case for

spheres. This is consistent with common intuition, gained from experience with objects such as collections of coins.

The packings generated for the cut spheres are not isostatic as can be seen from the contact numbers and as expected due to a pair of contacting flat faces constraining more than a single degree of freedom.

Acknowledgements

The Stichting voor Fundamenteel Onderzoek der Materie (FOM), financially supported by the Nederlandse Organisatie voor Wetenschappelijk Onderzoek (NWO) is acknowledged for both general funding and providing support for AW to travel to Australia and stay at the Research School of Chemistry where a significant component of this work took place. We thank the Australian Partnership for Advanced Computing (APAC) for computational facilities.

6

On contact numbers in random rod packings

Abstract

Random packings of non-spherical granular particles are simulated by combining mechanical contraction and molecular dynamics, to determine contact numbers as a function of density. Particle shapes are varied from spheres to long thin rods. The observed contact numbers and packing densities agree well with experiments on granular packings. Contact numbers are also compared to caging numbers calculated for spherocylinders with arbitrary aspect ratio. The caging number for rods arrested by uncorrelated point contacts asymptotes towards $\langle\gamma\rangle = 9$ at high aspect ratio, strikingly close to the experimental contact number $\langle C\rangle = 9.8$ for long thin rods. These and other findings confirm that long thin rod packings are dominated by local arrest in the form of truly random neighbour cages. The ideal packing law derived for random rod-rod contacts, supplemented with a calculation for the average contact number, explains both absolute value and aspect-ratio dependence of the packing density of randomly oriented long thin rods.

6.1. Introduction

The random rod packing is a valuable reference for packed granular matter composed of elongated particles as can be found in fiber-reinforced and other fibrous materials [93–95], and anisotropic powders [33, 34]. This reference packing is a stacking of randomly oriented, rigid rods with a maximum particle volume fraction uniquely determined by the rod aspect ratio [33]. Similarly, disorderly packed granular spheres are modeled by the (Bernal) random sphere packing [11]. Spheres and rods actually belong to a whole family of random particle packings, with a density fixed by the particle shape [33, 35]. Interestingly, the maximum density does not occur for the Bernal sphere packing, but for slightly deformed spheres. This density maximum was first found for spherocylinders [35] and later also for prolate spheroids [106] and cut spheres [102].

An essential difference between randomly packed spheres and long thin rods is the following. Due to the excluded volume effects there are strong positional correlations in a sphere packing that are very difficult to incorporate in a packing law, i.e. a relation between packing density, particle shape and contact numbers. Despite additional rotational degrees of freedom, it is much easier to model the random packing density for rods, because correlations between rod-rod contacts vanish in the thin-rod limit [33]. This asymptotic behaviour has been clearly confirmed by simulations [35]. Absence of contact correlations entails an 'ideal' packing law (see Ref. [33] and also section 6.2.2), namely a linear dependence of the random rod packing density on the average contact number $\langle C \rangle$.

The evaluation of $\langle C \rangle$, however, is not trivial. Philipse [33] concluded from a fit of experimental rod packing densities to the thin-rod packing law that $\langle C \rangle = 10.8 \pm 0.4$. Only recently Blouwolff and Fraden [96] succeeded to directly count contacts in experimental random rod packings and they reported that for thin rods $\langle C \rangle$ is about 10. The authors rationalised this outcome via an 'isostatic' argument to which we return in section 6.2.2.

Computer simulations of random rod packings are needed, not only for a better understanding of experimental densities and contact numbers, but also to investigate issues that are experimentally difficult to assess. (An example is the contact number as a function of particle volume fraction, treated in section 6.3.1). For random packing of non-spheres simulation algorithms are available, such as event-driven molecular dynamics [139, 140] and the mechanical contraction method (MCM). The MCM generates reproducible random packings of spheres and various non-spherical shapes [35, 102] with densities that are slightly below values from event driven molecular dynamics [106]. However, the MCM has yielded contact numbers that are unphysical for high aspect ratio spherocylinders. Defining a contact via a threshold distance [35] yielded for thin

spherocylinders that $\langle C \rangle$ is about 3, which is too low to achieve mechanical stability and anyhow much below the experimental values mentioned above.

The aim of this study is firstly to reproduce experimental contact numbers by combining MCM and molecular dynamics (MD), secondly to investigate the dependence of $\langle C \rangle$ on the particle volume fraction and finally, to analyze contact numbers in terms of a mathematical caging problem. In section 6.2.1 we describe the simulation method and the evaluation of contact numbers employing expansion of particles that interact via a spring-dashpot model. The caging problem, i.e. finding the average minimal number of uncorrelated contacts needed to arrest a particle, has only been solved for spheres [28, 127] and 2-dimensional discs [103]. In section 6.2.2 we explain a numerical solution of the caging problem for spherocylinders with arbitrary aspect ratio. One of the issues in the discussion in section 6.3 is whether magnitude and aspect ratio dependence of contact numbers for randomly packed rods can be explained as a local caging effect.

6.2. Methods

6.2.1. Simulation method

The starting configuration is a random particle packing generated with the MCM [35]. The particles are then expanded in steps at a constant growth rate. Contacts created between particles are modeled as spring-dashpots following Silbert et al. [78] for spheres and Pournin et al. [109] for spherocylinders. The approach of these authors was adopted in the sense that only the normal component of the overlap was considered whose magnitude is calculated as the diameter minus the shortest distance between the two line segments forming the spherocylinders (see Fig. 6.1). The contact force acting between overlapping particles is then given by

$$\vec{f} = -\left(k\delta + \gamma \vec{v}_{rel} \cdot \hat{n}\right) \hat{n} \tag{6.1}$$

where k is a spring constant, δ is the amount of overlap between two particles, γ is a viscosity constant, $\vec{v}_{rel}$ is the relative velocity of the two particles and $\hat{n}$ is a unit vector in the direction of the shortest distance. All particles experience a weak background viscosity force. The particle positions are updated by integrating the Newton-Euler equations of motion using a simple Euler scheme [69]:

$$\begin{aligned} \dot{x} &= v \\ \dot{p} &= f \\ \dot{q} &= \frac{1}{2}\omega \star q \\ \dot{L} &= \tau \end{aligned} \tag{6.2}$$

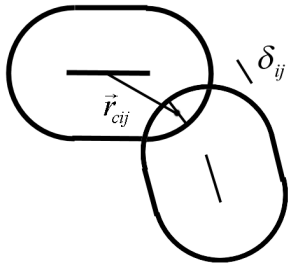

Figure 6.1: Illustration of the overlap δ that is shown as a line segment, $\hat{n}$ is the unit vector that points into the direction of the line segment, $\vec{r}_{cij}$ is the branch vector connecting the center of mass of a particle with the center of the overlap line, i. e. the contact.

where q is a quaternion representing the orientation of a particle, ω is the angular velocity, L is the angular momentum and τ is the total external torque.

The expansion of particles is terminated when a user-specified volume fraction is reached and after that the system is allowed to relax to zero energy. The final volume fraction is reached when it is no longer possible for the system to relax to zero potential energy. The expansion rate and viscosity of the particles were chosen such that the kinetic energy component of the total energy is small on average compared to the potential energy during the simulation run in order to keep the final structure as close as possible to the original starting configuration generated with the MCM and to maintain a disordered structure during the simulation.

6.2.2. Caging of non-spherical particles

The random contact equation [33] states that for a random packing with completely uncorrelated contacts, the volume fraction ϕ is given by

$$\phi = \frac{\langle C \rangle V_p}{V_{excl}} \tag{6.3}$$

where $\langle C \rangle$ is the average contact number per particle, V_p the particle volume and V_{excl} the orientationally averaged excluded volume for two particles. For spherocylinders with diameter D and a length L, the excluded volume [25] is

$$V_{excl} = \frac{4}{3}\pi D^3 + 2\pi L D^2 + \frac{\pi}{2} D L^2 \tag{6.4}$$

Substituting (6.4) into (6.3) we find for the limit of thin rods:

$$\phi \frac{L}{D} \sim \frac{\langle C \rangle}{2}; \text{for} \frac{L}{D} \gg 1 \tag{6.5}$$

This packing law for random long thin rods has been verified in experiments [33, 96] as well as simulations [35]. To calculate $\langle C \rangle$ one needs to define a mathematical problem to be solved. In a rod packing almost all particles are caged/jammed i.e. the particles cannot move because their movement is blocked by neighboring particles. Consequently,

an appropriate mathematical problem for $\langle C \rangle$ is to calculate the caging number $\langle \gamma \rangle$, defined as the minimum average number of contacts required to immobilize a particle by randomly placed contacts, where a contact can be a fixed point or another particle. Analytical solutions exist for 2-dimensional disks [127] and for 3-dimensional spheres caged by point contacts [28]. In Ref. [103] a caging number is calculated for rods ($\langle \gamma \rangle = 5$) where only the translations are blocked, which is a lower bound for the contact number in random rod packings.

Here, we show how to calculate the caging number $\langle \gamma \rangle$ for general shapes using a linear programming algorithm. In Ref. [141] it is shown that the relative acceleration of n contact points under the application of non-zero forces in a collection of rigid bodies can be written as the linear equation

$$A\vec{f} + \vec{b} = \vec{a} \tag{6.6}$$

where A is a symmetric and positive semi-definite n x n matrix, $\vec{f}$ is a vector whose elements are all larger than zero representing a positive pushing force and $\vec{a}$ is a vector whose elements consist of the relative accelerations of the n contact points. Rigid bodies are not allowed to overlap, which requires $\vec{a} \geq 0$, which can be written as a so-called Linear Complementarity Problem (LCP) [142], which is defined as follows:

$$A\vec{f} + \vec{b} \geq 0,\ \vec{f} \geq 0 \text{ and } \vec{f}^T \left(A\vec{f} + \vec{b} \right) = 0 \tag{6.7}$$

In the caging problem contacts are placed on a rigid body until all translations and rotations are blocked for the body. A body is caged if the relative acceleration at all contact points is zero under the application of a non-zero force [138] and we can use a LCP solver to determine whether a body is caged or not by examining the total force acting on a body. For a spherocylinder, the fixed contact points are randomly distributed on the spherocylinder with the restriction that the probability to place a point on a hemi-spherical cap or the cylindrical part is proportional to their respective surface areas.

6.3. Results and discussion

6.3.1. Molecular dynamics simulation results

A random sphere gas consisting of 2048 particles was contracted with the MCM to a volume fraction of 0.49. The spheres were then grown in size at various growth rates and the average contact number was recorded as a function of volume fraction (Fig. 6.2a). A lower growth rate keeps the spheres in contact resulting in a higher contact number. At a volume fraction of around 0.60 the average contact number becomes the same irrespectively of the growth rate. Similar results were obtained in the work of Silbert et al. [78] where the packing properties depended on the coefficient of restitution and the friction coefficient. The same procedure was followed for spherocylinders of aspect

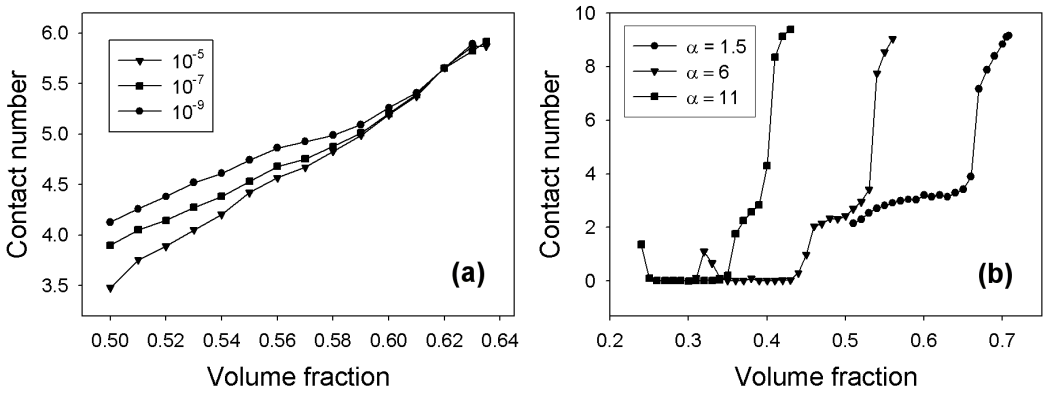

Figure 6.2: Evolution of contact number as a function of volume fraction for random packings with expanding particles. (a) Spheres with different growth rates (b) Spherocylinders with aspect ratio $\alpha = \frac{L}{D} = 1.5$ (circles), 6 (triangles) and 11 (squares) with growth rate 10^{-7}.

ratio 1.5, 6 and 11 with results shown in Fig. 6.2b. In contrast to spheres, where the contact number increases roughly linearly with volume fraction, spherocylinders show a sharp non-linear increase in contact number from about 3 up to a value between 9 and 10 for growth rate 10^{-7}.

As the volume fraction increases the distribution of contact numbers keeps roughly the same shape (Fig. 6.3) but the average shifts to a higher value. Note also that the average contact number (Fig. 6.2b) at the maximum density is fairly insensitive to the aspect ratio. This is consistent with the trend in the average caging number in Fig. 6.10.

The sharp non-linear increase in contact number in Fig. 6.2b for the spherocylinders could indicate a phase transition such that upon increasing the volume fraction of the random spherocylinder packings, the amount of order is increased in the packings due to alignment of spherocylinders. Graphical rendering of the packings (Fig. 6.4), however, shows that the sharp increase in Fig. 6.2b is not caused by particle alignment but apparently by particles suddenly coming into contact with each other.

A study of the nematic order parameter S (Fig. 6.5) confirms that the packings remain disordered as the particles grow in size but the spikes in the order parameter indicate small orientational changes in the packing. Donev et al. [97] calculated S for spheroids and found a value in the order of 0.05 consistent with the values in Fig. 6.5.

As the volume fraction increases, more particles come into contact and motion is progressively hindered. The percentage of caged particles was calculated, defining a caged particle as a particle whose translations and rotations are blocked by the presence of its contacting neighbors [28, 127]. It should be noted that the percentage of caged spheres does not provide a criterion for the stability of a sphere packing. A packing can be static where non-caged spheres rest on other spheres. Furthermore, caging is a local criterium and for modeling global jamming more complicated linear programming

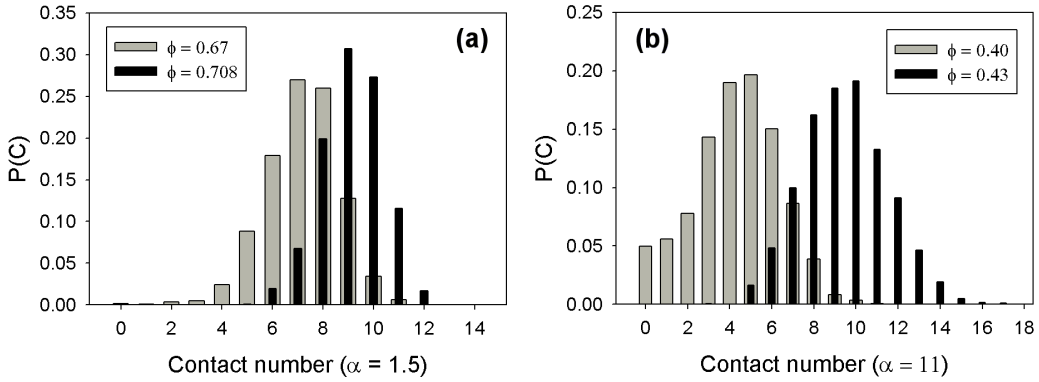

Figure 6.3: Distribution of contact numbers in random rod packings at different volume fractions for aspect ratio $\alpha = 1.5$ (a) and 11 (b). Black bars represent the maximum random packing density for the given aspect ratio.

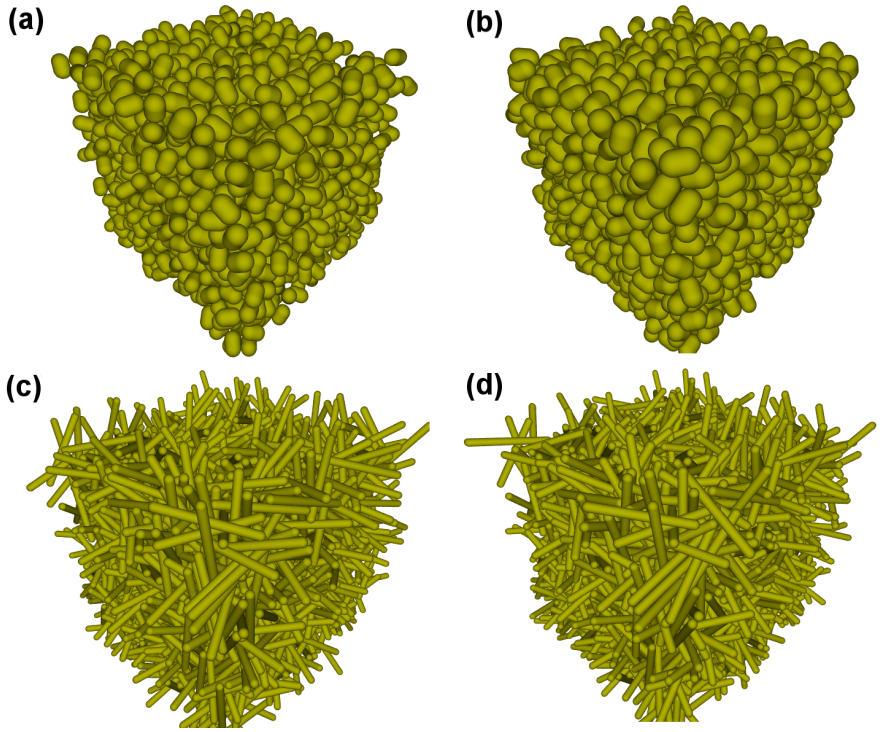

Figure 6.4: Graphical rendering of several packings. (a) Rods with aspect ratio 1.5 at $\phi = 0.51$ and at their maximum random packing density (b) $\phi = 0.708$. (c) Rods with aspect ratio 11 and $\phi = 0.40$ and at their maximum density (d) $\phi = 0.43$. These images indicate that the steep rise in contact number in Fig. 6.2b is not accompanied by a significant structural change.

algorithms are necessary [143] but it appears that long thin rods form an exception to this due to their highly uncorrelated entanglement. Nevertheless, a packing with a large percentage of non-caged spheres will certainly be unstable. Slower expansion rates

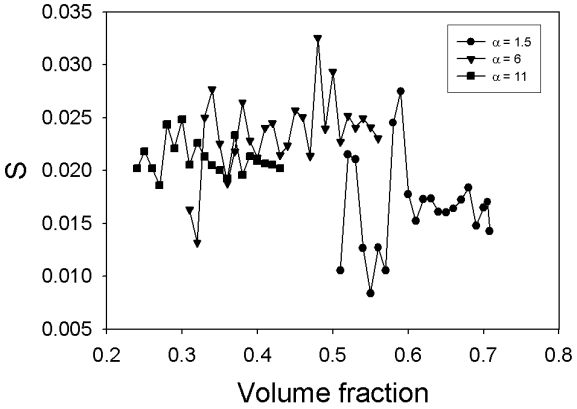

Figure 6.5: Order parameter S as a function of volume fraction for spherocylinders with aspect ratio 1.5 (circles), 6 (triangles) and 11 (squares). Upon increasing the volume fraction no significant increase in the amount of order is observed.

produce packings with more caged spheres as can be seen in Fig. 6.6a. The starting configuration was generated with the MCM. Possibly, a slow expansion rate leaves the cages intact whereas a higher rate destroys the initial cages, resulting in more non-caged spheres at lower volume fractions. A growth rate lower than 10^{-9}, for example 10^{-10}, did not produce more caged spheres but a percentage similar to 10^{-9}. This explanation is supported by the graph of the contact number versus volume fraction (Fig. 6.2a): for higher growth rates the contact number is lower at the same volume fraction indicating a higher percentage of non-caged spheres. At around 0.61 volume fraction the percentage of non-caged spheres converges for all growth rates, while for $\alpha = 1.5$ this rate independence is obtained for $\phi > 0.68$, see Fig. 6.6b.

The caging of spherocylinders was studied as described in section 6.3. In Fig. 6.6b the percentage of non-caged particles is plotted as a function of volume fraction for different growth rates. For the caging of rods only the blocking of translations and rotations perpendicular to the axis of symmetry were checked. The percentage of non-caged spheres and spherocylinders is directly correlated to the contact number as can be seen by comparing Figs. 6.2 and 6.6.

Fig. 6.2b and Fig. 6.6c show clear similarities; when the contact number sharply increases, the fraction of non-caged particles sharply decreases and plotting the percentage of non-caged particles as a function of contact number (Fig. 6.7) shows that the percentage of non-caged particles is almost independent of aspect ratio.

So far packing properties of spherocylinders with three different aspect ratios have been studied with the hybrid MCM-MD method, which yielded packings with different volume fractions but having roughly the same contact number. To see how the contact number depends on the aspect ratio, and whether it depends on the method, we now

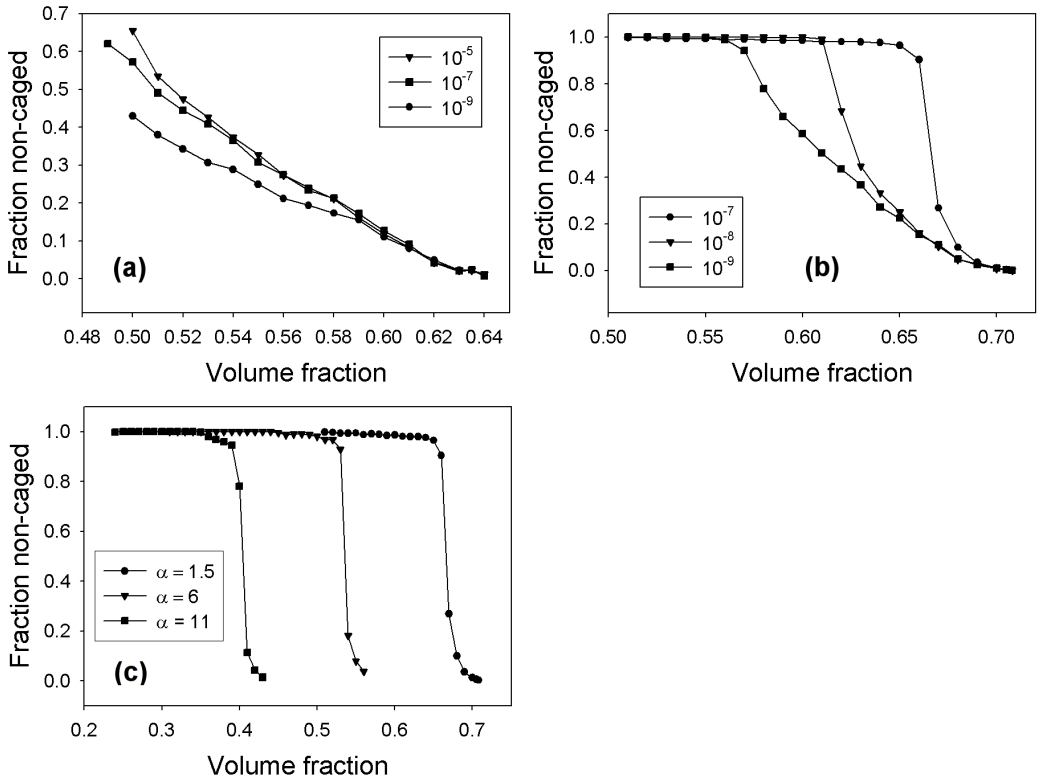

Figure 6.6: Fraction non-caged particles as a function of volume fraction for different expansion rates in case of (a) spheres and (b) spherocylinders with aspect ratio $\alpha = 1.5$. (c) Fraction of non-caged rods with aspect ratio $\alpha = 1.5$ (circles), 6 (triangles) and 11 (squares) in the quasi-static limit with growth rate 10^{-7}.

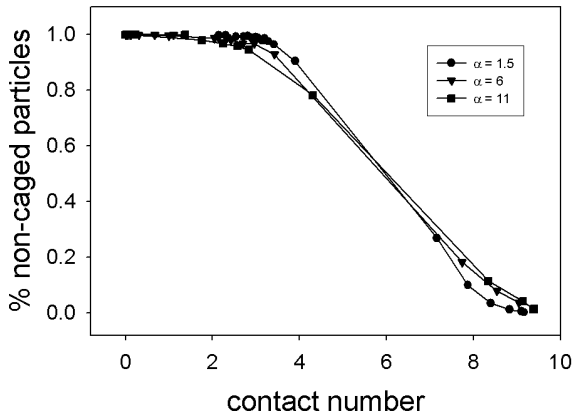

Figure 6.7: Fraction of non-caged particles as a function of contact number from data of Fig. 6.2b and Fig. 6.6c showing that the percentage of non-caged particles is almost independent of the aspect ratio for growth rate 10^{-7}.

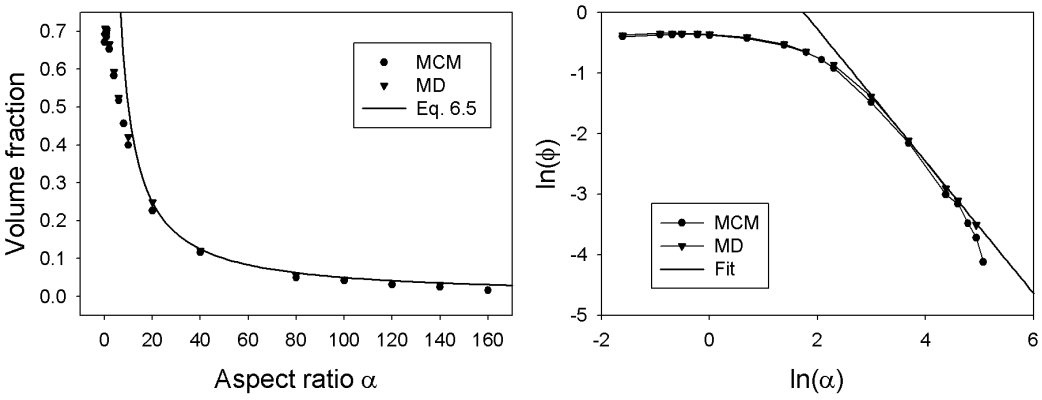

Figure 6.8: Volume fraction of a random spherocylinder packing as a function of aspect ratio (circles) MCM and (triangles) MD. (b) Log-log plot of the volume fraction as a function of aspect ratio with a slope -1.08.

consider in more detail the volume fraction and contact number as a function of aspect ratio. In Fig. 6.8 the volume fraction of a random spherocylinder packing is plotted as a function of aspect ratio for the MCM and the MD simulation of growing particles. The shapes of the curves are very similar and the volume fraction obtained via the MD simulation is slightly higher, as expected, since the MCM packings are used as starting configuration for the growth procedure. Note that the simulation data approach the long thin rod packing law (6.5) at an aspect ratio in the range 10 - 20. This is also the aspect ratio range in Fig. 6.10 in which the caging number asymptotes to its constant value in accordance with (6.5).

Though the volume fractions between the two methods do not differ much, there is a difference in the contact number (Fig. 6.9). For the MD simulation the contact numbers are clearly higher and comparable to the results from Blouwolff and Fraden [96] for uncompacted rods. Blouwolff and Fraden give an argument for the contact number in random rod packings, which we briefly recapitulate here. For N rods, there will be $N_c = N\langle C\rangle/2$ contacts and N_c contact equations that must be satisfied. Rods have 5 degrees of freedom, so there are a total of $5N$ variables specifying the configurations of the rods. The number of constraint equations must be less than the number of variables, yielding $N\langle C\rangle/2 \leq 5N$ and $\langle C\rangle \leq 10$. Mechanical stability gives 5 force-torque equations per particle. The number of mechanical stability equations cannot exceed the number of force variables, thus, $5N \leq N\langle C\rangle/2$ or $10 \leq \langle C\rangle$. Combining these two limits gives the isostatic value $\langle C\rangle = 10$. In [102, 137] it is noted that the isostatic contact value is not reached when spherocylinders are only slightly deviating from spheres. The number of degrees of freedom changes discontinuously and via the isostatic conjecture the number of contacts should change discontinuously too which, however, is not observed in computer simulations.

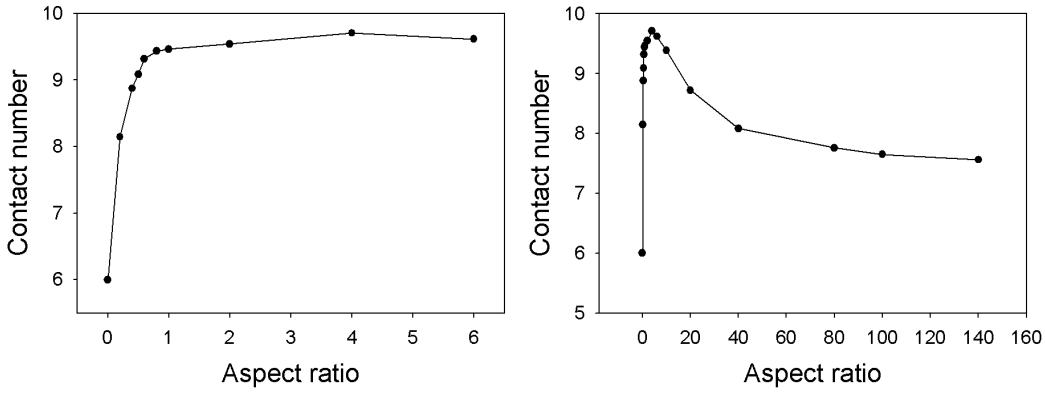

Figure 6.9: Contact number $\langle C \rangle$ as a function of aspect ratio for random spherocylinder packings. The dip in contact number after aspect ratio 6 is probably due to the packings being not completely jammed and further densification should be possible.

In Fig. 6.9 the contact number is plotted as a function of aspect ratio for random spherocylinder packings. The contact number increases monotonically and asymptotes towards a value between 9 and 10, which agrees quite well with the direct experimental value $\langle C \rangle = 9.8 \pm 0.3$ found in Ref. [96]. The finding that $\langle C \rangle$ asymptotes towards a constant value implies according to the random contact equation (6.5) the scaling $\phi L/D =$ constant for $L/D >> 1$, which has also been found experimentally [33]. In the next section a physical explanation for this constant will be given in terms of a local caging argument. The molecular dynamics procedure allows for slightly denser packings with better-defined contacts. The value of 10 is not reached but possibly implementing a "shaking" algorithm, which shakes the packings without inducing a nematic phase allows for further densification and increase of contact number.

In Ref. [138] it was shown that the parking number for spheres is about 8.4 but that it is not possible to pack each sphere with that contact number locally due to excluded volume effects. A contact number below the parking number is more optimal for a dense disordered packing. When slightly deviating from spheres the surface area of the particles hardly changes and also the excluded area as described for spheres in Ref. [127] will not alter significantly. Thus the parking number [27] for small aspect ratio spheroids and spherocylinders is expected to be around the same value as for spheres, which is below 10 and the parking number is an upper bound for the number of contacts that can be placed at random. It should be noted that the parking number is not really well-defined for higher aspect ratio spheroids and spherocylinders. As contacts are added randomly the available parking space decreases due to the non-overlap condition. At a certain point only spherocylinders with the right orientation will fit in that space which induces alignment in the particles.

6.3.2. Caging number for spherocylinders

Using the formalism described in section 6.2.2 we reproduced the exact caging number $\langle\gamma\rangle = 5$ for two-dimensional disks caged by uncorrelated point contacts [103]. We determined the caging number for infinitely long rods, considering only translations and rotations perpendicular to the axis of symmetry to be blocked (thus the rods can always move along and rotate around their long axis). The result for two- and three-dimensional rods is, respectively, $\langle\gamma\rangle = 5$ and $\langle\gamma\rangle = 9$. The caging number for spherocylinders as a function of aspect ratio was calculated (Fig. 6.10) where contacts are placed randomly on the cylindrical part or the hemi-spherical end caps with a probability proportional to the surface area of the cylindrical respectively hemi-spherical surface. For aspect ratio zero the caging number for 3-d spheres $\langle\gamma\rangle = 7$ is reproduced; a number derived analytically elsewhere [28]. For high aspect ratios $\langle\gamma\rangle$ approaches the value of 9 for infinite rods, as expected, since the probability of placing a contact on an end cap vanishes in the thin rod limit. Interestingly, immediately upon deviating from spheres (see Fig. 6.10) the caging number jumps to around 12 and then starts to decrease. Although we have reproduced limiting cases with our method for which we have the analytical solutions, it is difficult to numerically solve the LCP and it is not completely sure whether the results for almost spherical particles are numerically robust. However, the increase in caging number as such is physically plausible since the volume fraction of a random packing increases upon deviating from spheres which supports the fact that it becomes harder to cage or jam the non-spherical particles.

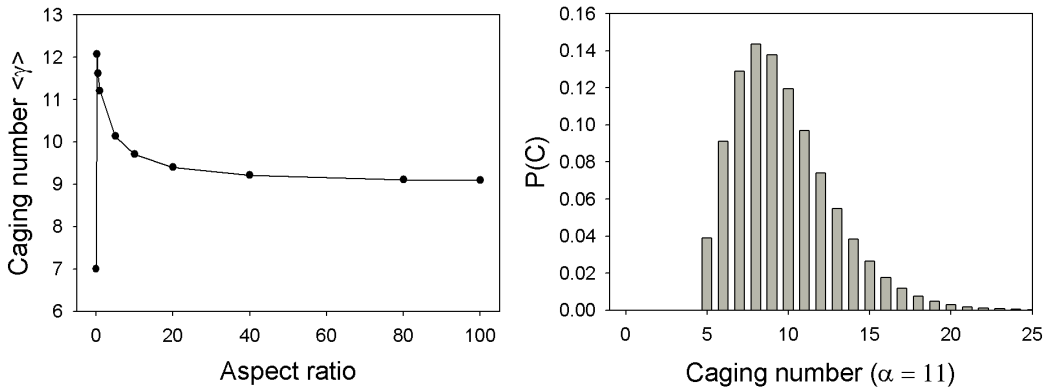

Figure 6.10: (a) Average number of contacts required to block rotations and translations perpendicular to the axis of symmetry for a spherocylinder as a function of its aspect ratio. (b) Distribution of contacts for the caging number of a spherocylinder with aspect ratio 11

Even though the caging number is a local contact number, the limiting value of $\langle\gamma\rangle = 9$ is surprisingly close to the isostatic value of 10 and average contact numbers from experiments $\langle C\rangle = 10.8\pm0.4$ [33] and $\langle C\rangle = 9.8\pm0.3$ [96]. Somewhere in the aspect ratio

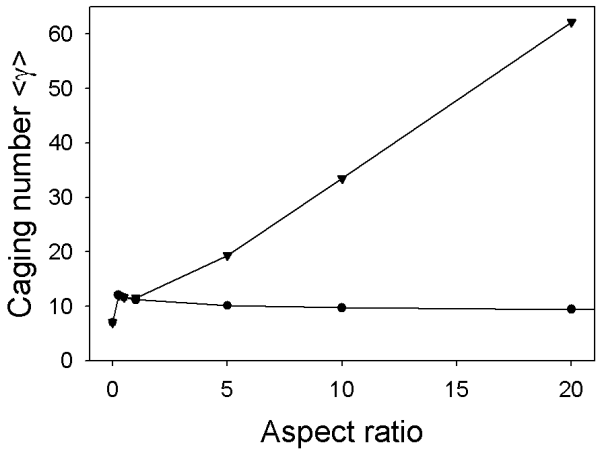

Figure 6.11: (triangles) Average number of contacts required to block rotations perpendicular to the axis of symmetry and all translations for a spherocylinders as a function of its aspect ratio. (circles) Fig. 6.10a

.

range 15 - 20 the caging number has become almost constant which is where the random contact equation yields a good comparison with experiments [33, 35]. High aspect ratio thin rods have uncorrelated contacts making the point contact approximation a valid choice where an extra contact could make sense to satisfy global jamming conditions. Interestingly, our results match well with simulations on semi-flexible rods, where a caging number of 8 was found [144].

In Fig. 6.11 the caging number is plotted as a function of aspect ratio, for the case where also translations along the axis of symmetry are required to be blocked. Here, the caging number is completely dominated by the probability to place a contact on both hemi-spherical caps, which becomes infinitesimally small in the limit of infinite aspect ratio yielding a sharp increase in the contact number. In view of the experimental and simulated contact numbers it is clear that in random thin rod packings the large majority of rods is unblocked at its ends. It should be noted that any small motion of rods parallel to their main axis has little effect on the random packing density because these axes are randomly oriented.

6.4. Conclusions

Performing molecular dynamics simulations on packings prepared with the mechanical contraction method is an efficient method for generating random packings with volume fractions and contact numbers comparable to experimental packings. In the limit of jamming, the packing properties such as contact number and percentage of caged spheres become independent of simulation parameters for random sphere packings. For spherocylinder packings the contact number rises sharply at a critical volume fraction

until a value between 9 and 10 at the jamming point, in line with the caging number $\langle\gamma\rangle = 9$, the isostatic value $\langle C\rangle = 10$ and the experimental value $\langle C\rangle = 9.8 \pm 0.3$. The percentage of non-caged spherocylinders follows the same trend as the contact number as expected. The amount of order as a function of volume fraction does not increase substantially as the particles expand in size while keeping the aspect ratio constant.

The caging number for rods arrested by uncorrelated point contacts asymptotes towards $\langle\gamma\rangle = 9$ at high aspect ratio according to the LCP calculation. This value is strikingly close to the experimental contact number $\langle C\rangle = 9.8$ for thin rods, which confirms that thin-rod packings are dominated by local effects in the form of truly random neighbour cages. The aspect ratio independence of the thin rod caging number further validates the random contact equation. Together with a value for the contact number, either from an isostatic argument or a caging analysis, this equation quantitatively explains the density of a random thin rod packing.

7

Expanding random rod packings and their possible relevance for biological cell motility

Abstract

Rod packings are simulated by growing randomly oriented, non-overlapping spherocylinders out of a random distribution of particle centres. This expansion method yields maximum random packing densities as a function of aspect ratio that are very similar to densities obtained via contraction of a dilute gas of spherocylinders, already having their final size (see Chapter 5). This similarity confirms that the random packing density represents a 'geometrical state' which only depends on particle geometry. For the expanding packings, stress on a wall is studied as a function of volume fraction and particle shape. The force generated by a growing packing might be relevant for the motility mechanism of certain biological cells that propel themselves via polymerization of randomly oriented filaments.

7.1. Introduction

A collection of randomly oriented hard rods can be quenched to a maximum packing density that is uniquely determined by the aspect ratio of the particles [93, 95]. Moreover, in the limit of long thin rods, the random packing density is linearly proportional to the inverse aspect ratio, in accordance with the long thin rod packing law [33, 34]. These insights have been further confirmed in Chapter 5 of this thesis. Moreover, in Chapter 6 we have analysed the contact numbers in a random rod packing, such that from the thin-rod packing law we can predict the packing density for a given (high) aspect ratio. This unique aspect-ratio dependence strongly suggests that the random rod packing density manifests a 'geometrical state'.

One motivation for the present chapter is to further explore this idea, by generating random packings via a route different from the contraction method we used so far (see Chapters 5 and 6 and Ref. [35]). This route is, instead of contracting a given collection of rods, to grow spherocylinders out of a gas of particle centres with a random orientation. It is not immediately obvious that such an expansion should produce the same final state as the contraction method. For example, it is conceivable that, given enough insertion attempts, a sufficiently thin rod always finds an orientation for some further growth in length without intersecting another rod. That possibility could lead to a maximum density that depends on the simulation route followed.

A second motivation for investigating a growth procedure is to study the expansive forces generated by the growing rods. If the density is indeed only determined by the aspect ratio, it follows that randomly growing rods must exert a stress on container walls because the density is inversely proportional to the aspect ratio. This stress development is also interesting because of a possible, rather unexpected biological application. Stewart [145] pointed out that expansion by a random thin-rod packing might be a good model for the motility of certain biological cells related to polymerization of random filaments.

In section 7.2 we first briefly explain the expanding-rod-packing (ERP) model for cell motility, referring for cell-biological details to the work of Stewart and co-workers [122, 146–148].

7.2. Background and methods

7.2.1. Random rods and cell-motility

In Fig. 7.1 an electron tomography of major sperm protein (MSP) filaments near a vesicle is shown [122]. The vesicles that assemble fibers are resealed fragments of the membrane from the leading edge of the cell. The close up shows that the tail produced by the motile machinery of amoeboid sperm of the nematode *Ascaris suum* consists of a disordered packing of rod-like filaments. Near the edge of the vesicle short

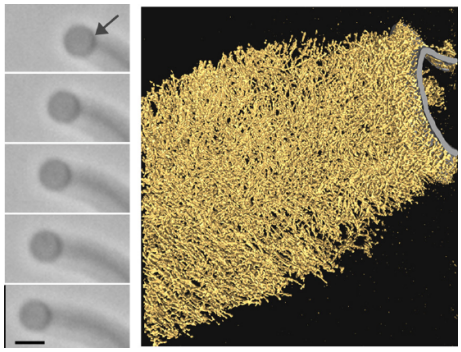

Figure 7.1: Electron tomography of major sperm protein filaments near the vesicle's edge [122]. (left) Moving vesicle producing a tail (right) Close up of the vesicle's edge.

filaments are packed at high density while further away longer filaments are packed at low density. This packing effect is explained by the random thin-rod packing law [33] for rigid rods, which states that the volume fraction of the packing is inversely proportional to the aspect ratio of the rods and was verified with experiments [33, 96] and computer simulations [35, 102].

This raises the question what is the mechanism behind the movement of the vesicle. A possible mechanism is that the movement is caused by expansion of the filament network. As the filaments grow in length, their aspect ratio increases and according to the thin-rod packing law their packing density decreases, which means that the total volume occupied increases. This increase in volume results in a net pushing force on the vesicle. Another pushing force occurs from the short filaments ratcheting around and colliding with the vesicle and the supporting tail. By generating the tail from high aspect ratio filaments less building material is needed to construct the tail because higher aspect ratio filaments pack less dense, which also results in more efficient movement.

Experimental support for this idea came from experiments done with a mutant D83R, which is an altered form of MSP (the protein that polymerizes to form filaments). The mutation alters the structure of the protein sufficiently to alter its polymerization properties so that it produces shorter filaments [122]. Shorter filaments should not have a big impact on the vesicle movement speed if only ratcheting is important because shorter filaments pack at a higher density, which leads to more ratcheting. On the other hand the structure of the tail and the expansion of the network depend very much on the aspect ratio. The experimental results show that vesicles that produce shorter filaments move more slowly, suggesting that the expansion of the rod network is a possible mechanism for the vesicle to move with a higher efficiency [122].

7.2.2. Simulation methods

To asses the plausibility of the mechanism described in the previous paragraph we deviced some extra simulations complementing the work already done with the mechanical contraction method (MCM) [35]. The original MCM contracted the volume of the periodic simulation box until a random dense packing was created of spherocylinders with a fixed aspect ratio. For the vesicle movement described in the previous paragraph the filaments grow in length and it is not a priori clear whether the volume fraction is still inversely proportional to the aspect ratio upon increasing the aspect ratio dynamically.

To test this we modified the original contraction method in the following way: The volume of the periodic simulation box remains constant during the simulation and the starting configuration consists of a gas of spherocylinders of aspect ratio 10^{-4} with a random orientation at a user-specified density. At each step in the simulation the length of the spherocylinders is increased. The simulation is stopped when it is no longer possible to remove overlap between the growing spherocylinders and the final volume fraction and aspect ratio is recorded. Varying the starting density of spherocylinders generates random packings of spherocylinders with a different aspect ratio. A high number density results in a dense packing of short aspect ratio spherocylinders while a low number density gives a low volume fraction packing with high aspect ratio spherocylinders.

In the previous simulation the volume of the simulation box was held fixed, while the conclusion was that the vesicle moved due to an expanding network of rods and thus an increasing volume. To model this more closely, a simulation was started with a random close packing of spherocylinders with aspect ratio 10^{-4} and a random orientation built in. Then, the aspect ratio is increased at each step, while keeping the volume of the simulation box constant. This is the same as the first simulation. At first, increasing the aspect ratio resulted in packings with a higher volume fraction than the starting random close packing volume fraction. When the overlap could not be removed anymore, the volume fraction and aspect ratio was recorded. Then, the volume of the periodic box was increased with a fixed amount and the rods were grown further in size until it was no longer possible to grow further. The volume fraction and aspect ratio are recorded again and the volume of the simulation box is increased again. This process was repeated for a fixed number of times.

Finally, simulations were done that mimicked the experimental setup more closely. The simulation framework of Chapter 6 was used to perform molecular dynamics on expanding spherocylinders. The starting configuration was a random close packing of spherocylinders with a movable wall placed below the packing. The spherocylinders were grown in length with a user specified growth rate and new spherocylinders were added at a constant rate. Spherocylinders interacted with the wall in the same way as

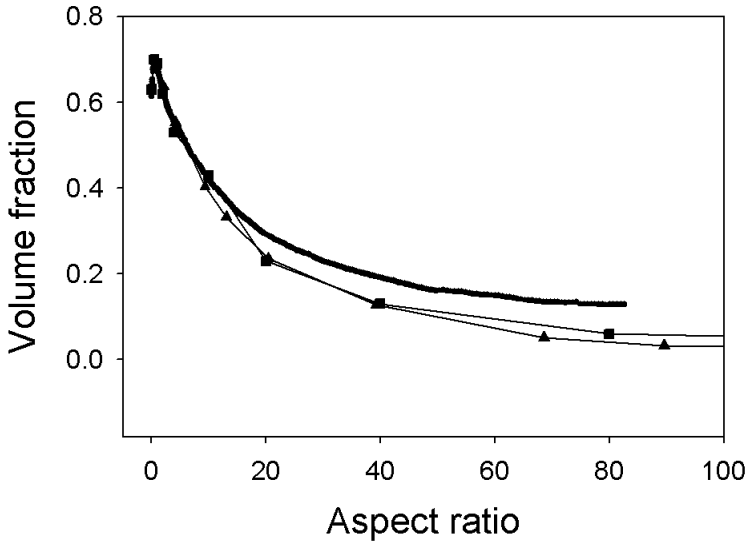

Figure 7.2: Original MCM [35] (squares) Growing from a gas of particles in a fixed volume (triangles) Starting from a random close sphere packing and increasing the volume in steps (circles).

with each other, through spring forces applied when overlapping as described in Chapter 6. The amount of force was recorded on the movable wall and if it was larger than a threshold, the wall was moved. Typical simulation parameters are $k = 10^4$, $\gamma = 100$ and $\gamma_{bg} = 0.1$.

7.3. Results and discussion

In Fig. 7.2 the volume fraction is plotted as a function of aspect ratio for random packings of spherocylinders for the various simulations. The original MCM and the spherocylinders growing from a gas show almost the same curve, whereas starting from a dense packing shows the same curve for short aspect ratios (less than about 10),whereas for higher aspect ratios the volume fraction is higher than for the other two methods.

Fig. 7.3 shows a graphical rendering of various stages in the simulation as the wall moves downward. The structure of the tail remains disordered as the simulation progresses but small ordering along the direction of movement does occur. As the rods expand and new rods are added close to the wall, a force is exerted on the wall, which is plotted in Fig. 7.4. The force occurs in spikes indicating that the wall makes contact with rods and moves and waits for a new contact to occur. The actual magnitude of the force depends on simulation parameters.

Furthermore, the change in pressure was measured upon contracting a random packing of spheres and spherocylinders with movable walls (Fig. 7.5). A prominent difference between spheres and spherocylinders is that the sphere packing shows a smooth increase

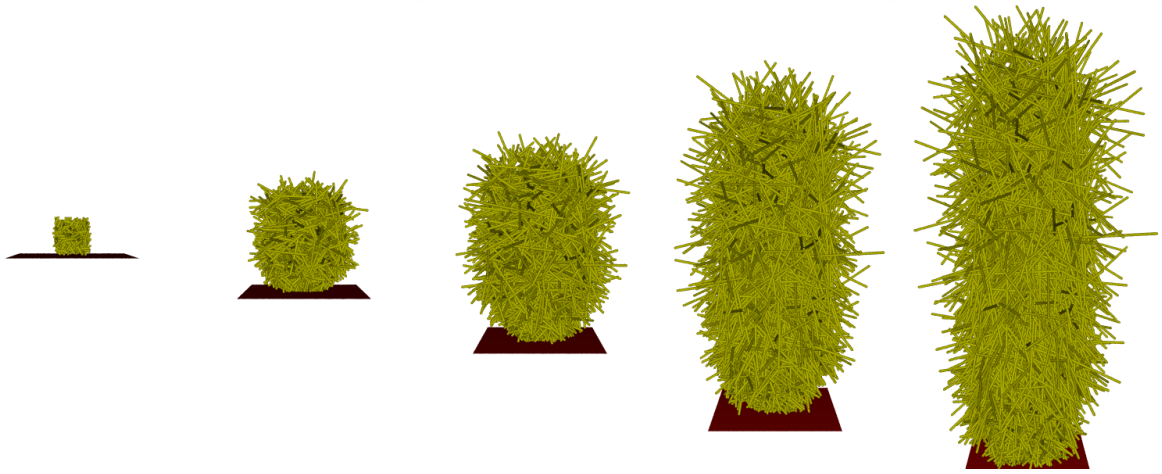

Figure 7.3: Graphical rendering of several stages in the simulation as the wall moves downwards due to the pushing force of the expanding tail.

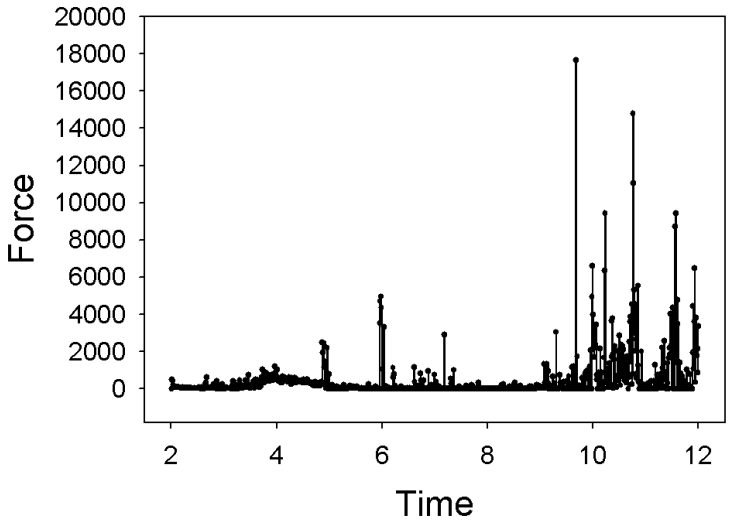

Figure 7.4: Force (N) on the wall as a function of time.

in pressure on the walls while the spherocylinders show a spiked increase. However, more simulations need to be done with different parameters such as aspect ratio, viscosity and wall movement speed in order to draw more solid conclusions from the results.

7.4. Conclusions

The volume fraction of random spherocylinders is inversely proportional to the aspect ratio regardless of the chosen simulation method, which confirms that the random rod packing density represents an almost path-independent geometrical state. All performed simulations indicate that an expansion of a rod network is a plausible model for the

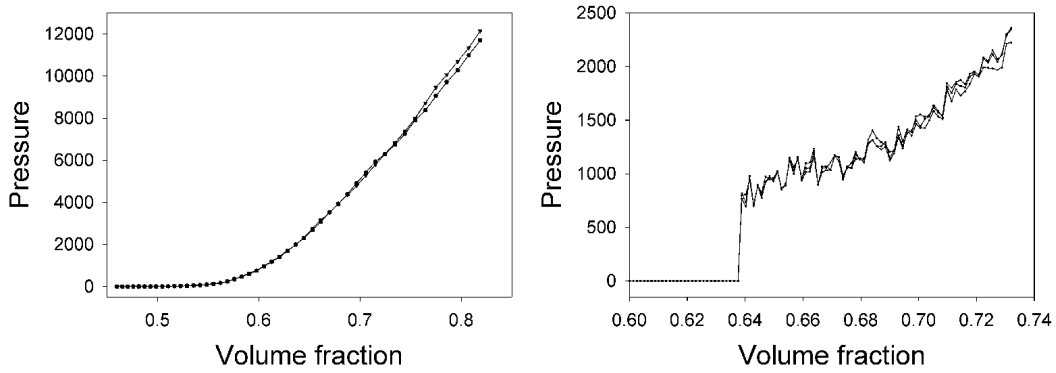

Figure 7.5: Measurement of pressure (Pa) on the walls while contracting a packing of (a) spheres and (b) spherocylinders with aspect ratio 1.5.

contribution of randomly polymerizing filaments to the motility of certain biological cells.

Acknowledgements

The possible relevance of the packing law for random thin rods to cell motility was first put forward to us by Murray Stewart (MRC Laboratory of Molecular Biology). The topic is part of an ongoing collaboration between his group and Thomas Roberts and co-workers from the department of Biological Science, Florida State University, with input from our lab on theory and simulations for randomly packed rods. Stefan Luding and Stephen Williams are acknowledged for valuable discussions and Thijs Vlugt for his invaluable help with setting up computational facilities.

Bibliography

[1] A. Vrij and R. Tuinier. *Structure of concentrated colloidal dispersions*, volume IV of *Fundamentals of Interface and Colloid Science*. Elsevier, Amsterdam, 2005.

[2] A. P. Philipse. *Particulate colloids: Aspects of preparation and characterization*, volume IV of *Fundamentals of Interface and Colloid Science*. Elsevier, Amsterdam, 2005.

[3] T. Heath. *A history of Greek mathematics*, volume II. Oxford Clarendon Press, Oxford, 1921.

[4] T. Heath. *A manual of Greek mathematics*. Dover, 2003.

[5] B. B. Mandelbrot. *The fractal geometry of nature*. Freeman, San Francisco, 1982.

[6] J. Kepler. *The six-cornered snowflake*. Oxford Clarendon Press, 1966.

[7] T. C. Hales. *Ann. Math.*, 162:1065, 2005.

[8] D. Bideau and A. Hansen. *Disorder and granular media*. Random materials and processes. Elsevier, Amsterdam, 1993.

[9] T. Aste and D. Weaire. *The pursuit of perfect packing*. Institute of Physics Publishing, 2000.

[10] J. D. Bernal. *Trans Faraday Soc.*, 33:27, 1937.

[11] J. D. Bernal. *Nature*, 183:141, 1959.

[12] D. Turnbull and M. H. Cohen. *Nature*, 203:964, 1964.

[13] M. Stroeven. *Discrete numerical modelling of composite materials*. PhD thesis, TU Delft, 1999.

[14] P. Stroeven and M. Stroeven. *Image Anal. Stereol.*, 19:85, 2000.

[15] D. Hull. *An introduction to composite materials*. Cambridge University Press, Cambridge, 1987.

[16] H. S. Katz and J. V. Milewski. *Handbook of fillers and reinforcement for plastics*. Van Nostrand Reinhold, New York, 1987.

[17] R. M. German. *Particle packing characteristics*. Metal Powder Industries Federation, Princeton, 1989.

[18] W.A. Gray. *The packing of solid particles*. Chapman and Hall, London, 1968.

[19] R. Zallen. *The physics of amorphous solids*. Wiley, New York, 1983.

[20] D. J. Cumberland and R. J. Crawford. *The packing of particles*, volume 6 of *Handbook of powder technology*. Elsevier, Amsterdam, 1987.

[21] W. O. Smith, P. D. Foote, and P. F. Busang. *Phys. Rev.*, 34:1271, 1929.

[22] S. Sacanna, L. Rossi, A. Wouterse, and A. P. Philipse. *J. Phys.: Cond. Matter*, 19:376108, 2007.

[23] D. van Asten. *Bachelor thesis, Universiteit Utrecht*, 2006.

[24] H. Wadell. *J. of Geology*, 43:250, 1935.

[25] L. Onsager. *Ann. N. Y. Acad. Sci.*, 51:627, 1949.

[26] H. S. M. Coxeter. *Trans. NY Acad. Sci.*, 11:320, 1962.

[27] M. L. Mansfield, L. Rakesh, and D. A. Tomalia. *J. Chem. Phys.*, 105:3245, 1996.

[28] E. A. J. F. Peters, M. Kollmann, Th. M. A. O. M. Barenbrug, and A. P. Philipse. *Phys. Rev. E*, 63:021404, 2001.

[29] A. P. Philipse. *Colloids and Surfaces A : Physicochem. Eng. Aspects*, 213:167, 2003.

[30] A. Donev, S. Torquato, F. H. Stillinger, and R. Connelly. *J. Comp. Phys.*, 197:139, 2004.

[31] A. Donev, S. Torquato, F. H. Stillinger, and R. Connelly. *J. Appl. Phys.*, 95:989, 2004.

[32] P. J. Steinhardt, D. R. Nelson, and M. Ronchetti. *Phys. Rev. B*, 28:784, 1983.

[33] A. P. Philipse. *Langmuir*, 12:1127, 1996.
[34] A. P. Philipse. *Corrigendum Langmuir*, 12:5971, 1996.
[35] S. R. Williams and A. P. Philipse. *Phys. Rev. E*, 67:051301, 2003.
[36] J. D. Bernal. *Nature*, 188:111, 1960.
[37] G. D. Scott. *Nature*, 194:956, 1962.
[38] G. D. Scott and D. M. Kilgour. *J. Appl. Phys.*, 2:863, 1969.
[39] G. Mason. *Nature*, 217:733, 1968.
[40] J. B. Knight, C. G. Fandrich, C. N. Lau, H. M. Jaeger, and S. R. Nagel. *Phys. Rev. E*, 51:3957, 1995.
[41] E. R. Nowak, J. B. Knight, E. Ben-Naim, H. M. Jaeger, and S. R. Nagel. *Phys. Rev. E*, 57:1971, 1998.
[42] C. C. Mounfield and S. F. Edwards. *Physica A*, 210:279, 1994.
[43] G. T. Seidler, G. Martinez, L. H. Seeley, K. H. Kim, E. A. Behne, S. Zaranek, B. D. Chapman, S. M. Heald, and D. L. Brewe. *Phys. Rev. E*, 62:8175, 2000.
[44] T. Aste, M. Saadatfar, and T. J. Senden. *Phys. Rev. E*, 71:061302, 2005.
[45] G. Y. Onoda and E. G. Liniger. *Phys. Rev. Lett.*, 64:2727, 1990.
[46] A. van Blaaderen and P. Wiltzius. *Science*, 270:1177, 1995.
[47] A. P. Philipse and C. Pathmamanoharan. *J. Colloid Interface Sci.*, 159:96, 1993.
[48] T. Eckert and E. Bartsch. *Phys. Rev. Lett.*, 89:125701, 2002.
[49] S. I. Henderson, T. C. Mortensen, S. M. Underwood, and W. van Megen. *Physica A*, 233:102, 1996.
[50] D.M.E. Thies-Weesie and A. P. Philipse. *J. Colloid Interface Sci.*, 162:470, 1994.
[51] R. K. McGeary. *J. Am. Ceram. Soc.*, 44:513, 1961.
[52] J. L. Finney. *Proc. R. Soc. London*, Ser. A 319:479, 1970.
[53] K. Gotoh and J. L. Finney. *Nature*, 252:202, 1974.
[54] R. K. Bordia. *Scripta Mettallurgica*, 18:725, 1984.
[55] J. G. Berryman. *Phys. Rev. A*, 27:1053, 1983.
[56] J. X. Liu and T. J. Davies. *Powder Metallurgy*, 40:48, 1997.
[57] S. F. Edwards and C. C. Mounfield. *Physica A*, 210:290, 1994.
[58] S. Torquato, T. M. Truskett, and P. G. Debenedetti. *Phys. Rev. Lett.*, 84:2064, 2000.
[59] J. Roux. arxiv:cond-mat/0405358. *http://arxiv.org/PS_cache/cond-mat/pdf/0405/0405358.pdf.*
[60] J. Roux. *Phys. Rev. E*, 61:6802, 2000.
[61] D. E. G. Williams. *J. Phys. C: Solid State Phys.*, 18:L181, 1985.
[62] W. Uhler and R. Schilling. *J. Phys. C: Solid State Phys.*, 18:L979, 1985.
[63] D. Bideau, J. P. Troadec, and L. Oger. *C. R. Acad. Sci. Paris*, 297:319, 1983.
[64] D. Bideau, A. Gervois, L. Oger, and J.P. Troadec. *J. Phys. (Paris)*, 47:1697, 1986.
[65] T. Aste. *Phys. Rev. E*, 53:2571, 1996.
[66] J. A. Dodds. *J. Colloid Interface Sci.*, 77:317, 1979.
[67] H. J. H. Brouwers. *Phys. Rev. E*, 74:31309, 2006.
[68] D. Frenkel and B. Smit. *Understanding molecular simulation*. Academic Press, San Diego, 2002.
[69] M. P. Allen and D. J. Tildesley. *Computer Simulation of Liquids*. Oxford Science Publications, 1987.
[70] D. C. Rapaport. *The Art of Molecular Dynamics Simulation*. Cambridge University Press, 2004.
[71] E. L. Hinrichsen, J. Feder, and T. Jossang. *J. Stat. Phys.*, 44:793, 1986.
[72] D. W. Cooper. *Phys. Rev. A*, 38:522, 1988.

[73] C. H. Bennett. *J. Appl. Phys.*, 43:2727, 1971.
[74] D. J. Adams and A. J. Matheson. *J. Chem. Phys.*, 56:1989, 1972.
[75] E. L. Hinrichsen, J. Feder, and T. Jossang. *Phys. Rev. A*, 41:4199, 1990.
[76] A. Donev. *Jammed packings of hard particles*. PhD thesis, Princeton University, 2006.
[77] B. D. Lubachevsky, F. H. Stillinger, and E. N. Pinson. *J. Stat. Phys.*, 64:501, 1991.
[78] L. E. Silbert, D. Ertas, G. S. Grest, T. C. Halsey, and D. Levine. *Phys. Rev. E*, 65:031304, 2002.
[79] W. Schaertl and H. Sillescu. *J. Stat. Phys.*, 77:1007, 1994.
[80] H. A. Makse, D. L. Johnson, and L. M. Schwartz. *Phys. Rev. Lett.*, 84:4160, 2000.
[81] J. D. Bernal and J. Mason. *Nature*, 188:910, 1960.
[82] K. L. Johnson. *Contact mechanics*. Cambridge University Press, Cambridge, 1985.
[83] H. A. Makse, N. Gland, D. L. Johnson, and L. M. Schwartz. *Phys. Rev. Lett.*, 76:3448, 1996.
[84] D. He, N. N. Ekere, and L. Cai. *Phys. Rev. E*, 60:7098, 1999.
[85] J. E. Marsden and A. J. Tromba. *Vector calculus*. W. H. Freeman and company, New York, 1996.
[86] F. X. Villarruel, B. E. Lauderdale, D. M. Mueth, and H. M. Jaeger. *Phys. Rev. E*, 61:6914, 2000.
[87] R. P. Zou. *Chem. Eng. Science*, 51:1177, 1996.
[88] R. P. Zou, A. B. Yu, and X. Y. Lin. *J. Am. Ceram. Soc.*, 82:933, 1999.
[89] A. B. Yu, R. P. Zou, and N. Standish. *J. Am. Ceram. Soc.*, 75:2765, 1992.
[90] A. B. Yu, R. P. Zou, and N. Standish. *Ind. Eng. Chem. Res.*, 35:3730, 1996.
[91] R. P. Zou and A. B. Yu. *Powder Technology*, 88:71, 1996.
[92] R. P. Zou, X. Y. Lin, A. B. Yu, and P. Wong. *J. Am. Ceram. Soc.*, 80:646, 1997.
[93] M. Nardin, E. Papirer, and J. Schultz. *Powder Technology*, 44:131, 1985.
[94] O. Rahli, L. Tadrist, and R. Blanc. *C. R. Acad. Sci. Paris*, 327:725, 1999.
[95] J. V. Milewski. *Ind. Eng. Chem. Prod. Res. Dev.*, 17:363, 1978.
[96] J. Blouwolff and S. Fraden. *Europhys. Lett.*, 76:1095, 2006.
[97] W. N. Man, A. Donev, F. H. Stillinger, M. T. Sullivan, W. B. Russel, D. Heeger, S. Inati, S. Torquato, and P. M. Chaikin. *Phys. Rev. Lett.*, 94:198001, 2005.
[98] A. P. Philipse, A. Nechifor, and C. Patmamanoharan. *Langmuir*, 10:4451, 1994.
[99] P. A. Buining and H. N. W. Lekkerkerker. *J. Phys. Chem.*, 97:11510, 1993.
[100] J. G. Parkhouse and A. Kelly. *Proc. R. Soc. London A*, 451:737, 1995.
[101] K. E. Evans and A. G. Gibson. *Composites Science and Technology*, 25:149, 1986.
[102] A. Wouterse, S. R. Williams, and A. P. Philipse. *J. Phys.: Cond. Matter*, 19:406215, 2007.
[103] A. P. Philipse and A. Verberkmoes. *Physica A*, 235:186, 1997.
[104] B. J. Buchalter and R. M. Bradley. *Phys. Rev. A*, 46:3046, 1992.
[105] J. D. Sherwood. *J. Phys. A: Math. Gen.*, 30:839, 1997.
[106] A. Donev, I. Cisse, D. Sachs, E. Variano, F. H. Stillinger, R. Connelly, S. Torquato, and P. M. Chaikin. *Science*, 303:990, 2004.
[107] G. T. Nolan and P. E. Kavanagh. *Powder Technology*, 84:199, 1995.
[108] J. P. Latham, Y. Lu, and A. Munjiza. *Geotechnique*, 51:871, 2001.
[109] L. Pournin, M. Weber, M. Tsukahara, J. A. Ferrez, M. Ramaioli, and T. M. Liebling. *Granular Matter*, 7:119, 2005.
[110] M. Adams, Z. Dogic, S. L. Keller, and S. Fraden. *Nature*, 393:349, 1998.
[111] C. R. A. Abreu, F. W. Tavares, and M. Castier. *Powder Technology*, 134:167, 2003.
[112] A. V. Petukhov, D. Aarts, I. P. Dolbnya, E. H. A. de Hoog, K. Kassapidou, G. J. Vroege, W. Bras, and H. N. W. Lekkerkerker. *Phys. Rev. Lett.*, 88:208301, 2002.
[113] A. P. Philipse and S. G. J. M. Kluijtmans. *Physica A*, 274:516, 1999.

[114] J. G. Wendel. *Math. Scand.*, 11:109, 1962.
[115] T. I. Quickenden and G. K. Tan. *J. Colloid Interface Sci.*, 48:382, 1974.
[116] A. Lawlor, D. Reagan, G. D. McCullagh, P. D. Gregorio, P. Tartaglia, and K. A. Dawson. *Phys. Rev. Lett.*, 89:245503, 2002.
[117] P. De Gregorio, A. Lawlor, P. Bradley, and K. A. Dawson. *Proc. Natl. Acad. Sci. U.S.A.*, 102:5669, 2005.
[118] K. De Lange-Kristiansen, A. Wouterse, and A. P. Philipse. *Physica A*, 358:249, 2005.
[119] T. Sitharam and N. Shimizu. *Proceedings of fourteenth Engineering Mechanics Conference, ASCE, Austin, Texas*, page 96, 2000.
[120] N. N. Sinelnikov, M. A. Mazo, and A. A. Berlin. *Colloid Journal*, 57(6):853, 1995.
[121] L. Schlaefli. *Gesammelte mathematische Abhandlungen I.* Basel, 1950.
[122] L. Miao, O. Vanderlinde, J. Liu, R. P. Grant, A. Wouterse, A. P. Philipse, M. Stewart, and T. M. Roberts. *To be submitted*, 2008.
[123] T. Aste. *J. Phys.: Cond. Matter*, 17:S2361, 2005.
[124] Z. H. Stachurski. *Phys. Rev. Lett.*, 90:155502, 2003.
[125] P.-G. de Gennes. *C. R. Physique*, 3:1263, 2002.
[126] M. Shahinpoor. *Powder Technology*, 25:163, 1980.
[127] A. Wouterse, M. Plapp, and A. P. Philipse. *J. Chem. Phys.*, 123:054507, 2005.
[128] W. M. Visscher and M. Bolsterli. *Nature*, 239:504, 1972.
[129] C. B. Barber, D. P. Dobkin, and H. T. Huhdanpaa. *ACM Trans. Math. Software*, 22:469, 1996.
[130] A. R. Kansal, S. Torquato, and F. H. Stillinger. *J. Chem. Phys.*, 117:8212, 2002.
[131] D. van der Beek, A. V. Petukhov, S. M. Oversteegen, G. J. Vroege, and H. N. W. Lekkerkerker. *Eur. Phys. J. E*, 16:253, 2005.
[132] R. P. A. Dullens, M. C. D. Mourad, D. G. A. L. Aarts, J. P. Hoogenboom, and W. K. Kegel. *Phys. Rev. Lett.*, 96:028304, 2006.
[133] G. J. Vroege and H. N. W. Lekkerkerker. *Rep. Prog. Phys.*, 55:1241, 1992.
[134] J. A. C. Veerman and D. Frenkel. *Phys. Rev. A*, 45:5632, 1992.
[135] A. Isihara. *J. Chem. Phys.*, 19:1142, 1951.
[136] S. F. Edwards and D. V. Grinev. *Phys. Rev. Lett.*, 82:5397, 1999.
[137] P. M. Chaikin, A. Donev, W. N. Man, F. H. Stillinger, and S. Torquato. *Ind. Eng. Chem. Res.*, 45:6960, 2006.
[138] A. Wouterse and A. P. Philipse. *J. Chem. Phys.*, 125:194709, 2006.
[139] A. Donev, S. Torquato, and F. H. Stillinger. *J. Comp. Phys.*, 202:737, 2005.
[140] A. Donev, S. Torquato, and F. H. Stillinger. *J. Comp. Phys.*, 202:765, 2005.
[141] D. Baraff. *Computer Graphics Proceedings (Siggraph)*, 23:223, 1989.
[142] D. Baraff. *Computer Graphics Proceedings (Siggraph)*, page 23, 1994.
[143] A. Donev, F. H. Stillinger, P. M. Chaikin, and S. Torquato. *Phys. Rev. Lett.*, 92:255506, 2004.
[144] D. Rodney, M. Fivel, and R. Dendievel. *Phys. Rev. Lett.*, 95:108004, 2005.
[145] M. Stewart. *Personal communication.*
[146] T. D. Pollard and G. G. Borisy. *Cell*, 112:453, 2003.
[147] T. M. Roberts, E. Salmon, and M. Stewart. *J. Cell Biol.*, 140:367, 1998.
[148] T. M. Roberts and M. Stewart. *J. Cell Biol.*, 149:7, 2000.

Summary

This thesis deals with the random packing of colloids and granular matter. A random packing is a stable disordered collection of touching particles, without long-range positional and orientational order. Random packings of particles with the same shape but made of different materials show large similarities, independent of particle size, indicating that particle shape is an important factor for their packing. The aim of this thesis is to further develop our understanding of the relation between particle shape and packing properties such as volume fraction occupied and contact numbers.

In Chapter 3, several contact numbers are introduced for spheres and their relation to sphere packings is discussed. For example, the caging number is defined as the average minimum number of randomly placed neighbour spheres on a single center sphere to immobilize that single sphere. The caging number utilizes the fact that particles cannot move in a stable packing because their motion is blocked by other particles. Analytic solutions are presented for the caging of two-dimensional disks, for neighbour disks that are larger than the center disk. An exact solution is given for neighbour disks with a radius smaller than the center disk by approximating the original problem. The approximated problem describes the original problem very well as was verified with computer simulation. Furthermore, a good approximation is given for the caging number of three-dimensional spheres. The caging number relates to loose random packing since it is the lowest contact number for which a single sphere is blocked. Another contact number, the so-called parking number relates to denser packings. It is defined as the average maximum number of spheres that can be placed randomly on a central sphere.

The contact numbers from Chapter 3 are then used in Chapter 4 to generate geometrical clusters from which global properties can be calculated as an ensemble average. This concept, which appears to work well when clusters of appropriate size are generated, is based on the absence of long-range order in a random packing, such that the packing can be considered as a collection of the aforementioned clusters. Loose as well as dense packings can be modeled by varying the rules for the generation of clusters. Thus, by varying the microscopic rules the macroscopic properties are altered. Essential findings are a lower bound on volume fraction for random loose packing that is surprisingly close to the freezing volume fraction for hard spheres and, for random close packing, the observation of an unexpected split peak in the distribution of volume fractions for the local configurations. Our ensemble analysis also highlights the importance

of collective and global effects in random sphere packings by comparing clusters generated via local rules to random sphere packings and clusters that do include collective effects.

Chapter 5 deals with the effect of the particle shape on the packing properties of particles. Packings are created with the mechanical contraction method (MCM), which is extended to handle general convex shapes. Shapes studied are spherocylinders, spheroids and cut spheres. It appears that for short aspect ratios, spheroids and spherocylinders pack very similar and both show a density maximum at about the same aspect ratio. At large aspect ratios spherocylinders pack more dense than spheroids because the ratio between particle volume and excluded volume is larger for spherocylinders than spheroids with equal aspect ratio. The influence of a flat face on packing properties can be studied carefully by using cut spheres. It turns out that the contribution of the flat face starts to become important at aspect ratio of two. Significant order is found for high aspect ratio cut spheres in the form of stacks of aligned particles, which are quantified with several parameters. Below aspect ratio two the particles form stable disordered packings which are insensitive to the simulation parameters.

Contact numbers are an important property for particle packings and in Chapter 6 a Molecular Dynamics (MD) study is performed to improve the determination of the contact number for spherocylinders as was previously determined using the MCM only. The latter method yields a contact number of three for high aspect ratio spherocylinders, which is too low compared to recent experiments on thin rod packings. Packings that are slightly more dense and have better defined contacts can be generated by doing MD on packings generated with the MCM and a better agreement with experiments was reached. A study is performed on the caging number as a function of volume fraction for spheres and spherocylinders by slowly growing them in size. Furthermore, a linear programming method is introduced to calculate the caging number for spherocylinders with arbitrary finite aspect ratios, as well as infinitely long rods. At high aspect ratios the spherocylinder caging number asymptotes to the constant value for infinite rods, in agreement with the observation in experiments and simulations that for random thin rods, the product of packing density and aspect ratio is a constant.

Several simulation methods for expanding rod packings are presented in Chapter 7. The volume fraction is still inversely proportional to the aspect ratio for these expanding packings independent of the simulation method chosen. The simulations show that expansion of rod packings could be a plausible additional mechanism for the movement of certain biological cells.

Samenvatting

Dit proefschrift beschrijft de invloed van de vorm van een deeltje op het stapelen van de betreffende deeltjes. De deeltjes in dit proefschrift zijn onderdeel van de zogenaamde granulaire materie maar kunnen ook colloiden zijn. Als voorbeeld kan het stapelen van sinaasappels aangehaald worden. De sinaasappels kunnen netjes één voor één ordelijk in een doos gelegd worden maar ze kunnen er ook met bakken tegelijk ingestort worden, waarbij ze een 'random' stapeling vormen. Andere voorbeelden van willekeurige deeltjes stapelingen die vaak voorkomen zijn: zand, grint, koffiepoeder, rijst, plantzaden en noten.

Dit onderzoek richt zich op wanordelijke stapelingen van verschillende deeltjes vormen, zoals bollen, afgeplatte bollen, spheroids (M&M's) en spherocylinders (Tic Tac vorm), waarbij wordt gekeken naar het ingenomen volume en de struktuur van de onderlinge contacten met elkaar. Er wordt gekeken naar hoe de vorm van het deeltje de pakking beinvloedt, sinaasappels zullen net iets anders stapelen dan M&M's en Tic Tacs. Dit kan grote gevolgen hebben voor bijvoorbeeld de industriële applicatie van deeltjes stapelingen in chemische reaktoren, waar de vloeistof langs de pakking stroomt en vervolgens reageert. De manier waarop de vloeistof stroomt wordt grotendeels bepaald door de structuur van de gestapelde deeltjes.

Na de literatuurstudie over deeltjes stapelingen in hoofdstuk 2, wordt in hoofdstuk 3 het kooiingsprobleem voor twee-dimensionale schijven zowel analytisch als op de computer opgelost. Een schijf is gekooid als die niet meer kan bewegen doordat de beweging geblokt wordt door andere schijven of zogenaamde punt contacten. Schijven worden willekeurig geplaatst op de omtrek van de centrale schijf en het kooiingsgetal is het gemiddelde aantal schijven dat geplaatst moet worden om te zorgen dat de centrale schijf niet meer kan bewegen. Verder wordt een benadering gegeven voor de kooiing van bollen in drie dimensies. Het kooiingsgetal is belangrijk voor willekeurige pakkingen omdat in zo'n pakking de meeste deeltjes niet kunnen bewegen en vormt dus een ondergrens voor het contact getal in deze pakkingen. Het parkeernummer is verwant aan het kooiingsgetal: het is het gemiddelde maximum aantal deeltjes dat willekeurig geplaatst kan worden op een centraal deeltje.

In hoofdstuk 4 worden deze getallen gebruikt om een model op te stellen voor pakkingen van bollen met verschillende dichtheden, zoals bijvoorbeeld wanneer men koffie poeder voorzichtig in een bus giet zal het poeder los gepakt zijn. Door te tikken op de wand van de bus zal de koffie dichter pakken en kan er meer koffie in de bus. (Houdt er

dan rekening mee dat de koffie dan ook sterker smaakt bij hetzelfde aantal scheppen.) Het model genereert een flink aantal clusters van bollen volgens gespecifeerde regels en vervolgens wordt het gemiddelde ervan uitgerekend en vergeleken met experimentele data en computer gegenereerde pakkingen. Op deze wijze worden uit microscopische regels macroscopische eigenschappen, zoals bijvoorbeeld de dichtheid, bepaald.

Hoofdstuk 5 onderzoekt de invloed van de deeltjesvorm op de struktuur van de gevormde pakkingen met behulp van de Mechanische Contractie Methode (MCM). Dit is een computationele methode waarbij begonnen wordt met een wolk van stilstaande deeltjes en waar vervolgens het volume van de wolk mechanisch wordt verkleind. Het volume van de wolk wordt net zolang verkleind totdat het niet meer mogelijk is om het verder te verkleinen doordat de deeltjes dicht tegen elkaar aangedrukt zijn.

Het blijkt dat spheroids (M&M's) vergelijkbaar stapelen als spherocylinders (Tic Tacs) voor lage lengte-diameter verhoudingen. Wanneer de lengte-diameter verhouding vergroot wordt dan gaan spherocylinders (lange staafjes) beter pakken dan M&M's doordat de ratio van het deeltjes volume met het uitgesloten volume voor spherocylinders groter is. In gedachten kan men een spheroid pakking voorstellen en dan de deeltjes vervangen door spherocylinders, de structuur blijft hetzelfde maar de spherocylinders nemen meer ruimte in bij dezelfde lengte-diameter ratio.

Verder wordt in hoofdstuk 5 de invloed van deeltjes met een plat vlak op het stapelen kwantitatief onderzocht door middel van afgeplatte bollen. Door aan beide kanten van een bol een plakje af te snijden kunnen steeds dunnere plaatjes gevormd worden. Het blijkt dat het platte vlak in de afgeplatte bollen een grote invloed heeft op de stapeling. Lange dunne staafjes vormen willekeurige in elkaar genestte structuren, zoals bijvoorbeeld ook worden gevonden in vogelhuisjes van dunne takken, terwijl het platte vlak van de afgeplatte bollen ervoor zorgt dat de deeltjes plat tegen elkaar aan gaan liggen in rolletjes. De afgeplatte bollen pakken niet langer willekeurig maar vormen geordende structuren. Dit effect van ordening kan ook gezien worden in stapelingen van munten zoals bijvoorbeeld in een piraten schatkist, of een vat volgestort met pepermuntjes.

Het gemiddeld aantal contacten met andere staven dat een staaf heeft werd onderzocht met behulp van Moleculaire Dynamica door dit toe te passen op pakkingen gegenereerd met de MCM methode. Moleculaire Dynamica rekent de krachten uit die werken op ieder deeltje en berekend op die manier de nieuwe posities van de deeltjes. Tijdens de simulatie groeien de deeltjes langzaam in grootte en als ze elkaar beginnen te overlappen worden ze uit elkaar geduwd doordat er een mechanische veer tussen de deeltjes geplaatst wordt die ze uit elkaar duwt tot ze niet meer overlappen. Met deze methode is het mogelijk om pakkingen met een beter gedefinieerd contact getal te creeren. Verder is er met deze methode naar gekeken hoeveel bollen en staven gekooid zijn als een functie van de volume fractie van een packing. Om de kooiing van staven te berekenen is een nieuwe methode ontwikkeld gebaseerd op lineair programmeren. Het

gevonden kooigetal blijkt heel goed de stapelingsdichtheid van willekeurig georienteerde staafjes te verklaren.

Hoofdstuk 7 borduurt verder op hoofdstuk 5 en 6 en laat zien dat pakkingen gemaakt van groeiende deeltjes ook een omgekeerd evenredig verband tussen volume fractie en aspect ratio van de deeltjes hebben. Het effect van de expansie van de pakking als de deeltjes groeien, zoals aangetoond met de simulaties, laat zien dat dit een plausibel mechanisme kan zijn voor de voortbeweging van sommige specifieke biologische cellen.

Publications

This thesis is based on the following publications:

Chapter 3: A. Wouterse, M. Plapp and A. P. Philipse, "On the caging of two- and three-dimensional hard spheres", J. Chem. Phys., 123, 054507 (2005)

Chapter 4: A. Wouterse and A. P. Philipse, "Geometrical cluster ensemble analysis of random hard sphere packings", J. Chem. Phys., 125, 194709 (2006)

Chapter 5: A. Wouterse, S. R. Williams and A. P. Philipse, "Effect of particle shape on the density and microstructure of random packings", J. Phys.: Condens. Matter, 19, 406215 (2007)

Chapter 6: A. Wouterse, S. Luding and A. P. Philipse, "On contact numbers in random rod packings", submitted

Chapter 7 summarizes our contribution to: L. Miao, O. Vanderlinde, J. Liu, R. P. Grant, A. Wouterse, A. P. Philipse, M. Stewart and T. M. Roberts, "The role of filament packing dynamics in powering amoeboid cell motility", to be submitted

Other publications:

K. de Lange Kristiansen, A. Wouterse and A. P. Philipse, "Simulation of random packing of binary sphere mixtures by mechanical contraction", Physica A, 358, 249 (2005)

S. Sacanna, L. Rossi, A. Wouterse and A. P. Philipse, "Observation of a shape dependent density maximum in random packing of colloidal silica ellipsoids", J. Phys.: Condens. Matter, 19, 376108 (2007)

A. Yethiraj, A. Wouterse, B. Groh and A. van Blaaderen, "Nature of an electric-field-induced colloidal Martensitic transition", Phys. Rev. Lett., 92, 058301 (2004)

A. Yethiraj, J. Thijssen, A. Wouterse and A. van Blaaderen, "Large electric-field-induced colloidal single crystals for photonic applications", Adv. Mater., 16, 596 (2004)

Dankwoord

Graag wil ik een aantal mensen bedanken voor het helpen met het tot stand komen van dit proefschrift. Allereerst bedank ik mijn promotor Albert Philipse voor het nemen van het initiatief dat tot dit proefschrift leidde en voor al je nuttige suggesties en bijdragen aan het onderzoek. Thijs Vlugt bedank ik hartelijk voor zijn waardevolle hulp met het opzetten van het rekencluster waarop een groot aantal van de berekeningen in dit proefschrift zijn uitgevoerd. I thank Stephen Williams for explaining the mechanical contraction method to me, for showing me around in Australia and taking me on a kangaroo trip. Also I would like to thank the other members of the Research school of Chemistry for the nice atmosphere. Mathis Plapp, Murray Stewart, Tom Roberts, Jos Brouwers, Tomaso Aste and Stefan Luding are greatly thanked for their valuable input on the various chapters in this thesis. Het drinken van koffie is goed voor het geheugen en daarom wil ik al mijn collega's van het Van 't Hoff laboratorium bedanken voor de gezellige koffie pauzes en de fijne sfeer op het lab. Emile wil ik bedanken voor het helpen met het rekencluster en voor het introduceren van de Wii en Hattrick voor de nodige ontspanning. Bonny wil ik bedanken voor de uitdaging van een antieke C++ compiler en Maria, Mark en Karel voor hun hulp met LaTeX. Karel ook bedankt voor onze GNU Linux discussies. David en Tjeerd, bedankt voor jullie input op het gebied van random packing. Mijn oud-kamergenoten Judith en Mircea voor de hartelijke ontvangst op het lab en mijn nieuwe kamergenoot Andriy voor het nauwkeurig lezen van het manuscript. Verder wil ik m'n vrienden bedanken voor al de ontspannende activiteiten, interessante films en hulp met GNU Linux. Tot slot wil ik mijn familie bedanken voor al hun steun en begrip de afgelopen jaren. Zonder jullie was het me nooit gelukt. Ma, Pa, Martin en Sunny bedankt.

Curriculum Vitae

De auteur van dit proefschrift werd geboren op 29 december 1978 in Utrecht. Vanaf 1991 bezocht hij het Anna van Rijn College te Nieuwegein, waaraan hij in 1997 het VWO-diploma behaalde. Aansluitend studeerde hij scheikunde en natuurkunde in de twin-variant aan de Universiteit Utrecht. Het doctoraal examen werd behaald in 2002 met als klein hoofdvak fysische en colloïd chemie en als hoofdvak zachte gecondenseerde materie. De auteur is in januari 2004 als onderzoeker in opleiding in dienst van de FOM verbonden aan het Van 't Hoff Laboratorium voor Fysische en Colloïd Chemie van de Universiteit Utrecht, waar hij onder leiding van Prof. Dr. A. P. Philipse het in dit proefschrift beschreven onderzoek uitgevoerd heeft.